INFORMATION TO USERS

This manuscript has been reproduced from the microfilm master. UMI films the text directly from the original or copy submitted. Thus, some thesis and dissertation copies are in typewriter face, while others may be from any type of computer printer.

The quality of this reproduction is dependent upon the quality of the copy submitted. Broken or indistinct print, colored or poor quality illustrations and photographs, print bleedthrough, substandard margins, and improper alignment can adversely affect reproduction.

In the unlikely event that the author did not send UMI a complete manuscript and there are missing pages, these will be noted. Also, if unauthorized copyright material had to be removed, a note will indicate the deletion.

Oversize materials (e.g., maps, drawings, charts) are reproduced by sectioning the original, beginning at the upper left-hand corner and continuing from left to right in equal sections with small overlaps.

ProQuest Information and Learning
300 North Zeeb Road, Ann Arbor, MI 48106-1346 USA
800-521-0600

UMI®

Reproduced with permission of the copyright owner. Further reproduction prohibited without permission.

Reproduced with permission of the copyright owner. Further reproduction prohibited without permission.

Combined Beamforming and Noise Cancellation

Jacek Dmochowski, B.Eng.

A thesis submitted to:

the Faculty of Graduate Studies and Research

in partial fulfillment of

the requirement for the degree of:

Master's of Applied Science

Ottawa-Carleton Institute for Electrical and Computer Engineering (OCIECE)

Department of Systems and Computer Engineering

Carleton University

Ottawa, Ontario, Canada

©Copyright

2005, Jacek Dmochowski

Reproduced with permission of the copyright owner. Further reproduction prohibited without permission.

Library and Archives Canada
Bibliothèque et Archives Canada

Published Heritage Branch
Direction du Patrimoine de l'édition

0-494-08371-9

395 Wellington Street
Ottawa ON K1A 0N4
Canada

395, rue Wellington
Ottawa ON K1A 0N4
Canada

Your file *Votre référence*
ISBN:
Our file *Notre reference*
ISBN:

NOTICE:
The author has granted a non-exclusive license allowing Library and Archives Canada to reproduce, publish, archive, preserve, conserve, communicate to the public by telecommunication or on the Internet, loan, distribute and sell theses worldwide, for commercial or non-commercial purposes, in microform, paper, electronic and/or any other formats.

The author retains copyright ownership and moral rights in this thesis. Neither the thesis nor substantial extracts from it may be printed or otherwise reproduced without the author's permission.

AVIS:
L'auteur a accordé une licence non exclusive permettant à la Bibliothèque et Archives Canada de reproduire, publier, archiver, sauvegarder, conserver, transmettre au public par télécommunication ou par l'Internet, prêter, distribuer et vendre des thèses partout dans le monde, à des fins commerciales ou autres, sur support microforme, papier, électronique et/ou autres formats.

L'auteur conserve la propriété du droit d'auteur et des droits moraux qui protège cette thèse. Ni la thèse ni des extraits substantiels de celle-ci ne doivent être imprimés ou autrement reproduits sans son autorisation.

In compliance with the Canadian Privacy Act some supporting forms may have been removed from this thesis.

While these forms may be included in the document page count, their removal does not represent any loss of content from the thesis.

Conformément à la loi canadienne sur la protection de la vie privée, quelques formulaires secondaires ont été enlevés de cette thèse.

Bien que ces formulaires aient inclus dans la pagination, il n'y aura aucun contenu manquant.

Canada

Reproduced with permission of the copyright owner. Further reproduction prohibited without permission.

The undersigned hereby recommends to the Faculty of Graduate Studies and Research acceptance of the thesis

Combined Beamforming and Noise Cancellation

Submitted by Jacek Dmochowski

In partial fulfillment of the requirements for the

Degree of Master's of Applied Science

Thesis Supervisor
Dr. Rafik A. Goubran

Chair, Department of Systems and Computer Engineering
Dr. Rafik A. Goubran
Carleton University
September 2005

Reproduced with permission of the copyright owner. Further reproduction prohibited without permission.

Abstract

This work examines combined beamformer-noise canceller (BF-NC) structures. A new paradigm for adaptive beamforming is presented: The front-end consists of a bank of arbitrary beamformers which are configured independently by a beam-steering module. A switching unit then cascades the beamformers with a multiple-reference adaptive noise canceller which provides sidelobe suppression.

The relationship between the front-end beamformers and cascaded adaptive noise cancellers is characterized by computing the beampattern, directivity, white noise gain, and signal-to-interference ratio (SIR) before and after the noise canceller stage. It is shown that the SIR gain offered by the desired signal beamformer varies inversely with the SIR gain contributed by the noise canceller.

It is also shown that signal enhancement is offered for a broad range of scenarios, including a speech desired signal and speech interference. An emphasis is placed on evaluating BF-NC structures in real environments. Experimental results reveal SIR improvements of up to 30 dB.

Reproduced with permission of the copyright owner. Further reproduction prohibited without permission.

Acknowledgments

This work was made possible through the funding provided by Ontario Graduate Scholarships (**OGS**), Communications and Information Technology Ontario (**CITO**), and the Department of Systems and Computer Engineering at Carleton University, at which the work was carried out.

I would like to personally thank Professor Mohamed El-Tanany for enabling the opportunity to work with Professor Rafik Goubran, the supervisor of this thesis. Professor Goubran has offered much technical expertise, guidance, and encouragement throughout the project, in addition to formulating the decoupled beamforming-noise cancellation design and facilitating interactions with industry partners. Franck Beaucoup contributed several helpful suggestions.

I would also like to thank my family for giving me the foundation from which I build my life around: my Mother for her endless love and care of me, my Father for establishing the value of education at an early age and for giving me the hard-earned opportunity to live and study in Canada.

To Shelley and Madeline, I am indebted for their continual support throughout my graduate studies. In particular, Shelley has supported me during the most difficult of times, offered endless affirmation, and worked hard to keep my spirits up. Both have brought much-needed balance into my life.

Reproduced with permission of the copyright owner. Further reproduction prohibited without permission.

Contents

Abstract iii
Acknowledgments iv
Contents v
List of Tables vii
List of Figures viii
List of Abbreviations xi

1. Introduction 1
   1.1 Signal Detection and Estimation 1
   1.2 Spatial Filtering 1
   1.3 Problem Statement and Thesis Objectives 2
   1.4 Thesis Contributions 3
   1.5 Thesis Organization 4

2. Background and Literature Review 6
   2.1 Adaptive Noise Cancellation 6
      2.1.1 Adaptive Noise Cancellation in the Presence of Uncorrelated Noise 7
      2.1.2 Adaptive Noise Cancellation in the Presence of Desired Signal Leakage ... 9
      2.1.3 Adaptation Control 10
      2.1.4 Multiple-Reference Adaptive Noise Canceller 10
      2.1.5 Problems with Adaptive Noise Cancellation 11
   2.2 Beamforming 12
      2.2.1 Beamforming Model 13
      2.2.2 Evaluation of Beamformers 15
      2.2.3 Fixed Beamforming 19
      2.2.4 Adaptive Beamforming 20

3. Simulation Environment and Experimental Setup 28
   3.1 Simulation Environment 28
   3.2 Experimental Setup 30

4. Decoupled Beamforming and Adaptive Noise Cancellation 34
   4.1 Decoupled Beamformer-Noise Canceller Model 34
   4.2 Decoupled Beamformer-Noise Canceller Structures 37
   4.3 Coupled, Blocking-Matrix Based Beamformer-Noise Canceller Structures .. 44
   4.4 Relationships between Beamforming and Noise Cancellation 47
      4.4.1 Signal-to-Interference Ratio as a Function of Signal-Interference Separation in a Decoupled Beamformer-Noise Canceller Structure 48
      4.4.2 Signal-to-Interference Ratio as a Function of Signal-Interference Separation in a Coupled Beamformer-Noise Canceller Structure 51
      4.4.3 Beampattern of a Decoupled Beamformer-Noise Canceller Structure ... 54
      4.4.4 Beampattern of a Coupled Beamformer-Noise Canceller Structure 55
      4.4.5 Frequency Dependency of Beampatterns 55
      4.4.6 White Noise Gain as a Function of Frequency 59

Reproduced with permission of the copyright owner. Further reproduction prohibited without permission.

4.4.7 Directivity as a Function of Frequency 60

5. Simulation Evaluation of Beamformer-Noise Canceller Structures 62
5.1 Investigation of Signal Nature in Beamformer-Noise Canceller Structures .. 62
5.2 Simulation Results 64

6. Experimental Evaluation of Beamformer-Noise Canceller Structures 73
6.1 Experimental Procedure 73
6.2 Experimental Results 74
6.3 Sensitivity of Blocking Matrix to Steering Errors 80

7. Conclusions and Future Work 83
7.1 Thesis Contributions 83
7.2 Concluding Remarks and Future Work 83

References 87

Reproduced with permission of the copyright owner. Further reproduction prohibited without permission.

List of Tables

Table 3.1. Origin of signals used in simulations. **29**

Table 3.2. Specifications of data acquisition unit. **31**

Table 5.1. Signal enhancement as a function of signal nature. **65**

Reproduced with permission of the copyright owner. Further reproduction prohibited without permission.

List of Figures

Figure 2.1. Classical adaptive noise canceller. 6

Figure 2.2. Model for adaptive noise cancellation with uncorrelated noise components in primary and reference inputs. 8

Figure 2.3. Model for adaptive noise cancellation with desired signal leakage..... 9

Figure 2.4. Multiple-reference adaptive noise canceller..... 11

Figure 2.5. Structure of a spatial filter: (left) Narrowband beamformer, (right) Broadband beamformer..... 12

Figure 2.6. Beamforming model consisting of signal source and noise field. 13

Figure 2.7. Near-field (left) and far-field (right) geometry. 15

Figure 2.8. Fixed beamforming: Delay-and-sum beamformer (left), Filter-and-sum beamformer (right). 20

Figure 2.9. Time-aligned signal model. 22

Figure 2.10. Decomposition of optimal weight selection. 22

Figure 2.11. Generalized Sidelobe Canceller..... 24

Figure 2.12. Novel approach to adaptive beamforming. 26

Figure 3.1. Layout of experiment room. 31

Figure 3.2. Multi-channel recording apparatus. 32

Figure 4.1. Decoupled beamforming-noise cancellation design..... 35

Figure 4.2. Decoupled beamformer-noise canceller structure with single interference source..... 38

Figure 4.3. Simple decoupled beamformer-noise canceller structure with two delay-and-sum beamformers and one noise canceller. 40

Figure 4.4. Magnitude response of Wiener solution in a decoupled beamformer-noise canceller structure..... 42

Reproduced with permission of the copyright owner. Further reproduction prohibited without permission.

Figure 4.5. Phase response of Wiener solution in a decoupled beamformer-noise canceller structure. 42

Figure 4.6. Generalized decoupled beamformer-noise canceller structure with multiple delay-and-sum beamformers and a multiple-reference noise canceller. 43

Figure 4.7. Coupled beamformer-noise canceller structure with blocking matrix.. 45

Figure 4.8. Magnitude responses of multi-channel Wiener solution in a coupled beamformer-noise canceller structure with blocking matrix. 46

Figure 4.9. Phase responses of multi-channel Wiener solution in a coupled beamformer-noise canceller structure with blocking matrix. 47

Figure 4.10. Signal-to-interference ratio relationships between beamformer and noise canceller in a decoupled beamformer-noise canceller structure. 49

Figure 4.11. Overall signal-to-interference ratio gain of a decoupled beamformer-noise canceller structure. 51

Figure 4.12. Signal-to-interference ratio relationships between beamformer and noise canceller in a coupled beamformer-noise canceller structure with blocking matrix. 52

Figure 4.13. Overall signal-to-interference ratio gain of a coupled beamformer-noise canceller structure with blocking matrix. 53

Figure 4.14. Beampatterns of a decoupled beamformer-noise canceller structure. 54

Figure 4.15. Beampatterns of a coupled beamformer-noise canceller structure with blocking matrix. 56

Figure 4.16. Frequency-dependency of beampatterns in a decoupled beamformer-noise canceller structure. 56

Figure 4.17. Addition of post-filter into decoupled beamformer-noise canceller. ... 58

Figure 4.18. Frequency-dependency of beampatterns in a coupled beamformer-noise canceller structure with blocking matrix 58

Figure 4.19. White noise gain as a function of frequency 60

Figure 4.20. Directivity index as a function of frequency. 61

Figure 5.1. Delay for causality in a decoupled beamformer-noise canceller structure. 63

Reproduced with permission of the copyright owner. Further reproduction prohibited without permission.

Figure 5.2. Delay for causality in a coupled beamformer-noise canceller structure. 63

Figure 5.3. Power spectral densities of male and female speech signals used in simulations. 66

Figure 5.4. Signal-to-interference ratio improvements as a function of frequency. 68

Figure 5.5. Output power spectral densities of interference only, as a function of frequency. 70

Figure 5.6. Output power spectral densities of desired signal only, as a function of frequency. 70

Figure 5.7. Convergence rates of beamformer-noise canceller structures. 72

Figure 6.1. Experimentally obtained signal-to-interference ratio improvements for the beamformer, decoupled beamformer-noise canceller, and coupled beamformer-noise canceller with blocking matrix, as a function of signal-source location..... 74

Figure 6.2. Sensitivity of desired signal beamformer to reverberation. 75

Figure 6.3. Effect of lowered beamformer directivity on performance of noise canceller. 76

Figure 6.4. Location at which blocking matrix offers greatest signal-to-interference ratio increase. 77

Figure 6.5. Locations at which blocking matrix is detrimental to performance..... 78

Figure 6.6. Signal-to-interference ratio improvements as a function of adaptive filter length in beamformer-noise canceller structures. 79

Figure 6.7. Reference signal-to-interference ratios under ideal conditions..... 81

Figure 6.8. Reference signal-to-interference ratios with steering error. 81

Reproduced with permission of the copyright owner. Further reproduction prohibited without permission.

List of Abbreviations

A-D	Analog-to-Digital
AGC	Automatic Gain Control
ANC	Adaptive Noise Cancellation, Adaptive Noise Canceller
BF-NC	Beamformer-Noise Canceller, Beamforming-Noise Cancellation
CSD	Cross-Spectral Density
DI	Directivity Index
DOA	Direction of Arrival
DSB	Delay-and-Sum Beamformer
FIR	Finite Impulse Response
FSB	Filter-and-Sum Beamformer
GSC	Generalized Sidelobe Canceller
GSVD	Generalized Singular Value Decomposition
IUNR	Interference-to-Uncorrelated-Noise Ratio
LCMV	Linearly Constrained Minimum Variance
MMSE	Minimum-Mean-Squared Error
MSE	Mean-Squared Error
MVDR	Minimum Variance Distortionless Response
NLMS	Normalized Least-Mean-Squares
PSD	Power-Spectral Density
SDB	Superdirective Beamformer
SIR	Signal-to-Interference Ratio
SNR	Signal-to-Noise Ratio

Reproduced with permission of the copyright owner. Further reproduction prohibited without permission.

SUNR	Signal-to-Uncorrelated Noise Ratio
VAD	Voice Activity Detection, Voice Activity Detector
WNG	White Noise Gain

Reproduced with permission of the copyright owner. Further reproduction prohibited without permission.

Chapter 1

Introduction

1.1 Signal Detection and Estimation

The detection and estimation of a desired signal in the presence of corruptive noise and interference is a classic problem that has spawned numerous approaches. Purely temporal approaches include frequency discrimination and optimal filtering [1-5]. Optimal or Wiener filter theory is based on the idea of selecting a filter that maximizes the signal-to-noise ratio (SNR) by performing least-squares minimization. Widrow's initial implementation of adaptive noise cancellation[1] (ANC) [6] introduced a spatial approach to the problem, in the form of a reference sensor that is positioned near the unwanted noise source. Array beamforming [7-8] has since emerged as the primary tool for estimating the desired signal when the bandwidths of the desired and interfering signals overlap.

1.2 Spatial Filtering

Spatial filtering is analogous to its temporal counterpart: The fact that desired and noise signals originate from different spatial locations is exploited to provide signal discrimination. Beamforming is the name given to spatial filtering approaches that are based on the collection of data over an array of sensors. Beamformers are subdivided into fixed and adaptive implementations: Fixed beamformer design is performed

[1] Throughout this paper, the terms "adaptive noise cancellation" and "noise cancellation" are used interchangeably. Likewise, a "noise canceller" is equivalent to an "adaptive noise canceller".

Reproduced with permission of the copyright owner. Further reproduction prohibited without permission.

independently of the signal characteristics, while adaptive designs are tailored to the specifics of the signal properties.

1.3 Problem Statement and Thesis Objectives

The primary application of the research presented in this thesis is the area of microphone-array based beamforming for speech enhancement. Present-day adaptive beamforming techniques are plagued by the effects of background noise, reverberation, and non-stationary signal environments, to which the algorithms are sensitive [9]. Fully-adaptive beamformers involve the constrained optimization process, which is computationally expensive [7]. Furthermore, the beam shapes formed by adaptive beamformers are intricate and thus not robust to moving signal sources. The Generalized Sidelobe Canceller (GSC) suffers from the desired signal cancellation phenomenon, which results from steering vector errors and correlated interference. The development of models based on stationary anechoic assumptions leads to such degradations in performance when operating under real conditions.

Even though adaptive beamformers such as the GSC combine front-end beamformers with a multiple-reference ANC, the identification of these structures as a combination of beamforming and noise cancellation has not been made. The structures are viewed as adaptive implementations of statistically optimum beamformers. In other words, the beamforming unit has not been decoupled from the noise cancellation unit.

It is surprising that even though the GSC clearly combines a multiple-reference ANC with front-end beamformers, this has not led to designs that are motivated by the properties of the ANC. For example, Widrow shows in [6] that the signal-to-interference ratio (SIR) at the output of an ANC is equal to the inverse of the SIR at the reference

Reproduced with permission of the copyright owner. Further reproduction prohibited without permission.

sensor. In other words, the key is to minimize the SIR at the reference noise canceller input. Why have we not designed a beamformer that minimizes the SIR and feeds the reference noise canceller input? Rather, the Linearly Constrained Minimum Variance (LCMV) approach has dominated adaptive beamformer design, even though it is not clear that this approach leads to optimal results in real environments. Perhaps restricting the weights of adaptive beamformers to those that yield a unity response in the direction of the desired signal prevents more robust beamformers from emerging.

It is not clear that trying to block the desired signal is the most effective way of creating a low SIR at the reference noise canceller inputs, as nulls are inherently very narrow. Rather, steering a wide beam to the interference leads to a greater allowable margin of steering error. Ideally, the reference beamformer should form both a null in the signal direction and a beam in the direction of the interference. To this date, such a structure has not been proposed.

This thesis proposes an alternative approach to adaptive beamformer design. A bank of arbitrary, stand-alone beamformers is cascaded with a multiple-reference ANC. The design of the front-end beamformers is performed independently of the ANC component. Auxiliary modules control the beam-steering, adaptation, and channel switching. This approach is termed the "decoupled beamformer-noise canceller (BF-NC) model". This thesis attempts to characterize the interoperation and dynamics involved when combining beamformers with noise cancellers. An experimental approach is stressed, and results obtained in real conditions are emphasized.

1.4 Thesis Contributions

This work contributes to the body of knowledge in beamforming and noise cancellation:

Reproduced with permission of the copyright owner. Further reproduction prohibited without permission.

1. The decoupled BF-NC model is identified [10-12]. It is shown that a decoupled BF-NC is effectively an adaptive beamformer, and may be implemented in fully-adaptive form.
2. The relationships between front-end beamformers and cascaded noise cancellers are defined by comparing the beampattern, directivity, white noise gain (WNG), and SIR achieved before and after the noise cancellation stage. It is shown that the SIR gain contributed by the desired signal beamformer is inversely related to the SIR gain contributed by the noise canceller [11-12]. The SIR gain of the beamformer increases for increased signal-interference physical separation. On the other hand, the SIR gain attained by the noise canceller decreases with increased signal-interference physical separation.
3. The applicability of BF-NC structures to various signal environments is established: This includes the case of a speech desired signal with speech interference.
4. An experimental model for evaluating BF-NC structures in real conditions is presented. Experimental results show that the inclusion of a voice activity detection (VAD) module allows for simpler, robust alternatives to coupled, blocking matrix-based approaches [11-12].

1.5 Thesis Organization

Chapter 1 introduces the general area of signal detection and estimation, presenting both temporal and spatial approaches. It also defines the problem statement and research objectives, presents the organization of the thesis, and summarizes the thesis contributions.

Reproduced with permission of the copyright owner. Further reproduction prohibited without permission.

Chapter 2 provides an overview of beamforming and noise cancellation theory, and reviews the work of previous researchers in the respective fields. The knowledgeable reader may proceed directly to Chapter 3.

Chapter 3 outlines the simulation environment and experimental setup used to obtain the results that are presented in this work, with an aim to facilitate reproduction of the results.

The essence of the thesis begins with Chapter 4, which presents the decoupled BF-NC model for signal enhancement. Comparisons with coupled, blocking matrix-based adaptive beamformers are made. Wiener solutions in BF-NC structures are given and allow for steady-state characterizations. It is shown that a BF-NC structure may be implemented in fully-adaptive form. Relationships between the front-end beamformers and cascaded noise cancellers are established in terms of the beampattern, directivity, WNG, and SIR.

Chapter 5 examines BF-NC structures in a simulated anechoic environment. The applicability of BF-NC structures to various signal natures is explored.

Chapter 6 sets out to evaluate combined BF-NC structures in real conditions. Results stem from experiments conducted in a large office-room. A procedure for measuring experimental signal enhancement is presented.

Concluding remarks are made in Chapter 7. Future research direction and open problems are also discussed.

Reproduced with permission of the copyright owner. Further reproduction prohibited without permission.

Chapter 2

Background and Literature Review

Sections 2.1 and 2.2 provide an overview of noise cancellation and beamforming theory, respectively. Notions fundamental to the understanding of the upcoming chapters are presented. The knowledgeable reader may proceed directly to Chapter 3.

2.1 Adaptive Noise Cancellation

The ANC process entails a scheme in which noise is subtracted from a received signal in an intelligent fashion to achieve a greater SNR [6]. Figure 2.1 depicts the operation of the classical noise canceller.

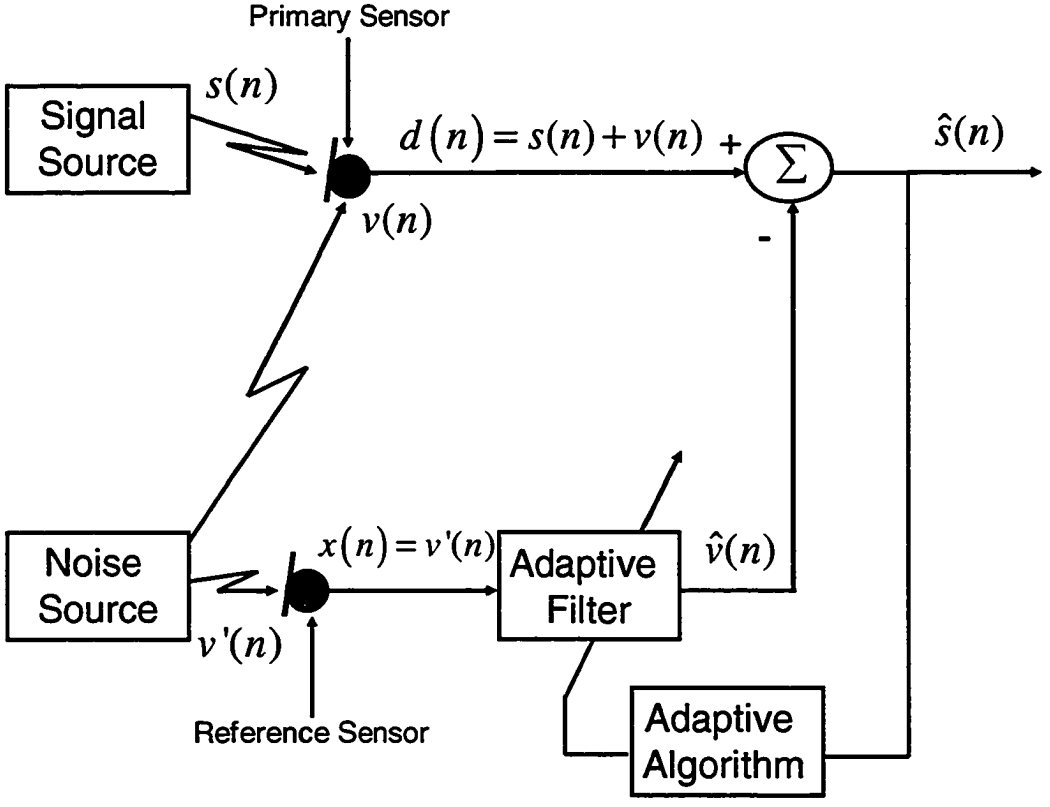

Figure 2.1. Classical adaptive noise canceller.

Reproduced with permission of the copyright owner. Further reproduction prohibited without permission.

A primary sensor is located in the vicinity of the desired signal source, while a reference sensor is positioned near the origin of the unwanted noise. An adaptive algorithm attempts to drive the tap weights of the adaptive filter to the impulse response between the noise source and the primary sensor. From the solution of the Wiener-Hopf equation, the least-squares Wiener solution of the ANC problem is given by [6]:

$$W_{NC}^{*}\left(e^{j\Omega}\right)=\frac{\Phi_{xd}\left(e^{j\Omega}\right)}{\Phi_{xx}\left(e^{j\Omega}\right)} \tag{2.1}$$

where $\Phi_{xd}\left(e^{j\Omega}\right)$ is the cross-spectral density (CSD) between the reference and primary noise canceller inputs, and $\Phi_{xx}\left(e^{j\Omega}\right)$ is the power-spectral density (PSD) of the reference input.

Initially, the ANC problem consisted of adapting the filter to minimize the noise canceller output power. The adaptation was performed in the presence of the desired signal. It is shown in [6] that minimizing the output power in such a manner maximizes the output SNR. There are two models for analyzing the performance of noise cancellers. The two models correspond to the two limiting factors in noise canceller performance.

2.1.1 Adaptive Noise Cancellation in the Presence of Uncorrelated Noise

Figure 2.2 depicts the ANC process with uncorrelated noise components in the primary and reference inputs. Widrow relates the performance of the ANC in this model to the levels of uncorrelated noise powers in the following manner. The ratio of uncorrelated-to-correlated noise power, as a function of frequency, at the primary sensor is given by [6]:

$$A\left(e^{j\Omega}\right)=\frac{\Phi_{m_0 m_0}\left(e^{j\Omega}\right)}{\Phi_{vv}\left(e^{j\Omega}\right)} \tag{2.2}$$

Reproduced with permission of the copyright owner. Further reproduction prohibited without permission.

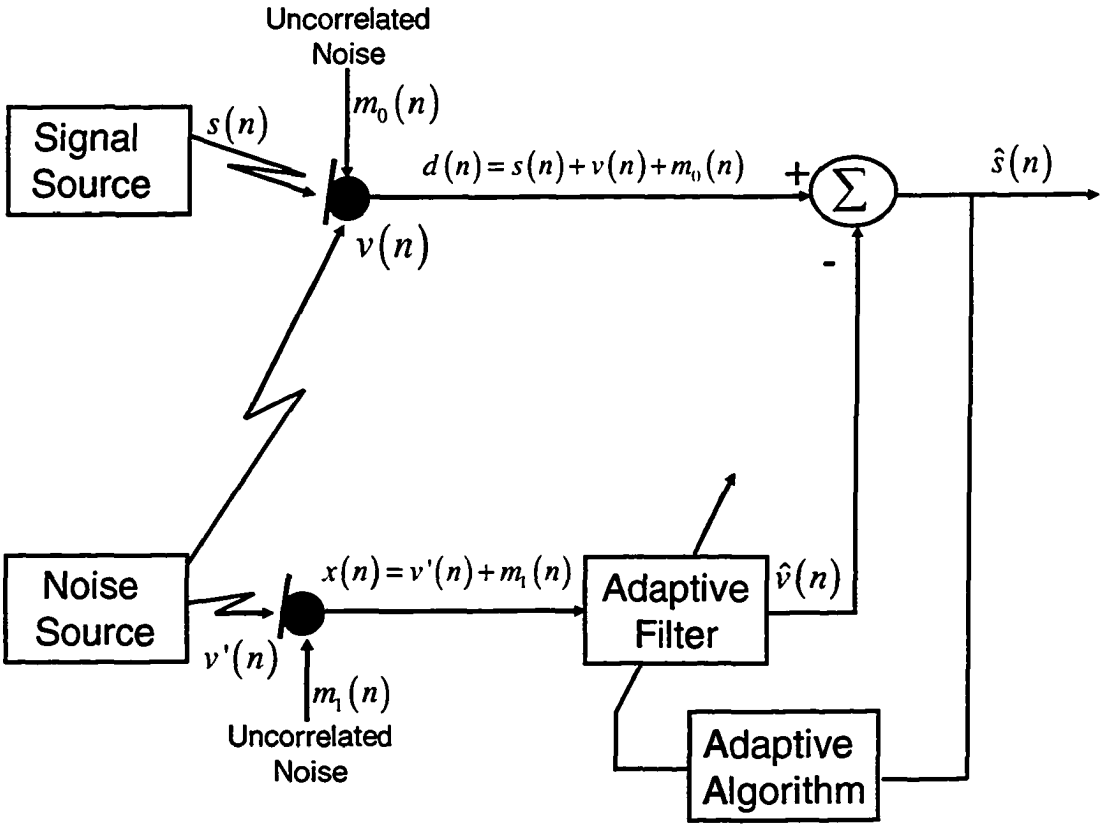

Figure 2.2. Model for adaptive noise cancellation with uncorrelated noise components in primary and reference inputs.

Likewise, the ratio of uncorrelated-to-correlated noise power at the reference sensor is [6]:

$$B\left(e^{j\Omega}\right)=\frac{\Phi_{m_1m_1}\left(e^{j\Omega}\right)}{\Phi_{v'v'}\left(e^{j\Omega}\right)} \tag{2.3}$$

The ratio of SNR at the output to the SNR at the primary sensor is then shown to be [6]:

$$\frac{SNR_{\text{output}}\left(e^{j\Omega}\right)}{SNR_{\text{primary}}\left(e^{j\Omega}\right)}=\frac{\left(A\left(e^{j\Omega}\right)+1\right)\left(B\left(e^{j\Omega}\right)+1\right)}{A\left(e^{j\Omega}\right)+A\left(e^{j\Omega}\right)B\left(e^{j\Omega}\right)+B\left(e^{j\Omega}\right)} \tag{2.4}$$

From (2.4), it is seen that the SNR enhancement offered by an ANC is inversely related to the level of uncorrelated noise power in the primary and reference inputs. For the

Reproduced with permission of the copyright owner. Further reproduction prohibited without permission.

special case of no uncorrelated noise, and assuming that the desired signal does not reach the reference sensor, the SNR improvement is infinite.

2.1.2 Adaptive Noise Cancellation in the Presence of Desired Signal Leakage

In the first ANC model, it is assumed that the reference sensor does not contain any desired signal components. The second ANC model, shown in Figure 2.3, takes into account the presence of the desired signal components in the reference input. This is termed "desired signal leakage." To simplify the analysis in this model, uncorrelated noise is ignored.

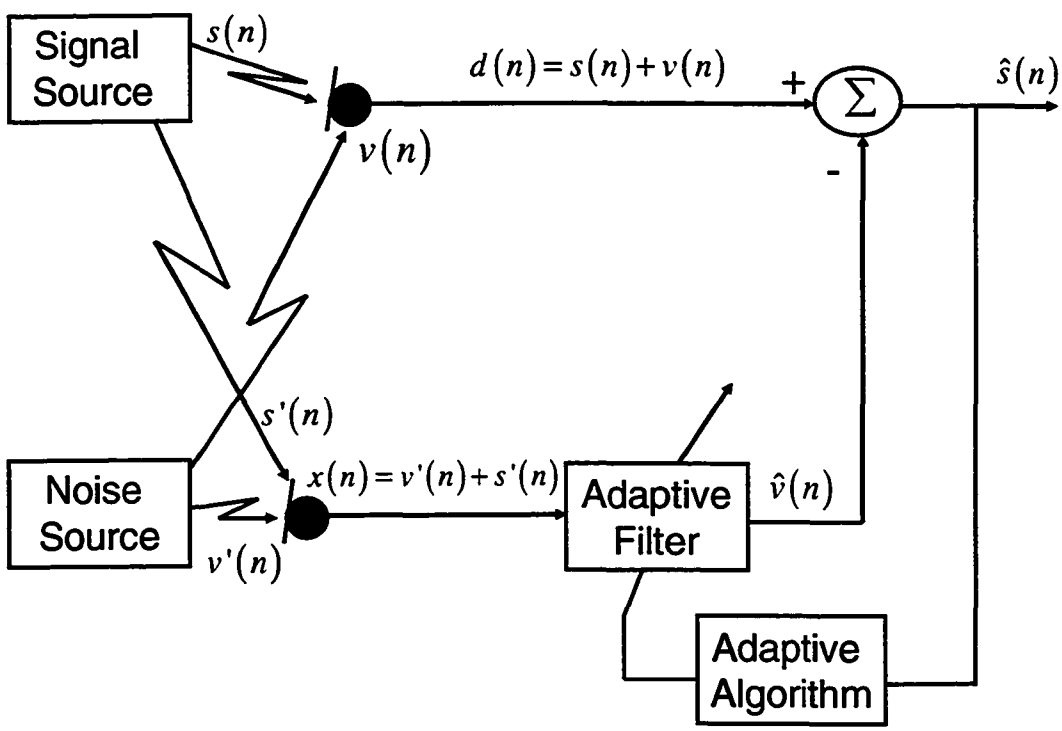

Figure 2.3. Model for adaptive noise cancellation with desired signal leakage.

Widrow shows that for the model of Figure 2.3, the output SNR is simply the inverse of the SNR at the *reference* input, at every frequency [6]:

Reproduced with permission of the copyright owner. Further reproduction prohibited without permission.

$$SNR_{\text{output}}\left(e^{j\Omega}\right) = \frac{1}{SNR_{\text{reference}}\left(e^{j\Omega}\right)} \tag{2.5}$$

The relationship of (2.5) is intuitively satisfying in that a low level of desired signal leakage leads to a high output SNR. Ignoring any uncorrelated noise, if there is no desired-signal at the reference sensor, the output is noise-free. The presence of the desired signal at the reference input leads to performance degradation, as the adaptive filter is partially driven to cancel the signal.

2.1.3 Adaptation Control

The notion of "adaptation control" [13-14] has enhanced the performance of noise cancellers. If adaptation is performed in the absence of the signal (i.e., noise only), the reference sensor will obviously not contain any desired signal component, and thus no signal cancellation will result. Adaptation control can be thought of as a "switched adaptive filter", where an external module controls the switching. When the desired signal is detected by this module, the step-size of the adaptive filter becomes zero, and thus adaptation is "frozen." Adaptation resumes when the signal becomes inactive. In the context of a speech desired signal and non-speech noise, a VAD module nicely serves as this external module.

2.1.4 Multiple-Reference Adaptive Noise Canceller

The presence of multiple noise sources necessitates the need for a noise canceller with multiple reference sensors, shown in Figure 2.4. For every additional noise source, an additional reference sensor and corresponding adaptive filter are inserted to model the transfer function from each noise source to the primary input. The multi-channel Wiener solution to the multiple-reference ANC problem is given by [6]:

Reproduced with permission of the copyright owner. Further reproduction prohibited without permission.

$$\begin{bmatrix} \Phi_{x_0x_0}(e^{j\Omega}) & \Phi_{x_0x_1}(e^{j\Omega}) & \cdots & \Phi_{x_0x_{M-2}}(e^{j\Omega}) \\ \Phi_{x_1x_0}(e^{j\Omega}) & \cdots & \cdots & \vdots \\ \vdots & \ddots & \ddots & \Phi_{x_{M-3}x_{M-2}}(e^{j\Omega}) \\ \Phi_{x_{M-2}x_0}(e^{j\Omega}) & \cdots & \Phi_{x_{M-2}x_{M-3}}(e^{j\Omega}) & \Phi_{x_{M-2}x_{M-2}}(e^{j\Omega}) \end{bmatrix} \begin{bmatrix} W^*_{NC,0}(e^{j\Omega}) \\ W^*_{NC,1}(e^{j\Omega}) \\ \\ W^*_{NC,M-2}(e^{j\Omega}) \end{bmatrix} = \begin{bmatrix} \Phi_{x_0d}(e^{j\Omega}) \\ \Phi_{x_1d}(e^{j\Omega}) \\ \\ \Phi_{x_{M-2}d}(e^{j\Omega}) \end{bmatrix} \quad (2.6)$$

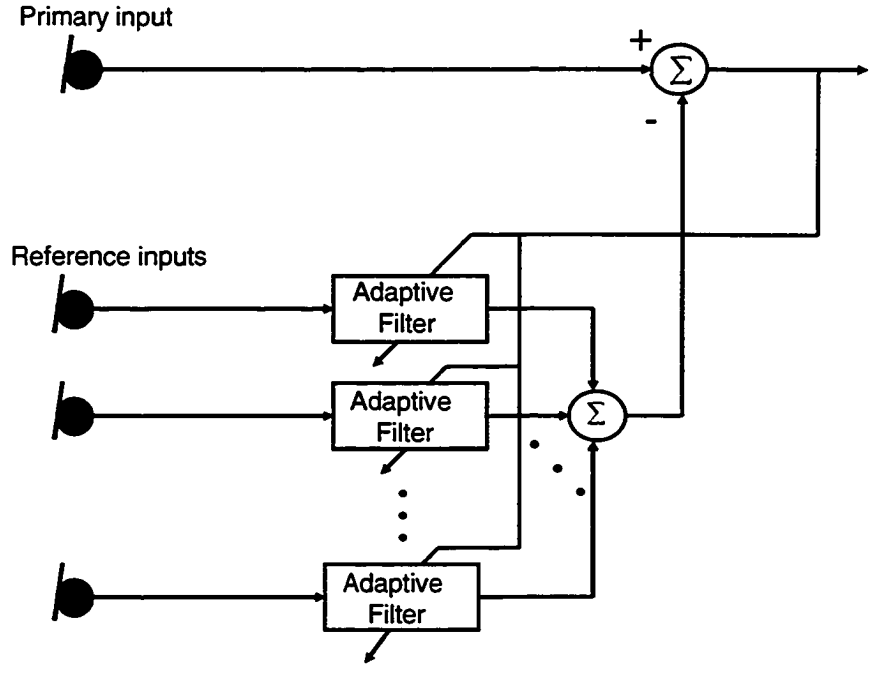

Figure 2.4. Multiple-reference ANC

where $\Phi_{x_ix_j}(e^{j\Omega})$ is the CSD between the i^{th} and j^{th} reference inputs, $\Phi_{x_id}(e^{j\Omega})$ is the CSD between the i^{th} reference input and the primary input, and $W^*_{NC,i}(e^{j\Omega})$ denotes the optimal transfer function of the i^{th} adaptive filter. Notice that in an ANC with M total sensors, there are M-1 reference sensors, and thus M-1 adaptive filters.

2.1.5 Problems with Adaptive Noise Cancellation

The placement of the primary and reference sensors is critical to the proper operation of the ANC. In some applications, it is not possible to place the reference sensor(s) near the

Reproduced with permission of the copyright owner. Further reproduction prohibited without permission.

noise source(s). Furthermore, the desired signal may leak into the reference sensor, leading to signal cancellation, particularly if the spectral content of the signal and noise is similar. The addition of an intelligent front-end may circumvent the latter two problems. A spatially-filtering front-end may be integrated into the noise cancellation process.

2.2 Beamforming

Much like temporal filtering allows us to perform frequency discrimination, spatial filtering allows us to distinguish between signals based on their propagation direction and origin. In order to perform temporal filtering, one collects data over a temporal aperture. Similarly, spatial filtering requires the collection of data over a spatial aperture: A continuous parabolic dish or a discrete array of sensors.

Beamforming is "the name given to a wide variety of array processing algorithms that, by some means, focus the array's signal-capturing abilities in a particular direction" [8]. A *beamformer* is then "a processor used in conjunction with an array of sensors to provide a versatile form of spatial filtering" [7]. The beamformer thus cleverly manipulates multiple replicas of the propagating wavefield in order to emphasize the signal originating from a particular direction.

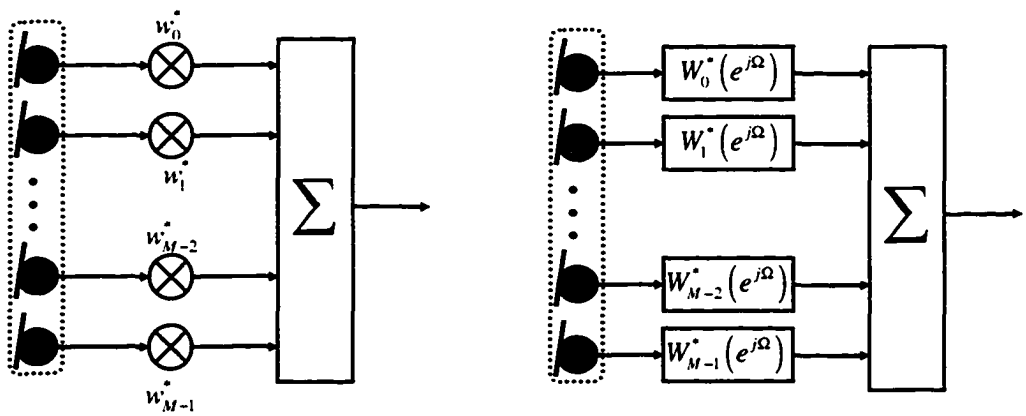

Figure 2.5. Structure of a spatial filter: (left) Narrowband beamformer, (right) Broadband beamformer.

Reproduced with permission of the copyright owner. Further reproduction prohibited without permission.

The general structure of spatial filters is shown in Figure 2.5. An array of sensors serves as the spatial aperture. For narrowband signal applications, the structure in the left pane of Figure 2.5 is suitable: The received signals are multiplied by a complex weight w_m^* before being summed. Broadband beamforming consists of passing the sensor outputs through finite impulse response (FIR) filters $W_m^*(e^{j\Omega})$ and then summing the filter outputs. The broadband beamformer on the right of Figure 2.5 represents the traditional beamformer.

2.2.1 Beamforming Model

Figure 2.6 depicts a common model for the beamforming process [9]. A discrete-time environment is assumed. The output of each sensor consists of a delayed and attenuated version of the desired signal, and a noise component. In this model, the noise is viewed as an additive sound field that exists at the sensors.

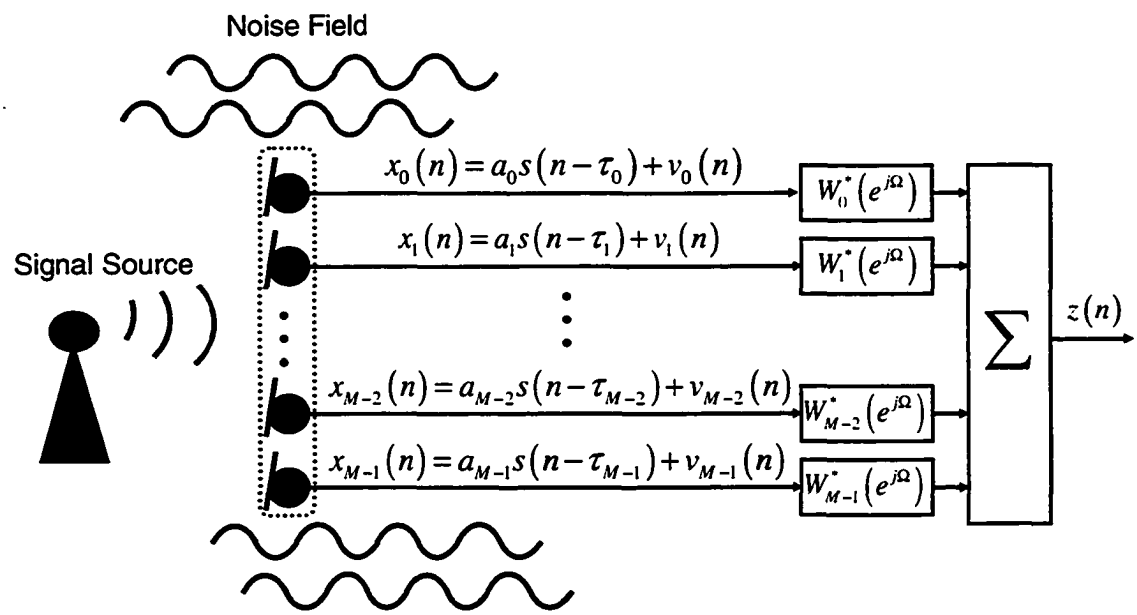

Figure 2.6. Beamforming model consisting of signal source and noise field.

Reproduced with permission of the copyright owner. Further reproduction prohibited without permission.

The M-element array output may be written in vector notation as:

$$\begin{bmatrix} x_0(n) \\ x_1(n) \\ \vdots \\ x_{M-1}(n) \end{bmatrix} = \begin{bmatrix} a_0 s(n-\tau_0) \\ a_1 s(n-\tau_1) \\ \vdots \\ a_{M-1} s(n-\tau_{M-1}) \end{bmatrix} + \begin{bmatrix} v_0(n) \\ v_1(n) \\ \vdots \\ v_{M-1}(n) \end{bmatrix} \tag{2.7}$$

or conveniently as:

$$\boldsymbol{x}(n) = \boldsymbol{a}\, s(n-\boldsymbol{\tau}) + \boldsymbol{v}(n) \tag{2.8}$$

Taking the Fourier transform of (2.8) leads to:

$$\boldsymbol{X}\left(e^{j\Omega}\right) = S\left(e^{j\Omega}\right)\boldsymbol{d} + \boldsymbol{V}\left(e^{j\Omega}\right) \tag{2.9}$$

where the vector **d** models the propagation of the signal to the array in the frequency domain:

$$\boldsymbol{d}^T = \begin{bmatrix} a_0 e^{-j\Omega\tau_0} & a_1 e^{-j\Omega\tau_1} & a_2 e^{-j\Omega\tau_2} & \cdots & a_{M-1} e^{-j\Omega\tau_{M-1}} \end{bmatrix} \tag{2.10}$$

Signal sources may be classified as belonging to either the "near-field" or "far-field" of the array. The distinction here is important, as for near-field sources, the wavefront is considerably curved with respect to the array dimensions, meaning that each sensor perceives a different direction of arrival (DOA). In the case of a far-field source, the wavefront is essentially a plane wave, and thus each sensor perceives approximately the same DOA. Figure 2.7 illustrates the difference between far and near-field sources.

When the source is in the far-field of the array, and the array consists of linear, equidistant sensors with inter-sensor distance d, the propagation vector becomes:

$$\boldsymbol{d}^T = \begin{bmatrix} 1 & e^{-j\Omega f_s c^{-1} d\cos\theta} & e^{-j\Omega f_s c^{-1} 2d\cos\theta} & \cdots & e^{-j\Omega f_s c^{-1}(M-1)d\cos\theta} \end{bmatrix} \tag{2.11}$$

Reproduced with permission of the copyright owner. Further reproduction prohibited without permission.

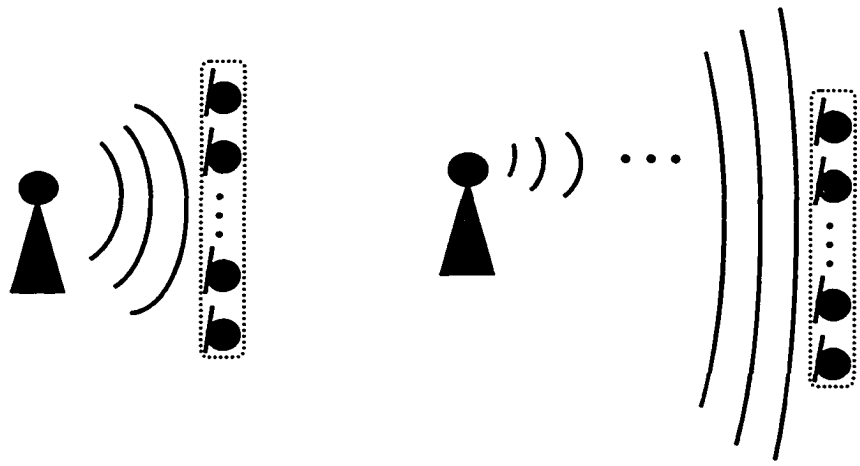

Figure 2.7. Near-field (left) and far-field (right) geometry.

where f_s is the sampling frequency, c is the speed of propagation, and θ is the DOA relative to the array axis.

The output of the beamformer is expressed as:

$$Z\left(e^{j\Omega}\right)=\sum_{m=0}^{M-1}W_m^*\left(e^{j\Omega}\right)X_m\left(e^{j\Omega}\right)=\boldsymbol{W}^H\boldsymbol{X} \tag{2.12}$$

where

$$\boldsymbol{W}=\left[W_0\left(e^{j\Omega}\right)\quad W_1^*\left(e^{j\Omega}\right)\quad\cdots\quad W_{M-1}\left(e^{j\Omega}\right)\right]^T \tag{2.13}$$

$$\boldsymbol{X}=\left[X_0\left(e^{j\Omega}\right)\quad X_1\left(e^{j\Omega}\right)\quad\cdots\quad X_{M-1}\left(e^{j\Omega}\right)\right]^T \tag{2.14}$$

and the dependency on frequency is dropped for readability[2].

2.2.2 Evaluation of Beamformers

Several performance metrics exist when it comes to the evaluation of beamformers. The *array gain* describes the improvement in SNR from sensor input to array output:

$$G=\frac{SNR_{\text{Array}}}{SNR_{\text{Sensor}}} \tag{2.15}$$

[2] From here on in, the dependence on frequency will be implied.

Reproduced with permission of the copyright owner. Further reproduction prohibited without permission.

where SNR_{Sensor} is the SNR at an arbitrary sensor, and SNR_{Array} is the SNR of the beamformer output. From the definition of the PSD and (2.12), it easily follows that the PSD of the beamformer output is given by:

$$\Phi_{ZZ} = \boldsymbol{W}^H \Phi_{XX} \boldsymbol{W} \tag{2.16}$$

where Φ_{XX} is CSD matrix of the array input:

$$\Phi_{XX} = \begin{bmatrix} \Phi_{X_0X_0} & \Phi_{X_0X_1} & \Phi_{X_0X_{M-1}} \\ \Phi_{X_1X_0} & \Phi_{X_0X_1} & \Phi_{X_1X_{M-1}} \\ \\ \Phi_{X_{M-1}X_0} & \Phi_{X_{M-1}X_0} & \Phi_{X_{M-1}X_{M-1}} \end{bmatrix} \tag{2.17}$$

and $\Phi_{X_nX_m}$ is the CSD between the n^{th} and m^{th} sensor outputs. The PSD of the array output for only the signal is then:

$$\Phi_{ZZ}\big|_{signal} = \Phi_{SS} \left| \boldsymbol{W}^H \boldsymbol{d} \right|^2 \tag{2.18}$$

where Φ_{SS} is the PSD of the desired signal. Likewise, the array output PSD for only the noise is given by:

$$\Phi_{ZZ}\big|_{\text{Noise}} = \Phi_{V_{\text{average}}V_{\text{average}}} \boldsymbol{W}^H \Phi_{VV} \boldsymbol{W} \tag{2.19}$$

where $\Phi_{V_{\text{average}}V_{\text{average}}}$ is the noise PSD averaged over the array elements, and Φ_{VV} is a normalized CSD matrix of the noise, with the normalization setting the trace of the matrix to M. Assuming a homogenous noise field, the coherence matrix Γ_{VV} already fulfills the normalization, and thus the array gain G may be written as:

$$G = \frac{\left| \boldsymbol{W}^H \boldsymbol{d} \right|^2}{\boldsymbol{W}^H \Gamma_{VV} \boldsymbol{W}} \tag{2.20}$$

Reproduced with permission of the copyright owner. Further reproduction prohibited without permission.

$$\Gamma_{VV} = \begin{bmatrix} 1 & \Gamma_{V_0V_1} & \cdots & \Gamma_{V_0V_{M-1}} \\ \Gamma_{V_1V_0} & 1 & \cdots & \Gamma_{V_1V_{M-1}} \\ \vdots & \vdots & \ddots & \vdots \\ \Gamma_{V_{M-1}V_0} & \Gamma_{V_{M-1}V_1} & \cdots & 1 \end{bmatrix} \tag{2.21}$$

where the elements of the coherence matrix are given by:

$$\Gamma_{V_nV_m} = \frac{\Phi_{V_nV_m}}{\sqrt{\Phi_{V_nV_n}\Phi_{V_mV_m}}} \tag{2.22}$$

where $\Phi_{V_nV_m}$ is the CSD between the n^{th} and m^{th} sensor outputs for *only the noise*. The array gain is most significant in applications where a noise field, as opposed to a noise source (interference) is the dominant corrupting entity. When the unwanted signal originates from a point in space, the SIR gain G_{SIR} is most appropriate:

$$G_{SIR} = \frac{\left|\boldsymbol{W}^H \boldsymbol{d}_s\right|^2}{\left|\boldsymbol{W}^H \boldsymbol{d}_i\right|^2} \tag{2.23}$$

where $\boldsymbol{d}_s$ and $\boldsymbol{d}_i$ are the propagation vectors of the signal and interference, respectively.

A related performance measure is the *beampattern*, which describes the response of the array to a complex exponential arriving at a certain DOA (described in a spherical coordinate system by the azimuth angle φ and elevation angle θ) and at a certain frequency:

$$H\left(e^{j\Omega}, \varphi, \theta\right)\Big|_{\text{dB}} = -10\log_{10}\left(\frac{\left|\boldsymbol{W}^H \boldsymbol{d}\right|^2}{\boldsymbol{W}^H \Gamma_{VV}\big|_{\text{Wavefront}} \boldsymbol{W}}\right) \tag{2.24}$$

where the coherence function of a wavefront is given by:

$$\begin{aligned} \Gamma_{V_nV_m}\Big|_{\text{Wavefront}} &= \exp\left(j\Omega\tau_{nm}\right) \\ \tau_{nm} &= \frac{f_s}{c}\left(l_{x,nm}\sin\theta\cos\varphi + l_{y,nm}\sin\theta\sin\varphi + l_{z,nm}\cos\theta\right) \end{aligned} \tag{2.25}$$

Reproduced with permission of the copyright owner. Further reproduction prohibited without permission.

where $l_{x,n\,m}$, $l_{y,n\,m}$, and $l_{z,n\,m}$ are the distances in the x, y, and z directions, respectively, between the n^{th} and m^{th} sensor. When the elements of the array are aligned to a co-ordinate axis, the beampattern function may be plotted using only a single direction argument.

The *directivity index* (DI) of a beamformer describes the ability of the array to suppress a spherically isotropic (diffuse) noise field, while preserving the desired signal. A spherically isotropic noise field is one where noise emanates from all directions with equal probability. The directivity index is simply the array gain computed with the coherence function of a diffuse noise field:

$$\mathrm{DI}\big|_{\mathrm{dB}} = 10\log_{10}\left(\frac{\left|\boldsymbol{W}^{H}\boldsymbol{d}\right|^{2}}{\boldsymbol{W}^{H}\boldsymbol{\Gamma}_{VV}\big|_{\mathrm{Diffuse}}\boldsymbol{W}}\right) \tag{2.26}$$

where the elements of the coherence matrix are given by:

$$\Gamma_{V_nV_m}\big|_{\mathrm{Diffuse}} = \frac{\sin\left(\Omega f_s l_{n\,m} c^{-1}\right)}{\Omega f_s l_{n\,m} c^{-1}} \tag{2.27}$$

and $l_{n\,m}$ is the distance between the n^{th} and m^{th} sensor.

Finally, the *white noise gain* (WNG) of an array is the ability of the array to suppress spatially uncorrelated noise at the sensors:

$$\mathrm{WNG}\big|_{\mathrm{dB}} = 10\log_{10}\left(\frac{\left|\boldsymbol{W}^{H}\boldsymbol{d}\right|^{2}}{\boldsymbol{W}^{H}\boldsymbol{\Gamma}_{VV}\big|_{\mathrm{White}}\boldsymbol{W}}\right) = 10\log_{10}\left(\frac{\left|\boldsymbol{W}^{H}\boldsymbol{d}\right|^{2}}{\boldsymbol{W}^{H}\boldsymbol{W}}\right) \tag{2.28}$$

This follows from the fact that the coherence matrix of a white noise field is simply the identity matrix.

Beamformers may be classified as being either "fixed" or "adaptive." In a fixed beamformer, the weights of (2.13) are chosen independently of the characteristics of the

Reproduced with permission of the copyright owner. Further reproduction prohibited without permission.

signals and noise. Conversely, the weights in an adaptive beamformer are chosen to optimize the response of the array such that the noise and interference have a minimal effect.

2.2.3 Fixed Beamforming

In a fixed beamformer, the weights are chosen such that the beamformer response best approximates a desired response [7]. Two common fixed beamformers are the delay-and-sum beamformer (DSB) and filter-and-sum beamformer (FSB).

Delay-and-sum beamforming is the oldest and simplest beamforming algorithm. It exploits the fact that there is naturally a direct relationship between DOA and inter-sensor delay. The algorithm applies variable delays to each sensor, in order to time-align the signal replicas, thus yielding a coherent summation of signal originating from some desired DOA. A DSB, shown on the left of Figure 2.8, consists of an array of sensors, whose outputs are individually delayed and weighted before being summed to form the beamformer output. The delays $\{\Delta_m\}\big|_{m=0}^{M-1}$ "steer" the beamformer to a particular DOA, while the scalar weights $\{w_m\}\big|_{m=0}^{M-1}$ shape the beam. In a FSB, shown on the right of Figure 2.8, linear filters precede the delay-and-sum operation. The transfer functions of the filters are usually identical, and correspond to the range of frequencies that contain the signal of interest. In the figure, these transfer functions have been denoted by H to distinguish them from the transfer functions of the FIR filters that comprise the traditional beamformer of Figure 2.5. Notice that a DSB with uniform weights may be conveniently expressed in the canonical form of (2.13) as:

$$\boldsymbol{W}\big|_{\text{DSB}} = \frac{1}{M}\boldsymbol{d} \tag{2.29}$$

Reproduced with permission of the copyright owner. Further reproduction prohibited without permission.

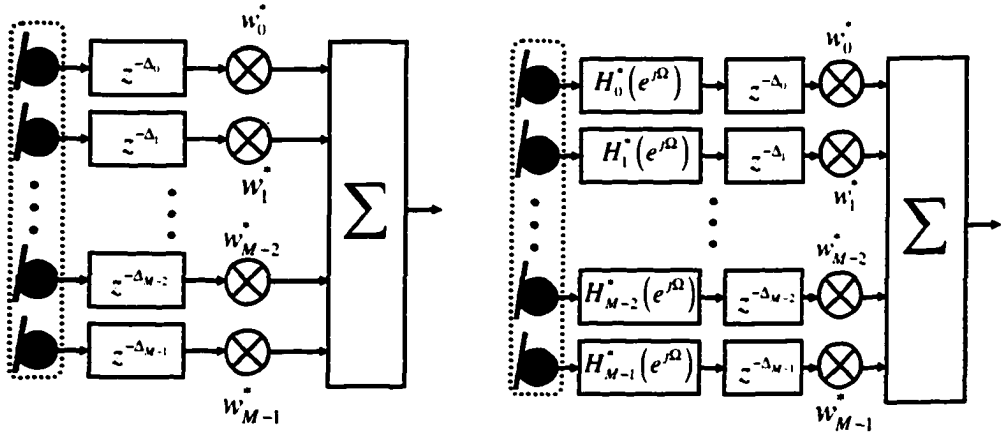

Figure 2.8. Fixed beamforming: Delay-and-sum beamformer (left), Filter-and-sum beamformer (right).

2.2.4 Adaptive Beamforming

The design of optimal beamformers consists of selecting the weights of (2.13) in such a manner that the effects of noise and interference are minimized. One way of doing this is to minimize the output power of the array, while keeping the response of the array to the desired signal at unity:

$$\min_{\boldsymbol{W}} \boldsymbol{W}^H \boldsymbol{\Phi}_{XX} \boldsymbol{W} \text{ subject to } \boldsymbol{W}^H \boldsymbol{d} = 1 \tag{2.30}$$

This constrained optimization is one example of the general LCMV beamforming [15] problem. The solution to this constrained optimization is known as the Minimum-Variance, Distortionless Response (MVDR) beamformer [16], and assuming a homogenous noise field, is given by [15,17]:

$$\boldsymbol{W} = \frac{\boldsymbol{\Gamma}_{VV}^{-1} \boldsymbol{d}}{\boldsymbol{d}^H \boldsymbol{\Gamma}_{VV}^{-1} \boldsymbol{d}} \tag{2.31}$$

It has also been assumed that there is no discrepancy between the DOA of the desired signal, and the "look-direction" of the array. The look-direction is the term given to the

Reproduced with permission of the copyright owner. Further reproduction prohibited without permission.

DOA to which the array is steered to, or focused on. From (2.31), to design an optimal array, one must have knowledge of the coherence matrix of the noise field, and then substitute this coherence matrix into (2.31) to obtain the optimal weights. The resulting beamformer is in the form of Figure 2.5. For example, when the coherence function of a diffuse noise field is used in (2.31), the resulting weights comprise the so-called "superdirective" beamformer (SDB), as it is the beamformer that maximizes the directivity. When the coherence function of a white noise field is used, the resulting weights are simply that of the DSB. In other words, the DSB is the optimal beamformer for maximizing the WNG.

Notice that in a broadband optimal beamformer, the weight selection must be performed at every frequency. The matrix inversion operation is computationally expensive, and if the statistics of the noise change, the beamformer will no longer be optimal. Therefore, an alternative implementation of the MVDR beamformer was proposed by Griffiths and Jim [18], and is outlined below.

If one time-aligns the received signal as shown in Figure 2.9, the optimal weight solution of the constrained optimization becomes:

$$\boldsymbol{W}\big|_{\text{time aligned}} = \frac{\mathbf{1}^T \left(\boldsymbol{\Gamma}_{vv}^{'}\right)^{-1}}{\mathbf{1}^T \left(\boldsymbol{\Gamma}_{vv}^{'}\right)^{-1} \mathbf{1}} \tag{2.32}$$

where $\boldsymbol{\Gamma}_{vv}^{'}$ is the coherence matrix of the delay-compensated noise field. More importantly, the solution of (2.32) can be decomposed into two orthogonal parts, one of which fulfills the linear constraint, while the other performs unconstrained optimization to minimize the output power. This is shown schematically in Figure 2.10.

Reproduced with permission of the copyright owner. Further reproduction prohibited without permission.

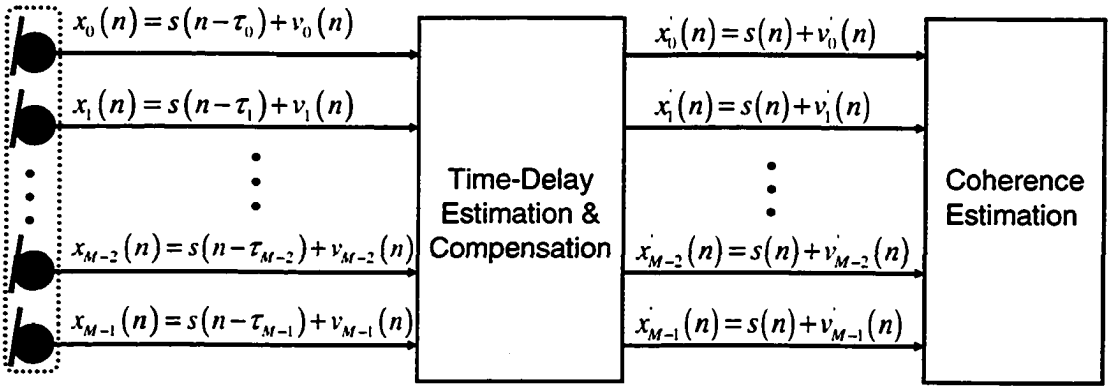

Figure 2.9. Time-aligned signal model.

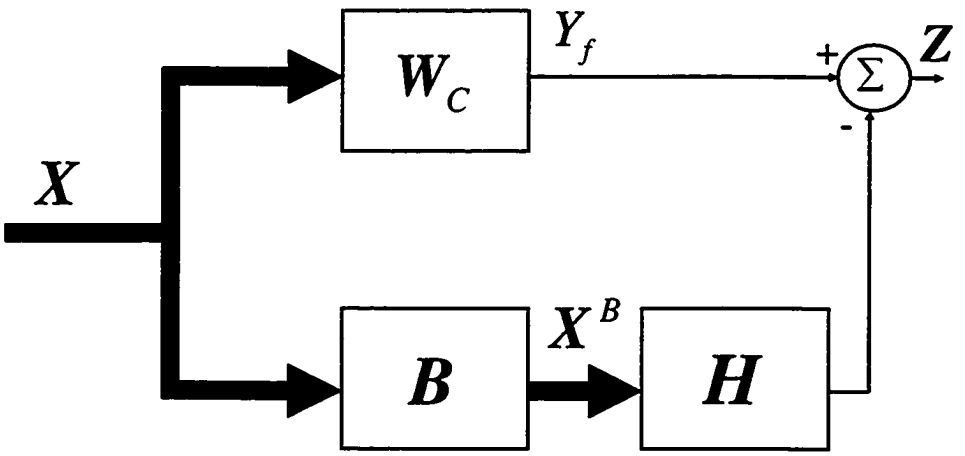

Figure 2.10. Decomposition of optimal weight selection.

The vector W^C (upper branch) represents the linear constraint, while the matrix B, termed the "blocking matrix", projects the time-aligned input vector X onto a noise-only subspace. The blocking matrix removes the desired signal from the observation vector. The noise-only output vector X^B is multiplied by the unconstrained optimal vector H and then subtracted from the output of the upper branch. It has been shown that this

Reproduced with permission of the copyright owner. Further reproduction prohibited without permission.

structure is equivalent to the optimal MVDR beamformer in canonical form [18-20], as long as:

$$\boldsymbol{W}_C = \frac{1}{M}\mathbf{1} \tag{2.33}$$

and the blocking matrix obeys the following properties:

- The size of the matrix must be *(M-1)* by *M*.
- The sum of the values in any row is zero.
- The rank of the matrix is *M-1*.

An example of a valid blocking matrix is the Griffiths-Jim matrix:

$$\boldsymbol{B} = \begin{bmatrix} 1 & -1 & 0 & 0 & \cdots & 0 \\ 0 & 1 & -1 & 0 & \vdots & 0 \\ \vdots & \ddots & \ddots & \ddots & \ddots & \vdots \\ 0 & \cdots & 0 & 0 & 1 & -1 \end{bmatrix} \tag{2.34}$$

The Griffiths-Jim matrix is a simple, fixed implementation of the blocking matrix. Multiple (more than two) channels may be subtracted to form each output, yielding a more elaborate signal blockage. The blocking matrix may be adaptive, such that reflections of the desired signal are also cancelled. Furthermore, the time-aligning that precedes the blocking matrix may also be updated adaptively to take into account movement of the desired signal source.

Since the lower branch of the decomposition performs an unconstrained optimization, a multiple-reference ANC may be employed to perform this task adaptively. These ideas form the basis for the GSC [18], which is shown in Figure 2.11. The delay L in the desired signal beamformer output is introduced to ensure causality in the adaptive transfer functions. The multiple-reference ANC is able to track changes in

Reproduced with permission of the copyright owner. Further reproduction prohibited without permission.

the statistics of the noise field. The Wiener solution of the multiple-reference canceller is given by [21]:

$$\boldsymbol{H} = \boldsymbol{\Phi}_{X^B X^B}^{-1} \boldsymbol{\Phi}_{X^B Y_f} \tag{2.35}$$

where $\boldsymbol{\Phi}_{X^B X^B}$ is the CSD matrix of the blocking matrix outputs, and $\boldsymbol{\Phi}_{X^B Y_f}$ is the CSD vector between the blocking matrix outputs and the DSB output (primary input of the multiple-reference noise canceller).

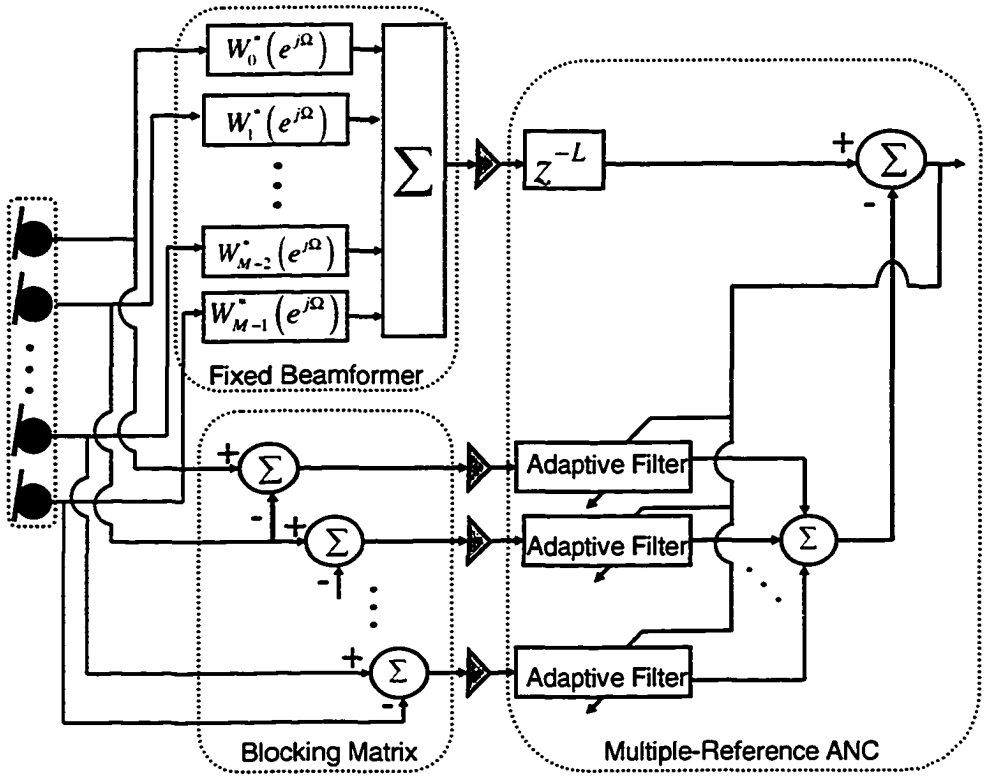

Figure 2.11. Generalized Sidelobe Canceller.

In Figure 2.11, it has been assumed that the signal source is located at broadside (perpendicular to the array axis), and thus delays are not needed after the sensors. Generally, delays are implemented at the outputs of the sensors to time-align the received

Reproduced with permission of the copyright owner. Further reproduction prohibited without permission.

signals with respect to the location of the signal source. The subtractions of the blocking matrix then remove any signal components for all array configurations.

Assuming a homogenous noise field, the optimal coefficients of the multiple-reference ANC may be computed using [9]:

$$\boldsymbol{H} = \left(\boldsymbol{B}\boldsymbol{\Gamma}_{vv}^{'}\boldsymbol{B}^{H}\right)^{-1}\boldsymbol{B}\boldsymbol{\Gamma}_{vv}^{'}\boldsymbol{W}^{C} \tag{2.36}$$

When the adaptive filters of the multiple-reference ANC are replaced by their corresponding Wiener solutions (i.e., after convergence), the GSC is equivalent to the beamformer of (2.31).

The GSC suffers from the desired signal cancellation phenomenon. Theoretically, the blocking matrix forms a deep null in the direction of the desired signal, and thus minimizes the SIR at the reference ANC inputs. However, the blocking matrix is sensitive to both steering errors and reverberation [9]. For example, reflections arriving at a direction other than the look-direction are undesirably passed. As a result, desired signal components leak through the blocking matrix to the ANC, and drive the adaptive filter taps to cancel the desired signal.

A number of researchers have tackled the robustness problems of the GSC. A notable approach is that of constraining the growth of the coefficients [16] in the multiple-input canceller, thus throttling the desired-signal cancellation phenomenon. Implementing a "leaky" adaptive algorithm [22] achieves a similar effect, although both of these approaches come at the cost of reduced directivity. A second general approach to the problem is that of dynamically adapting the steering direction [23-25]. Hoshuyama [26] combines several approaches, including a simple adaptation control module, into an elaborate GSC implementation that is insensitive to a certain amount of steering error.

Reproduced with permission of the copyright owner. Further reproduction prohibited without permission.

Notice that all of these approaches involve increasing the complexity of the GSC, which in its purest form is already computationally expensive. Furthermore, very few researchers have attempted to move away from the general blocking matrix approach to sidelobe cancellation, which is at the root of the robustness problems of the GSC.

Zheng, Goubran, and El-Tanany [27] propose a novel approach to adaptive beamforming, in the form of a bank of FSBs cascaded with a multiple-reference ANC. A switching module determines which beamformer output serves as the primary input, and feeds the others to the reference noise canceller inputs. The reference beamformers are steered to the various noise DOAs present, while the primary beamformer is steered towards the desired signal. The structure is shown in Figure 2.12.

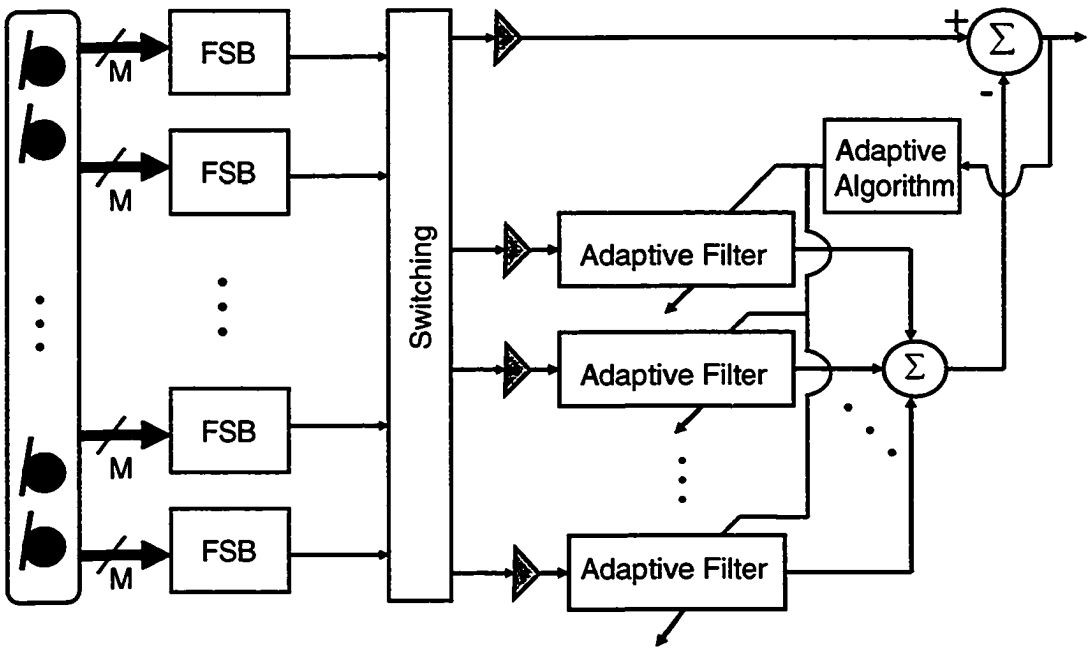

Figure 2.12. Novel approach to adaptive beamforming.

Reproduced with permission of the copyright owner. Further reproduction prohibited without permission.

Recently, a new technique for adaptive beamforming has been proposed in the form of the Generalized Singular Value Decomposition (GSVD) beamformer [28-32]. The GSVD approach does not require knowledge of the desired signal DOA or microphone location, and is thus a more robust technique than the GSC [9]. Combination of the GSVD beamformer with an ANC leads to substantial SNR gains. However, the high computational complexity of GSVD algorithms pose problems for operation in real-time [9].

Reproduced with permission of the copyright owner. Further reproduction prohibited without permission.

Chapter 3

Simulation Environment and Experimental Setup

3.1 Simulation Environment

The MATLAB© software is employed to carry out the simulations from which results in this work are obtained. An anechoic and lossless signal environment is modeled by omitting attenuation and reflection of propagating signals. Continuous-time signals are emulated in MATLAB's discrete-time environment by sampling at a high rate of $f_a = 80$ kHz. The propagation of these analog signals to the array is modeled as far-field, plane-wave propagation:

$$y_m(n) = s(n - n_m) \tag{3.1}$$

where y_m denotes the output of the m^{th} sensor, s is the source signal, and n_m denotes the propagation delay, from the source to the m^{th} array element:

$$n_m = \left[\frac{f_a (m-1) d \cos\theta}{c} \right] \tag{3.2}$$

where θ is the DOA with respect to the array axis, d is the inter-element spacing of the array, c is the speed of propagation, and $[\bullet]$ denotes the integer rounding operation. The analog-to-digital (A-D) conversion is then emulated in the digital domain as a downsampling operation, from $f_a = 80$ kHz to $f_s = 8$ kHz, where f_s is the sampling frequency at which the signal processing is performed. The downsampling operation includes a low-pass filtering operation with a cut-off frequency of $0.8 \cdot \frac{f_a}{2} \cdot \frac{1}{D}$, where:

Reproduced with permission of the copyright owner. Further reproduction prohibited without permission.

$$D = \frac{f_a}{f_s} = 10 \tag{3.3}$$

and is implemented in MATLAB with the *decimate* function. Note that the propagation of signals from source to array cannot be simulated at the sampling frequency, due to the poor resolution that would result. Simulating at a high frequency ensures a high spatial resolution, meaning that two nearby sources may be discriminated by the array.

The simulations employ a linear array with $M = 4$ uniformly spaced elements with an inter-element distance of $d = 0.046\,\text{m}$. The microphone elements are assumed to be omni directional and calibrated with unity gain. All signal sources are modeled as belonging to the far-field. The desired signal source is located at broadside, while the interfering source impinges on the array at an angle of 45° relative to the array axis. In all cases, the signal is uncorrelated with the interference. Table 3.1 lists the origin of the signals used in the simulations.

Table 3.1. Origin of signals used in simulations.

Signal	Origin
White noise signal	MATLAB, *randn* function
Male speech signal	TIMIT database: TEST\DR1\MDAB0\sa1.raw
Female speech signal	TIMIT database: TEST\DR1\FAKS0\sa1.raw
Uncorrelated white noise field at sensors	MATLAB, *randn* function

White noise is added at the sensors to model self-noise. This noise is obviously uncorrelated with the signals, and the signal-to-uncorrelated-noise ratio (SUNR) is 20 dB. The output of each sensor is filtered to the 300 – 3700 Hz range, using the MATLAB functions *fir1* to obtain the coefficients, and then *filter* to perform the FIR filtering.

Reproduced with permission of the copyright owner. Further reproduction prohibited without permission.

The *delay-and-sum beamforming* is performed with full knowledge of the propagating signal's DOA, such that the implemented delays are given by:

$$\Delta_m = -\left[\frac{f_s(m-1)d\cos\theta}{c}\right] \tag{3.4}$$

Notice that the delays are rounded to the nearest 8 kHz sample, and thus the beam-steering is not ideal.

The Normalized-Least-Mean-Square (NLMS) algorithm with a step-size of $\alpha = 0.1$ is chosen as the adaptive algorithm, with the adaptive filters consisting of 100 taps each. This high value is purposely chosen such that under-modeling does not occur. A delay of $L = 50$ samples is introduced into the desired signal beamformer output in order to ensure that the transfer functions between primary and reference noise canceller inputs are causal. It is well-known that the value of L does not affect the SNR at noise canceller output, as long as it is within a broad optimal range [6].

The simulation results reflect the assumption that the adaptation is performed in the absence of the desired signal. Furthermore, the results given are post-convergence, meaning that the optimal Wiener filters are in place prior to evaluation.

3.2 Experimental Setup

The experiments are performed in a large office-room, whose layout is shown in Figure 3.1. The room dimensions are: 11 m by 9.5 m by 3 m. The data acquisition unit consists of a circular, sector-based, 6-element microphone array, a pre-amplifier, a multi-channel computer sound card, and recording software. The sound sources are ordinary personal computer speakers. The sampling rate of the sound card is chosen to be 8 kHz, with a 16-

Reproduced with permission of the copyright owner. Further reproduction prohibited without permission.

bit A-D conversion. The apparatus is shown in Figure 3.2. The specifications of the data acquisition unit are given in Table 3.2.

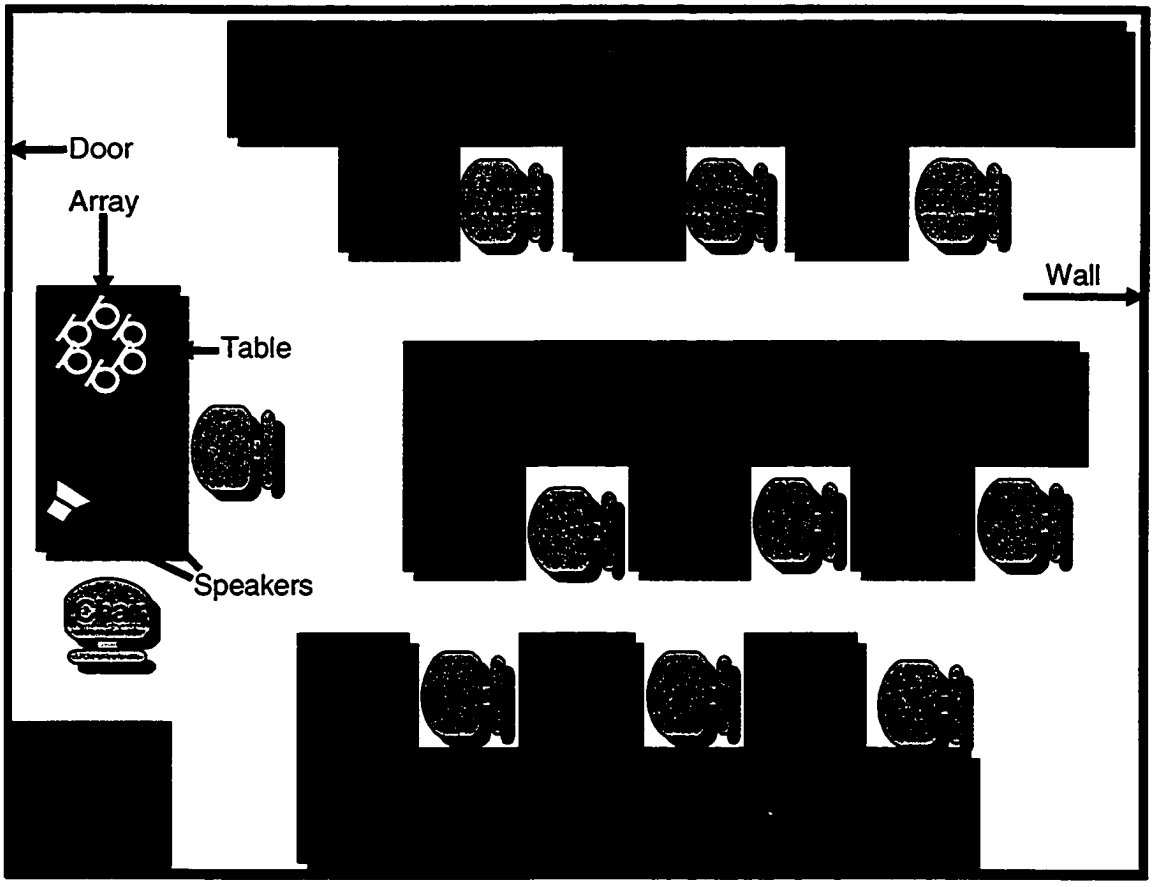

Figure 3.1. Layout of experiment room.

Table 3.2. Specifications of data acquisition unit.

Component	Specifications
Microphone array	6-element, sector-based, circular array with 10 cm diameter
Multi-channel sound card	M-Audio Delta 1010
Recording software	Adobe Audition, version 7.0
Personal computer	Dell Dimension DIM4600, Pentium 4, CPU 2.80 GHz
Audio playback software	Windows Media Player, version 9.00.003250
PC Loudspeaker	Harman/Kardon Multimedia Speaker System

Reproduced with permission of the copyright owner. Further reproduction prohibited without permission.

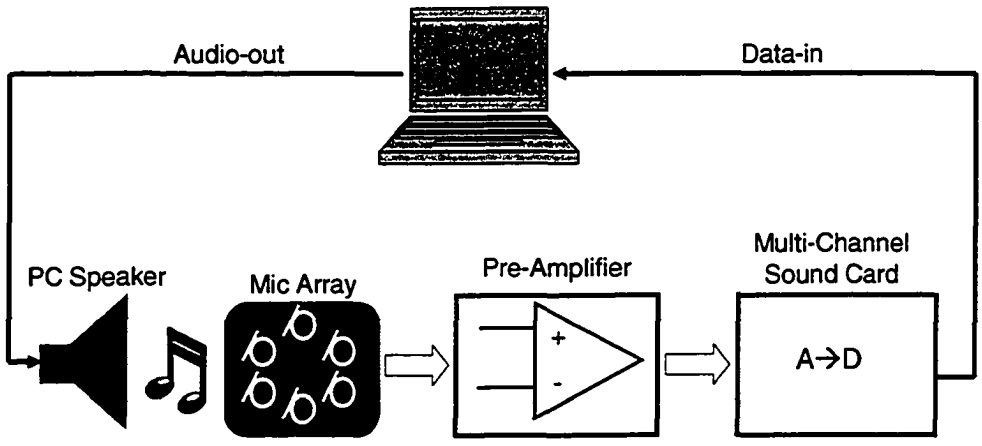

Figure 3.2. Multi-channel recording apparatus.

Throughout the experiment, the sound sources and microphone array rest on a wooden table. The microphone array is not calibrated. Both desired and interfering signals are chosen to be independent realizations of a band-limited (300 – 3700 Hz) white Gaussian process. The MATLAB function *randn* generates the unfiltered white noise sequence, and the functions *fir1* and *filter* performed the necessary band-pass filtering. This sequence is then converted into an audio track via the MATLAB *wavwrite* function, and outputted to the speaker by Windows Media Player.

The subsequent signal processing is performed in the MATLAB environment. In order to compute the optimal delays to perform *delay-and-sum beamforming* at the front-end, the Generalized Correlation Method [33] for time delay estimation with no frequency weighting is employed. To implement this method, the MATLAB function *xcorr* (with the normalized option 'on') is utilized. A reference sensor is chosen, and the outputs of the other five sensors are individually aligned to the output of the reference sensor. For each sensor output $y_m(n)$, the optimal delay for that sensor is calculated as:

Reproduced with permission of the copyright owner. Further reproduction prohibited without permission.

$$\Delta_m = \max_{\Delta_m} \left(\sum_{n=0}^{N-\Delta_m-1} y_m(n+\Delta_m)\, y^*_{\text{reference}}(n) \right) \tag{3.5}$$

where N is the length of the time series and $y_{\text{reference}}(n)$ is the output of the reference sensor. The reference sensor is chosen to be the microphone with the largest propagation delay.

A delay of $L=100$ samples is implemented at the desired signal beamformer output. The NLMS algorithm with a step-size of $\alpha=0.1$ is employed, with the adaptive filters having lengths of 200 taps. Longer filters have been used (as compared to that in the simulation model) to model reflected components that have a long delay. Experimental impulse responses are generally longer than anechoic impulse responses. The adaptation is performed with only the interference source playing.

Reproduced with permission of the copyright owner. Further reproduction prohibited without permission.

Chapter 4

Decoupled Beamforming and Adaptive Noise Cancellation

Beamformers and noise cancellers have a common goal: To enhance the desired signal, while suppressing the noise and interference. The drawbacks of noise cancellers are the need to install reference sensor(s) in the vicinity of the noise source(s), and the possibility of the desired signal leaking into the reference sensor(s). The SNR gains provided by stand-alone fixed beamformers are insufficient. In particular, the sidelobe levels of fixed beamformers are undesirably high. The integration of a beamforming front-end into the ANC process resolves all of these drawbacks: The ANC now has an intelligent front-end that removes the need for placing secondary sensors near the noise sources, and performs beam steering to distinguish the signal from the interference. Moreover, the sidelobe levels of the beamformer are reduced by cascading with the noise canceller.

The terminology of signal enhancement may sometimes be confusing: In this chapter, "interference" refers to signal sources that one is trying to suppress. "Noise" refers to unwanted, random sound fields that exist in the environment, particularly at the sensors.

4.1 Decoupled Beamformer-Noise Canceller Model

Figure 4.1 exhibits the decoupled BF-NC model. The front-end is composed of a bank of beamformers (denoted in the figure by 'BF') which may belong to any class of spatial filters: delay-and-sum, filter-and sum, constant-directivity [34], or super-directivity [35].

Reproduced with permission of the copyright owner. Further reproduction prohibited without permission.

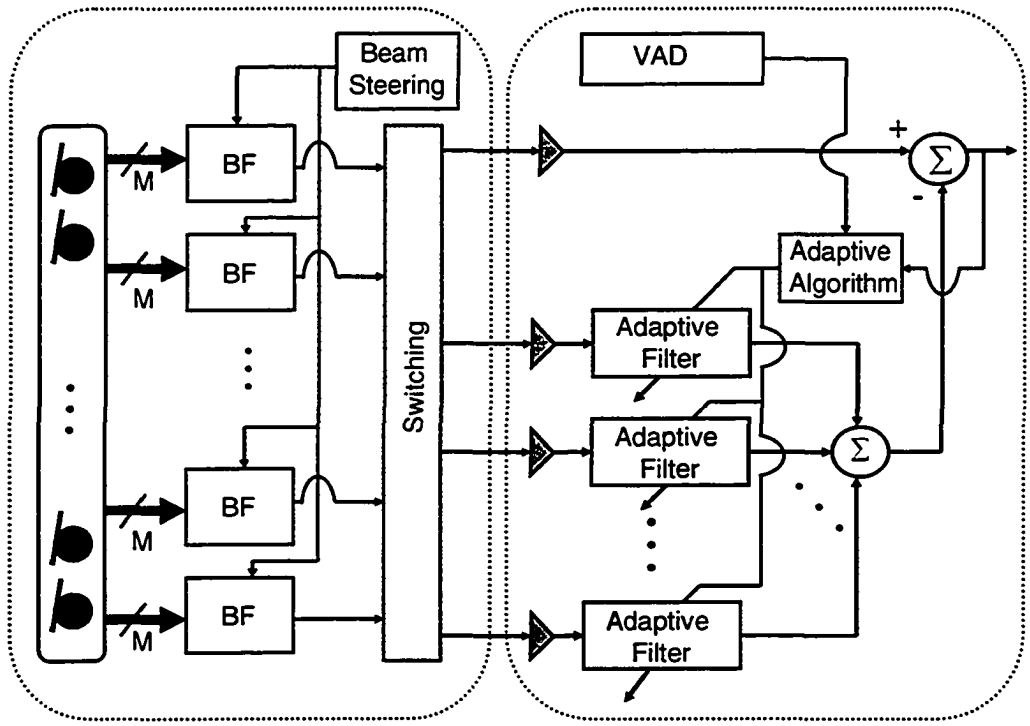

Figure 4.1. Decoupled beamforming-noise cancellation design.

The steering of these beamformers is performed by an intelligent beam-steering module, which will operate as a "look-up" table. The module scans the environment, determines the locations of the signal and interference sources, and then feeds the appropriate coefficients to the beamformers. It is important to understand that the design of these beamformers is performed independently of the noise canceller part of the system. The beamformers provide signal references that are then fed to the switching module, which then appropriately directs these references to the noise canceller. The desired signal reference is fed to the primary noise canceller input. Interfering signal references are connected to the reference noise canceller inputs. The noise cancellers provide added suppression at the DOAs that correspond to significant interference power.

The decoupled BF-NC scheme is a collection of independently-operated modules. The emphasis is no longer on optimizing one central structure, as in the MVDR

Reproduced with permission of the copyright owner. Further reproduction prohibited without permission.

beamformer. Rather, each individual component is optimized in isolation, and the components are combined accordingly. There is no restriction on the class of beamformers to be employed at the front-end. The multiple-reference noise canceller may be added to any configuration of spatial filters. The decoupled BF-NC paradigm varies significantly from that of the coupled GSC structure. Beamformers with more "robust" beams are implemented at the front-end, while significant attenuation of interfering sources is provided by the back-end noise cancellers. It is expected that decoupled BF-NC structures will prove beneficial in real environments that lead to performance degradations in conventional adaptive beamformers such as the GSC.

Blocking matrix-based adaptive beamformers are very limited in terms of designer degrees of freedom. In order to meet the conditions for equivalence with the MVDR beamformer, the desired signal beamformer must be delay-and-sum, while the coefficients of the blocking matrix are further restricted. The decoupled BF-NC model allows the designer to independently select the beamformers of the front-end, and then simply cascade them with the multiple-reference ANC. These beamformers may be designed to maximize the SIR at the primary noise canceller input, while minimizing the SIR at the reference noise canceller inputs. The GSC appears to be a subset of the more general decoupled BF-NC paradigm: When the reference beamformers are chosen to block the desired signal and the primary beamformer is a DSB, the GSC structure results. However, many other possibilities for the choice of the beamformers exist. From Widrow's assertions [6], it appears as though the design of the reference beamformers is most important in determining overall performance.

Reproduced with permission of the copyright owner. Further reproduction prohibited without permission.

The selection of beamformers should also take into account the effect of uncorrelated noise fields at the sensors. An ANC is not able to remove uncorrelated noise from its primary input, and thus, the beamformers at the front-end should minimize the uncorrelated noise level propagated to the ANC. Notice that a multiple-reference ANC adds the uncorrelated noise that accumulates in its individual reference inputs. Furthermore, the subtraction of adjacent channels, as is the case in Griffiths-Jim beamformers, is not optimal for suppressing white noise. A DSB is the ideal beamformer for suppressing white noise.

Combined BF-NC structures may be divided into two categories: The decoupled structures presented above, and coupled structures employing a blocking matrix [16]. A blocking matrix is a multiple-input, multiple-output beamformer designed to block the desired signal. The presence of multiple outputs necessitates the need for a multiple reference noise canceller. Throughout this chapter, a sample decoupled BF-NC structure is compared to a sample coupled structure. Moreover, it is assumed that only a single interference source exists. It should also be noted that in this work, "blocking matrix" implies "fixed blocking matrix." Adaptive blocking matrices are not considered in the comparisons.

4.2 Decoupled Beamformer-Noise Canceller Structures

Assuming a single source of interference, a multiple-reference noise canceller is not needed in the decoupled case, and thus the model of Figure 4.1 may be simplified to include only two beamformers and one noise canceller, as shown in Figure 4.2. The auxiliary modules have been omitted from the figure. Furthermore, the adaptive filter has been labeled with $W_{NC}^{*}\left(e^{j\Omega}\right)$, which denotes the transfer function of the Wiener solution.

Reproduced with permission of the copyright owner. Further reproduction prohibited without permission.

Each beamformer consists of a bank of FIR filters. The beamformer for the desired signal is denoted by:

$$\boldsymbol{W}_d\left(e^{j\Omega}\right)=\left[W_{d,0}\left(e^{j\Omega}\right)\;\; W_{d,1}\left(e^{j\Omega}\right)\;\; \cdots\;\; W_{d,M-1}\left(e^{j\Omega}\right)\right]^T \tag{4.1}$$

Likewise, the beamformer for the interfering signal, whose output feeds the reference noise canceller input, is:

$$\boldsymbol{W}_r\left(e^{j\Omega}\right)=\left[W_{r,0}\left(e^{j\Omega}\right)\;\; W_{r,1}\left(e^{j\Omega}\right)\;\; \cdots\;\; W_{r,M-1}\left(e^{j\Omega}\right)\right]^T \tag{4.2}$$

Letting the vector $\boldsymbol{X}\left(e^{j\Omega}\right)=\left[X_0\left(e^{j\Omega}\right)\;\; X_1\left(e^{j\Omega}\right)\;\; \cdots\;\; X_{M-1}\left(e^{j\Omega}\right)\right]^T$ denote the input to the array, and suppressing the dependence on frequency for brevity, it easily follows that the output of the BF-NC structure is:

$$Z=\boldsymbol{W}_d^H\boldsymbol{X}-\boldsymbol{W}_{NC}^*\boldsymbol{W}_r^H\boldsymbol{X}=\left(\boldsymbol{W}_d^H-\boldsymbol{W}_{NC}^*\boldsymbol{W}_r^H\right)X \tag{4.3}$$

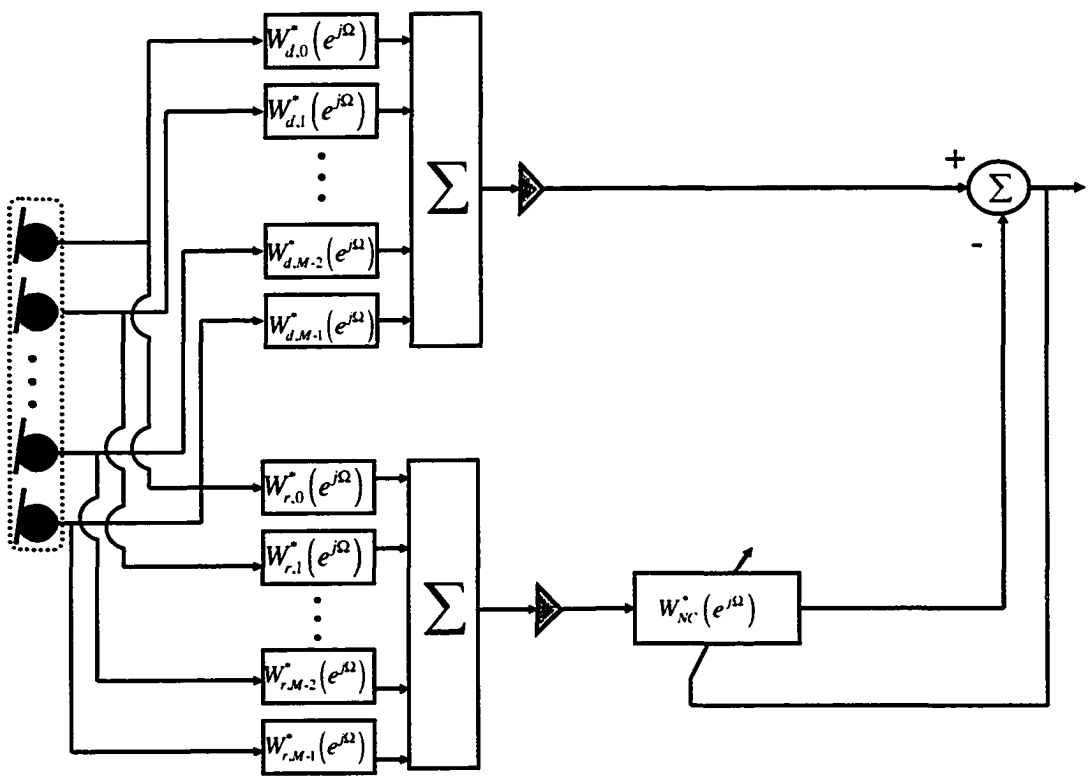

Figure 4.2. Decoupled beamformer-noise canceller structure with single interference source.

Reproduced with permission of the copyright owner. Further reproduction prohibited without permission.

The PSD of the output signal is then:

$$\Phi_{ZZ} = \left(W_d^H - W_{NC}^* W_r^H\right)\Phi_{XX}\left(W_d - W_{NC}W_r\right) \tag{4.4}$$

where Φ_{XX} is the CSD matrix of the array input. From (2.1), the Wiener solution of the noise canceller is given by:

$$W_{NC} = \frac{W_r^H \Phi_{XX}\big|_{\text{adaptation}} W_d}{W_r^H \Phi_{XX}\big|_{\text{adaptation}} W_r} \tag{4.5}$$

where $\Phi_{XX}\big|_{\text{adaptation}}$ is the CSD matrix of the array input during the adaptation period. From (4.4) and (4.5), it is evident that the decoupled BF-NC structure is effectively an adaptive beamformer with weights given by:

$$W_{\text{effective}} = W_d - \frac{W_r^H \Phi_{XX}\big|_{\text{adaptation}} W_d}{W_r^H \Phi_{XX}\big|_{\text{adaptation}} W_r} W_r \tag{4.6}$$

Therefore, the structure of Figure 4.2 may be implemented in the canonical form of Figure 2.5. The notation of (4.6) greatly simplifies the evaluation of combined BF-NC structures. For example, the WNG of the BF-NC structure is:

$$\text{WNG}_{\text{BF-NC}} = \frac{\left|W_{\text{effective}}^H d_s\right|^2}{W_{\text{effective}}^H W_{\text{effective}}} \tag{4.7}$$

where d_s is the propagation vector of the signal source to the array. Likewise, the directivity is given by:

$$\text{DI}_{\text{BF-NC}} = \frac{\left|W_{\text{effective}}^H d_s\right|^2}{W_{\text{effective}}^H \Gamma_{VV}\big|_{\text{Diffuse}} W_{\text{effective}}^H} \tag{4.8}$$

where $\Gamma_{VV}\big|_{\text{Diffuse}}$ is the coherence matrix of a diffuse noise field. The SIR gain of the BF-NC may be computed using:

Reproduced with permission of the copyright owner. Further reproduction prohibited without permission.

$$G_{\text{BF-NC}}^{\text{SIR}} = \frac{W_{\text{effective}}^{H} \Phi_{XX}|_{\text{Signal}} W_{\text{effective}}}{W_{\text{effective}}^{H} \Phi_{XX}|_{\text{Interference}} W_{\text{effective}}} \tag{4.9}$$

A simple decoupled BF-NC structure with a single noise canceller is presented in [10], and shown in Figure 4.3.

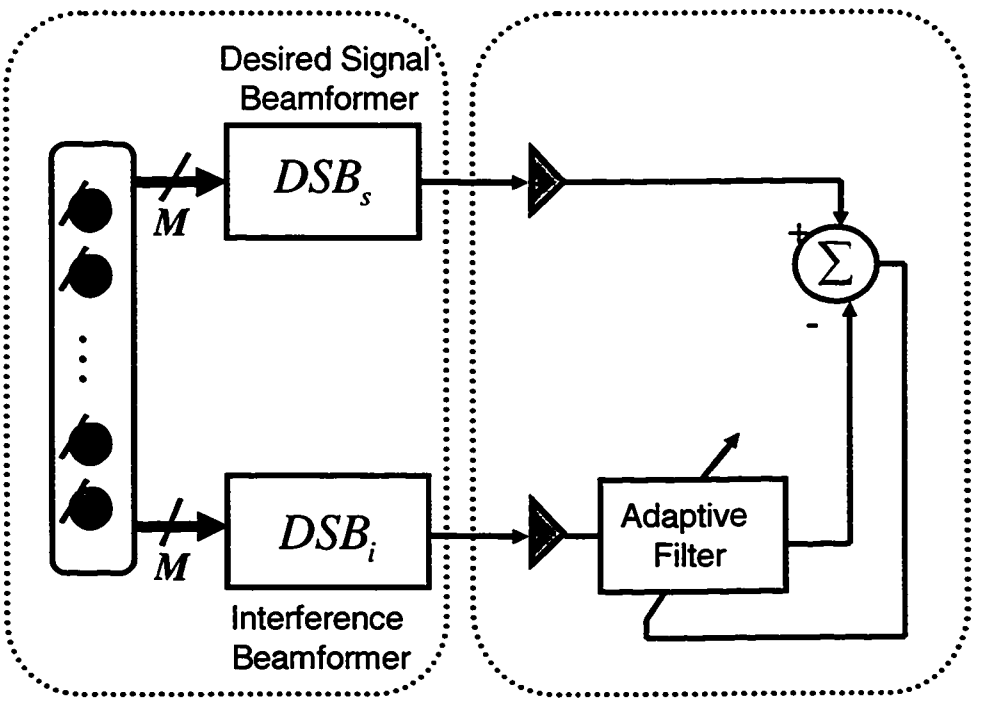

Figure 4.3. Simple decoupled beamformer-noise canceller structure with two delay-and-sum beamformers and one noise canceller.

Using the model of Figure 4.2, the structure is defined as:

$$W_d = \frac{1}{M} d_s \tag{4.10}$$

$$W_r = \frac{1}{M} d_i \tag{4.11}$$

Reproduced with permission of the copyright owner. Further reproduction prohibited without permission.

where $\boldsymbol{d}_s$ and $\boldsymbol{d}_i$ are the propagation vectors of the signal and interference, respectively. In other words, the upper beamformer is a DSB steered to the signal source, while the lower beamformer is a DSB steered to the interference. This is shown in the figure. Using (4.5), and assuming that the adaptation is performed with only the interference source active, the Wiener solution of this structure is easily found to be:

$$W_{NC} = \frac{1}{M}\boldsymbol{d}_i^H \boldsymbol{d}_s \tag{4.12}$$

Therefore, for this structure,

$$\boldsymbol{W}_{\text{effective}} = \frac{1}{M}\boldsymbol{d}_s - \frac{1}{M^2}\boldsymbol{d}_i^H \boldsymbol{d}_s \boldsymbol{d}_i \tag{4.13}$$

The magnitude and phase responses of the transfer function of (4.12) are shown in Figures 4.4 and 4.5, respectively. A linear array with $M = 4$ equidistant sensors with an inter-sensor spacing of $d = 0.046$ m is assumed to generate the plots. A white noise source with a DOA of 45° relative to the array axis is active during the adaptation. It is observed that the transfer function has a low-pass nature. The significance of this fact will become apparent in subsequent sections.

One advantage of employing such a structure is the reduced complexity: Only a single adaptive filter is needed. Furthermore, note that the desired signal cancellation phenomenon that occurs as a result of the sensitivity of the blocking matrix is averted, as one is no longer steering the reference beamformer to the desired signal. Even if the steering direction of the interference is misjudged, the SIR at the adaptive filter input will not increase greatly - One desires to have a low SIR at the adaptive filter input. Thus, the structure is more robust to steering vector errors. On the other hand, decoupled structures without a blocking matrix are not MVDR beamformers [9]. As will be shown in

Reproduced with permission of the copyright owner. Further reproduction prohibited without permission.

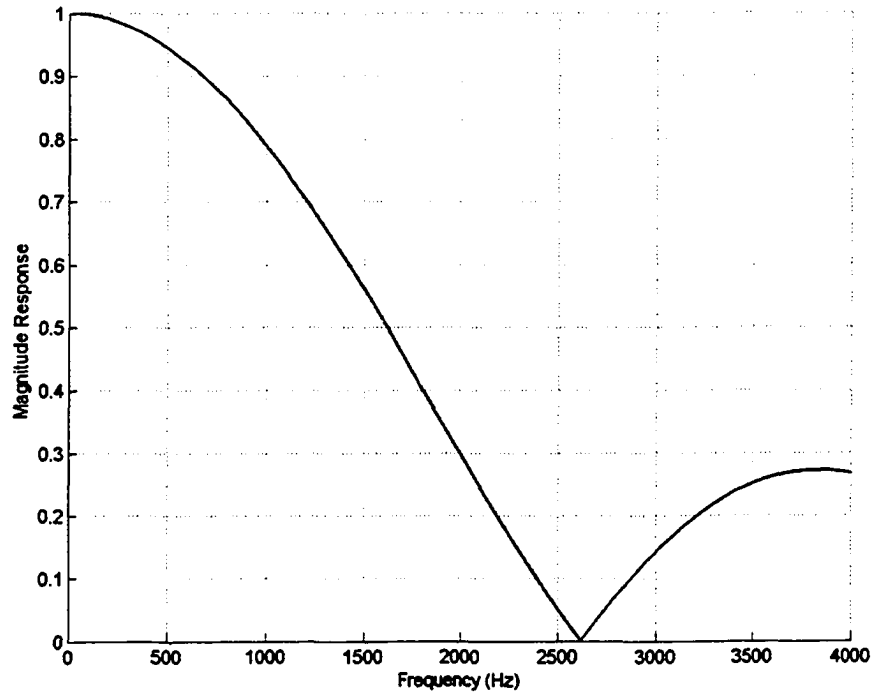

Figure 4.4. Magnitude response of Wiener solution in a decoupled beamformer-noise canceller structure.

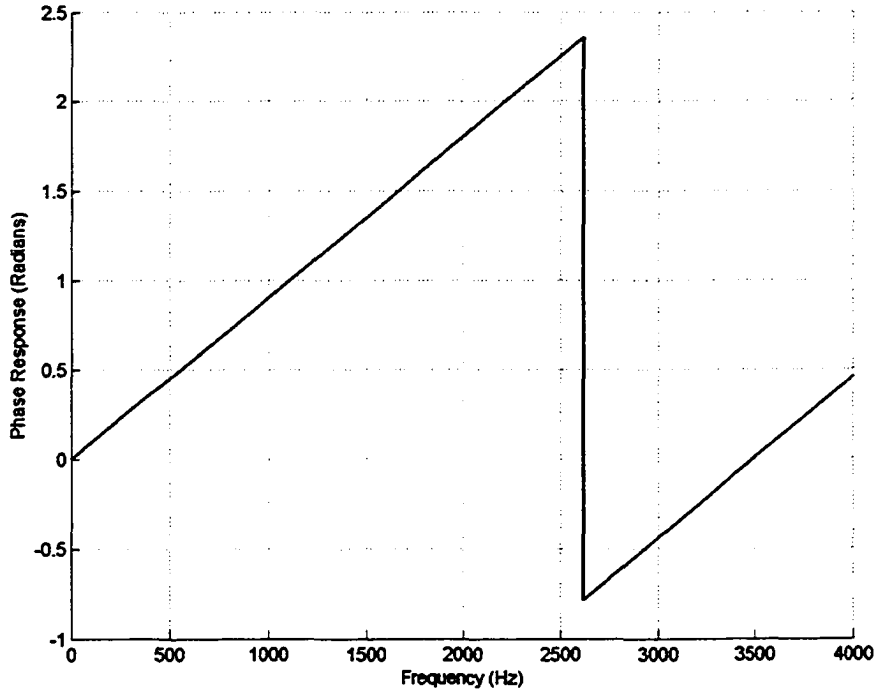

Figure 4.5. Phase response of Wiener solution in a decoupled beamformer-noise canceller structure.

Reproduced with permission of the copyright owner. Further reproduction prohibited without permission.

upcoming sections, the blocking matrix is needed to ensure a unity response to the desired signal at all times.

The structure in Figure 4.3 is applicable to environments with a single interference source. The structure may easily be generalized to an arbitrary number of interferers, N_i, by adding a lower branch for every additional source of interference. Each additional branch consists of a DSB steered to the corresponding interference source, and an adaptive filter to remove this interference from the primary input. This generalized structure is shown in Figure 4.6.

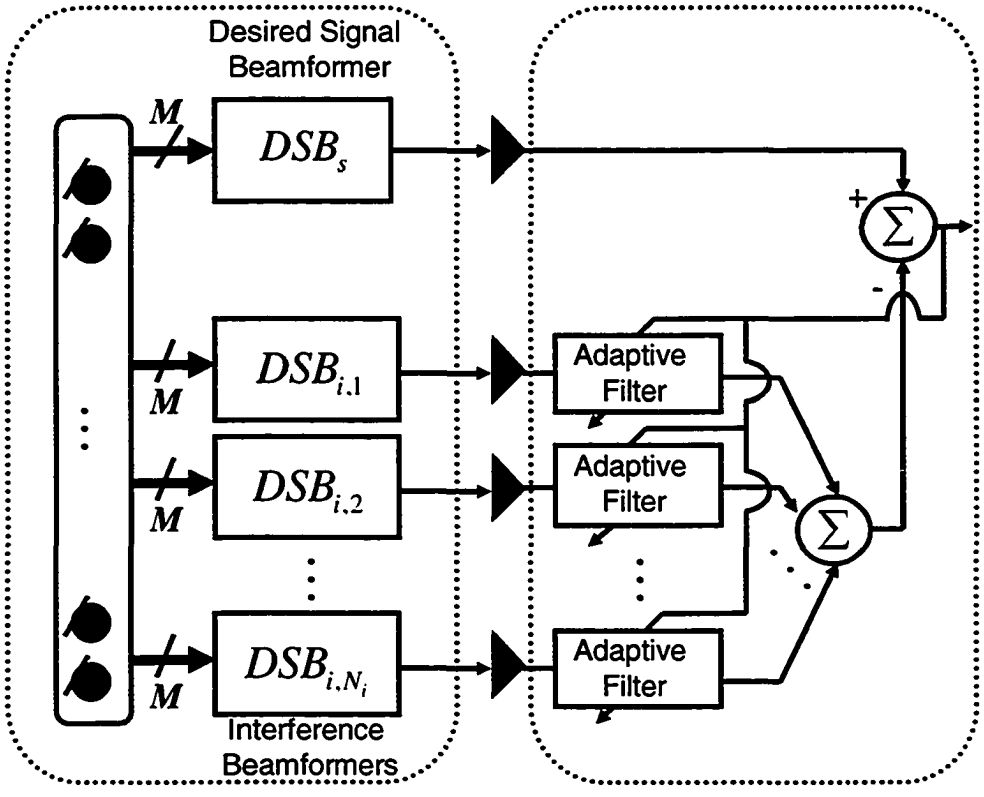

Figure 4.6. Generalized decoupled beamformer-noise canceller structure with multiple delay-and-sum beamformers and a multiple-reference noise canceller.

Reproduced with permission of the copyright owner. Further reproduction prohibited without permission.

4.3 Coupled, Blocking Matrix-Based Beamformer-Noise Canceller Structures

Figure 4.7 depicts the coupled BF-NC model with a blocking matrix. The role of the blocking matrix is to transform the input signals to an interference-only subspace. In the coupled BF-NC scheme, the blocking matrix comprises the reference beamformers. In other words, each reference beamformer has a simple delay-and-subtract structure. It has been shown [16] that for an M-element array, the blocking matrix $\mathbf{B}$ must have $M-1$ rows and M columns, and thus, a multiple-reference ANC is needed. In the figure, the adaptive filters are labeled with their corresponding Wiener solutions. Furthermore, the Griffiths-Jim blocking matrix has been shown:

$$\mathbf{B}=\begin{bmatrix} 1 & -1 & 0 & \cdots & 0 \\ 0 & 1 & -1 & \cdots & 0 \\ \vdots & \ddots & \ddots & \ddots & \vdots \\ 0 & 0 & \cdots & 1 & -1 \end{bmatrix} \tag{4.14}$$

This blocking matrix may be viewed as a bank of DSBs, each of which have only two non-zero weights, namely 1 and -1. The m^{th} blocking matrix output is then represented as the output of a DSB with weights $W_{BM,m}$. Using this notation, the output of the overall structure is given by:

$$Z = W_d^H X - \sum_{m=0}^{M-2} W_{NC,m}^* W_{BM,m}^H X = \left(W_{\mathrm{d}}^H - \sum_{m=0}^{M-2} W_{NC,m}^* W_{BM,m}^H \right) X \tag{4.15}$$

where $W_{NC,m}$ is the Wiener solution of the m^{th} adaptive filter. The output PSD is thus:

$$\Phi_{ZZ} = \left(W_d^H - \sum_{m=0}^{M-2} W_{NC,m}^* W_{BM,m}^H \right) \Phi_{XX} \left(W_d - \sum_{m=0}^{M-2} W_{NC,m} W_{BM,m} \right) \tag{4.16}$$

Reproduced with permission of the copyright owner. Further reproduction prohibited without permission.

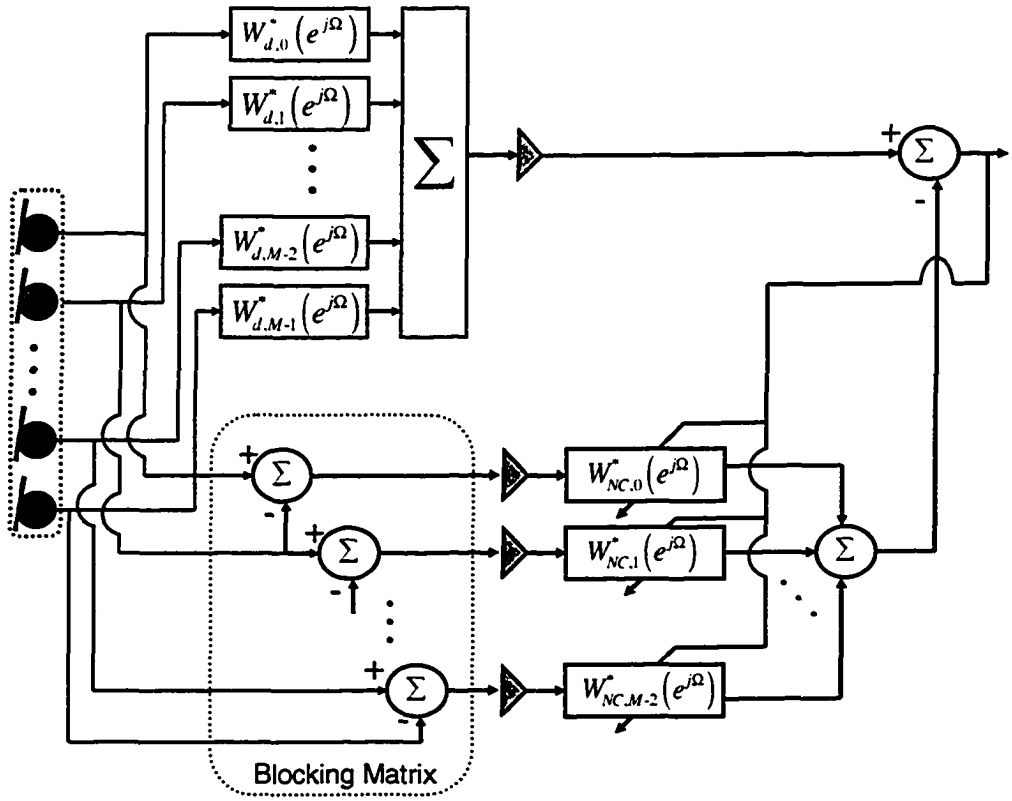

Figure 4.7. Coupled beamformer-noise canceller structure with blocking matrix.

The multi-channel Wiener solution in (4.16) is given by [9]:

$$\boldsymbol{W}_{NC} = \left[W_{NC,0} \quad W_{NC,1} \quad \cdots \quad W_{NC,M-2} \right]^T = \left(\boldsymbol{B}\boldsymbol{\Phi}_{xx}\big|_{adaptation} \boldsymbol{B}^H \right)^{-1} \boldsymbol{B}\boldsymbol{\Phi}_{xx}\big|_{adaptation} \boldsymbol{W}_d \quad (4.17)$$

From (4.15), one sees that the overall structure may be implemented in canonical form with the adaptive weights given by:

$$\boldsymbol{W}_{\text{effective}}\big|_{\text{coupled}} = \mathbf{W}_{\text{d}} - \sum_{m=0}^{M-2} W_{NC,m} \boldsymbol{W}_{BM,m} \quad (4.18)$$

Figures 4.8 and 4.9 depict the multi-channel Wiener solutions of (4.17). Once again, a linear array with $M = 4$ equidistant sensors and an inter-sensor spacing of $d = 0.046$ m is assumed. Adaptation is performed with a white noise source impinging on the array at a direction of arrival of 45° relative to the array axis. Once again, the magnitude

Reproduced with permission of the copyright owner. Further reproduction prohibited without permission.

responses are low-pass in nature. Note that in Figure 4.8, the curves for $m=0$ and $m=2$ are identical, and thus the only the latter curve is visible.

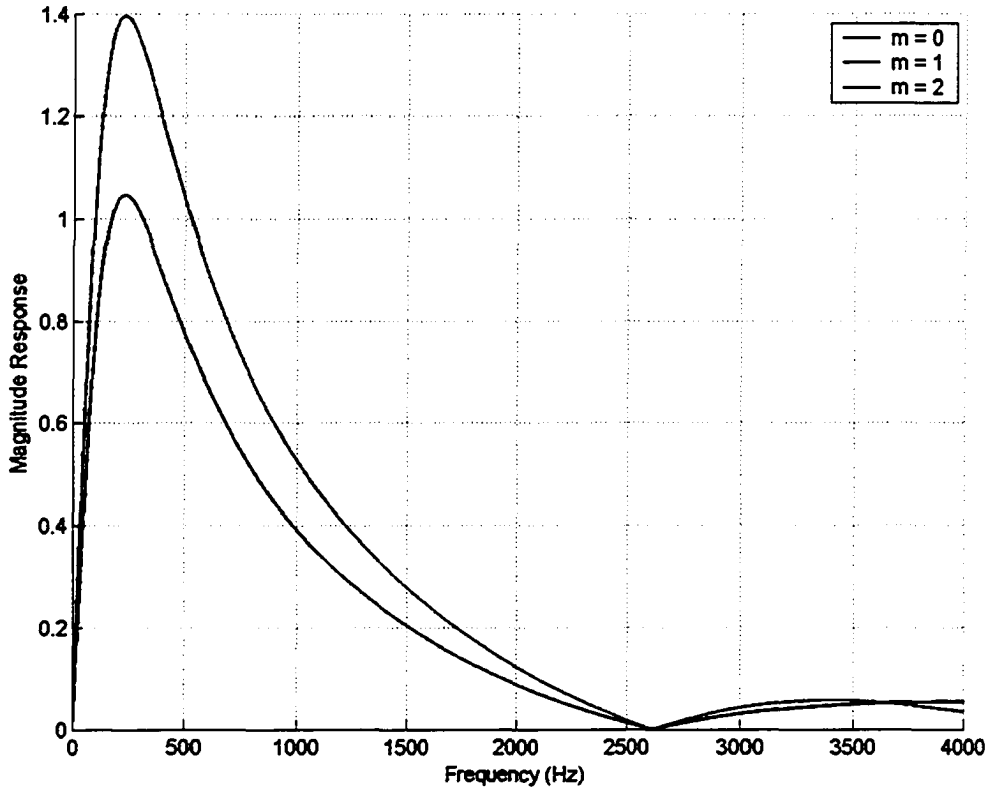

Figure 4.8. Magnitude responses of multi-channel Wiener solution in a coupled beamformer-noise canceller structure with blocking matrix. The curves for *m=0* and *m=2* are identical.

The WNG, directivity, and SIR gain of the structure may be determined by substituting the effective weights of (4.18) into (4.7), (4.8), and (4.9), respectively. A well-known implementation of coupled BF-NC with a blocking matrix is the GSC [16] structure. Please refer to section 2.2.4 for full details of the GSC. The GSC is an alternate form of the MVDR (superdirective) beamformer, which avoids the constrained optimization process. However, the GSC suffers from the desired-signal cancellation phenomenon, which occurs when the desired-signal look-direction is misjudged. As a result, the signal leaks into the adaptive filter inputs, driving the adaptation to cancel the

Reproduced with permission of the copyright owner. Further reproduction prohibited without permission.

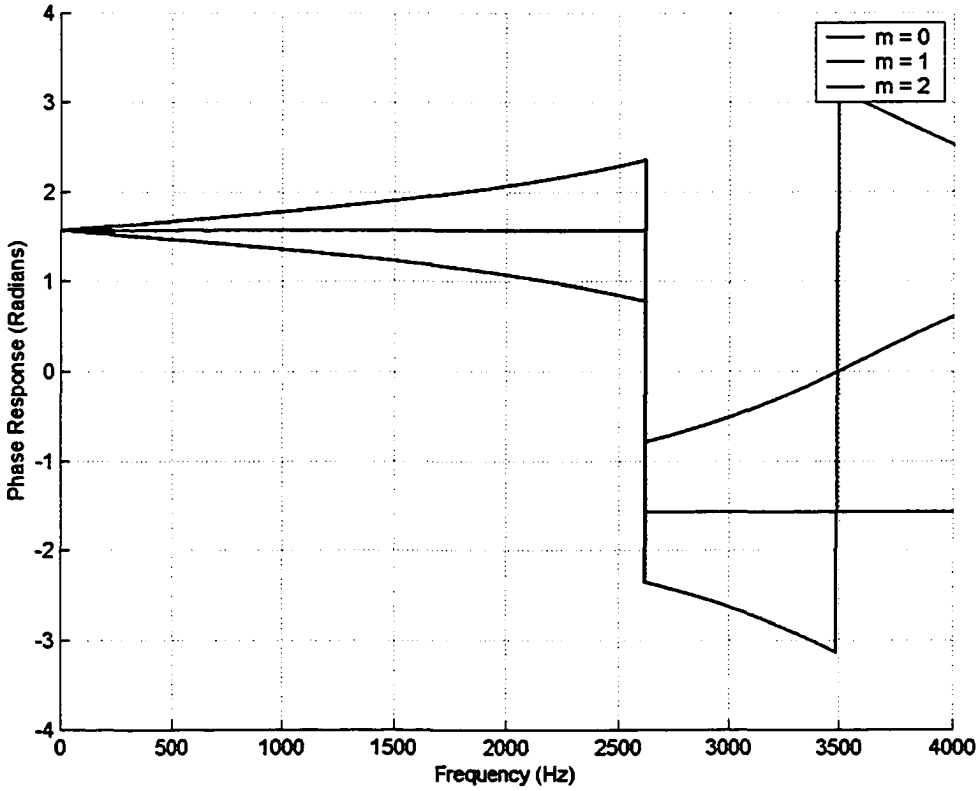

Figure 4.9. Phase responses of multi-channel Wiener solution in a coupled beamformer-noise canceller structure with blocking matrix.

signal. Moreover, the structure requires *M-1* adaptive filters, which is only one less than the standard adaptive beamformer.

4.3 Relationships between Beamforming and Noise Cancellation

It is instructive to analyze the relationship between the performance of the beamforming and noise canceling units of combined BF-NC structure. To that end, note that the WNG, DI, and SIR gains may be computed for only the desired-signal beamformer, prior to the ANC:

$$\mathrm{WNG}_{\mathrm{BF}} = \frac{\left|\boldsymbol{W}_d^H \boldsymbol{d}\right|^2}{\boldsymbol{W}_d^H \boldsymbol{W}_d} \tag{4.19}$$

Reproduced with permission of the copyright owner. Further reproduction prohibited without permission.

$$\mathrm{DI}_{\mathrm{BF}} = \frac{\left|\boldsymbol{W}_d^H \boldsymbol{d}\right|^2}{\boldsymbol{W}_d^H \boldsymbol{\Gamma}_{VV}\big|_{\mathrm{diffuse}} \boldsymbol{W}_d} \tag{4.20}$$

$$\mathrm{G}_{\mathrm{BF}}^{\mathrm{SIR}} = \frac{\boldsymbol{W}_d^H \boldsymbol{\Phi}_{XX}\big|_{\mathrm{signal}} \boldsymbol{W}_d}{\boldsymbol{W}_d^H \boldsymbol{\Phi}_{XX}\big|_{\mathrm{interference}} \boldsymbol{W}_d} \tag{4.21}$$

The improvements in signal enhancement offered by the inclusion of the ANC are then:

$$\mathrm{WNG}_{\mathrm{NC}} = \mathrm{WNG}_{\mathrm{BF\text{-}NC}} - \mathrm{WNG}_{\mathrm{BF}} = \frac{\left|\boldsymbol{W}_{\mathrm{effective}}^H \boldsymbol{d}\right|^2}{\boldsymbol{W}_{\mathrm{effective}}^H \boldsymbol{W}_{\mathrm{effective}}} - \frac{\left|\boldsymbol{W}_d^H \boldsymbol{d}\right|^2}{\boldsymbol{W}_d^H \boldsymbol{W}_d} \tag{4.22}$$

$$\mathrm{DI}_{\mathrm{NC}} = \mathrm{DI}_{\mathrm{BF\text{-}NC}} - \mathrm{DI}_{\mathrm{BF}} = \frac{\left|\boldsymbol{W}_{\mathrm{effective}}^H \boldsymbol{d}\right|^2}{\boldsymbol{W}_{\mathrm{effective}}^H \boldsymbol{\Gamma}_{VV}\big|_{\mathrm{diffuse}} \boldsymbol{W}_{\mathrm{effective}}} - \frac{\left|\boldsymbol{W}_d^H \boldsymbol{d}\right|^2}{\boldsymbol{W}_d^H \boldsymbol{\Gamma}_{VV}\big|_{\mathrm{diffuse}} \boldsymbol{W}_d} \tag{4.23}$$

$$\mathrm{G}_{\mathrm{NC}}^{\mathrm{SIR}} = \mathrm{G}_{\mathrm{BF\text{-}NC}}^{\mathrm{SIR}} - \mathrm{G}_{\mathrm{BF}}^{\mathrm{SIR}} = \frac{\boldsymbol{W}_{\mathrm{effective}}^H \boldsymbol{\Phi}_{XX}\big|_{\mathrm{signal}} \boldsymbol{W}_{\mathrm{effective}}}{\boldsymbol{W}_{\mathrm{effective}}^H \boldsymbol{\Phi}_{XX}\big|_{\mathrm{interference}} \boldsymbol{W}_{\mathrm{effective}}} - \frac{\boldsymbol{W}_d^H \boldsymbol{\Phi}_{XX}\big|_{\mathrm{signal}} \boldsymbol{W}_d}{\boldsymbol{W}_d^H \boldsymbol{\Phi}_{XX}\big|_{\mathrm{interference}} \boldsymbol{W}_d} \tag{4.24}$$

Examination of the relationships between the quantities of (4.22) to (4.24) and those of (4.19) to (4.21) sheds light into the inter-operation of the beamforming and noise canceling components.

4.4.1 Signal-to-Interference Ratio as a Function of Signal-Interference Separation in a Decoupled Beamformer-Noise Canceller Structure

The SIR gains of the beamforming and noise canceling units have been determined for various signal-interference separations. The two-DSB, one-ANC structure of Figure 4.3 is implemented to compute the SIR gains. An $M = 4$ element, uniformly-spaced, linear array with an inter-element spacing of 0.046 m is assumed. The desired signal source is located at broadside, while the interference impinges on the array at an angle of 45° with respect to the array axis. There is a perfect correspondence between array steering and the signals' DOAs. Uncorrelated noise with a SUNR of 20 dB is added at the microphone array. The sampling frequency is 8 kHz, and the results are averaged over

Reproduced with permission of the copyright owner. Further reproduction prohibited without permission.

the 300 Hz – 3.7 kHz frequency band. Adaptation is performed in the absence of the desired signal. The SIR gains of the noise canceller are shown for both noise canceller models: The model of Figure 2.2 which ignores the path from desired signal source to reference noise canceller input, and the model of Figure 2.3, which includes this path. Figure 4.10 shows the SIR relationships.

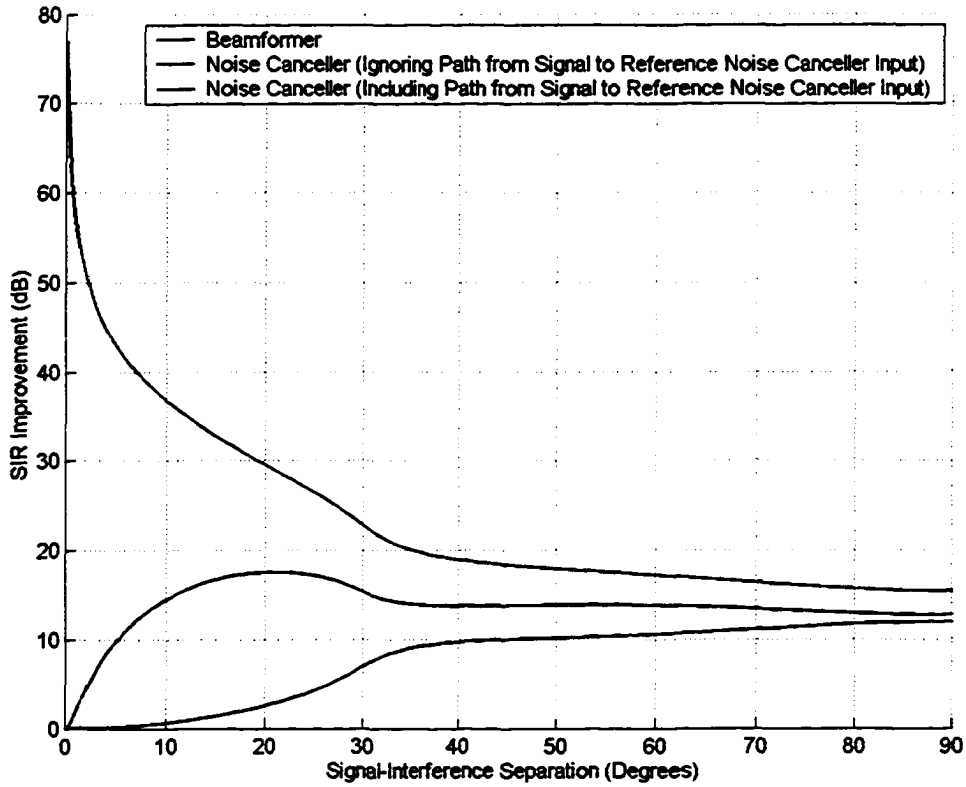

Figure 4.10. Signal-to-interference ratio relationships between beamformer and noise canceller in a decoupled beamformer-noise canceller structure.

The curve clearly illustrates the opposing nature of the beamforming and noise canceling units. While the beamformer benefits from increased signal-interference separation, the SIR gain of the noise canceller tends to decrease with increased separation.

Reproduced with permission of the copyright owner. Further reproduction prohibited without permission.

A beamformer is a structure that thrives on spatial separation between desired signal and interference sources. The beampattern function generally decreases as one moves away from the steering direction. Since the amount of interference leaked through the desired signal beamformer decreases as the interference source moves away from the look-direction, the SIR at the beamformer output will increase for increased signal-interference separation. On the other hand, a noise canceller is a purely temporal device that relies on correlation between its primary and reference inputs to convert the adaptive filter input to the desired signal. Intuitively, the correlation between beamformer outputs decreases as the steering directions of the beamformers move away from each other. Formally, note that the level of interference reduction in the noise canceller is related to the interference-to-uncorrelated-noise ratio (IUNR) at the primary input, according to (2.4). As the interference source moves away from the desired signal look direction, the level of interference at the primary noise canceller input decreases. However, the level of uncorrelated noise at the primary noise canceller input obviously does not depend on the position of the interference, and thus the IUNR decreases with increased signal-interference separation. Consequently, the SIR gain of the ANC decreases as the signal-interference separation increases.

Notice that when taking into account the path from signal to reference noise canceller input, for small signal-interference separation (i.e., $0^\circ - 20^\circ$), the ANC suffers from a large amount of leakage of the desired signal into its reference input, according to (2.5). This occurs because the steering directions of the two beamformers are similar. As a result, the desired signal is passed through the interference beam.

Reproduced with permission of the copyright owner. Further reproduction prohibited without permission.

Figure 4.11 shows the overall SIR gain of the decoupled BF-NC as a function of signal-interference separation. It is apparent that the angle of optimal signal-interference separation is 90°. This result is intuitively satisfying: A combined BF-NC may be effectively viewed as an adaptive beamformer. It stands to reason that an adaptive beamformer will provide the most discrimination with maximum separation between the signal sources.

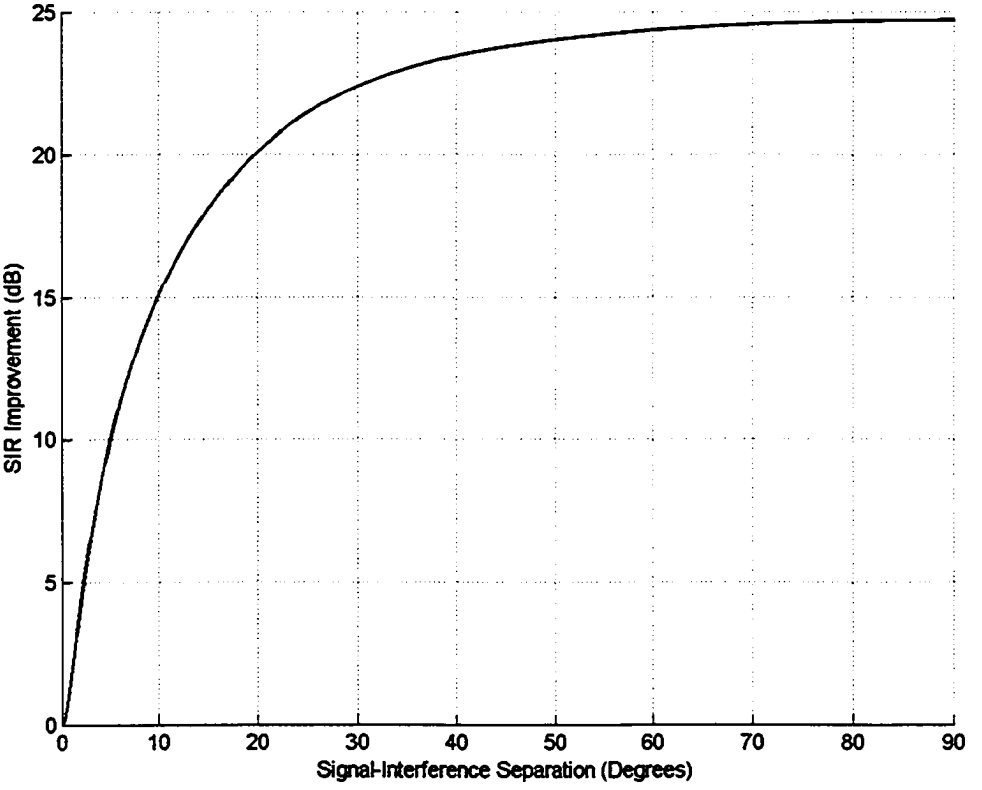

Figure 4.11. Overall signal-to-interference ratio gain of a decoupled beamformer-noise canceller structure.

4.4.2 Signal-to-Interference Ratio as a Function of Signal-Interference Separation in a Coupled Beamformer-Noise Canceller Structure

The SIR relationships have also been computed for the case of a coupled BF-NC with a blocking matrix, as in the structure of Figure 4.7. A DSB is employed as the desired signal beamformer. All parameters are the same as in the previous section. The

Reproduced with permission of the copyright owner. Further reproduction prohibited without permission.

respective SIR gains are shown as a function of signal-interference separation in Figure 4.12. Figure 4.13 shows the overall SIR gain of the coupled structure as a function of signal-interference separation.

Once again, the inverse relationship between the SIR gain of the beamformer and that offered by the noise canceller is apparent. However, ignoring the path from signal to reference noise canceller inputs does not affect the curve. This is because the blocking

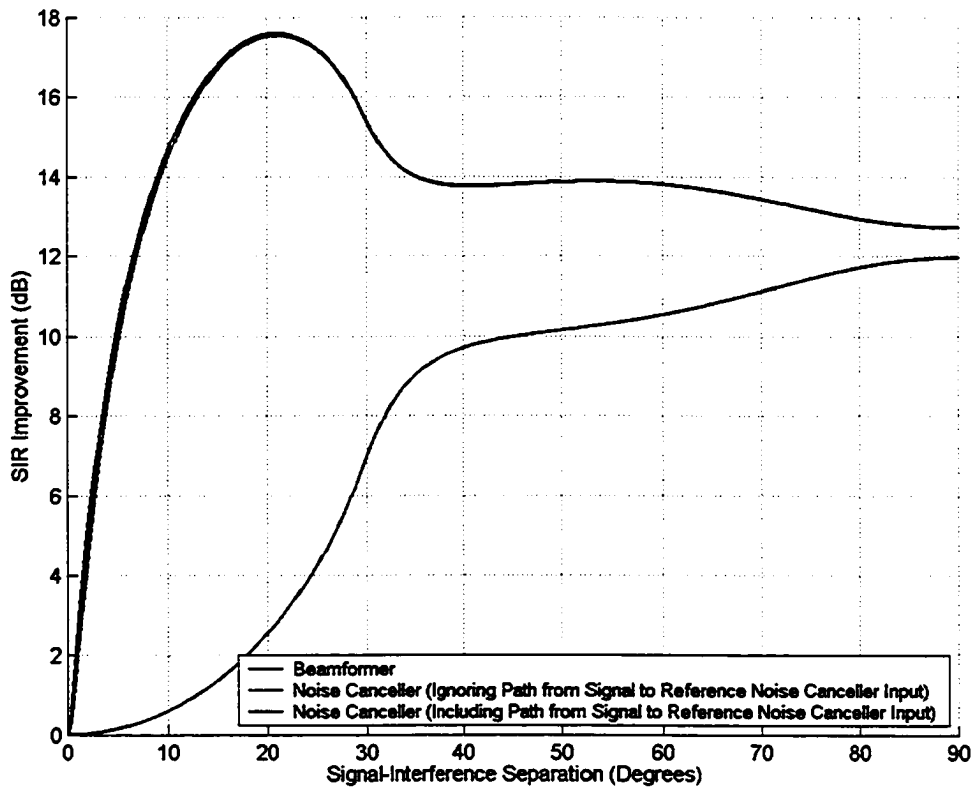

Figure 4.12. Signal-to-interference ratio relationships between beamformer and noise canceller in a coupled beamformer-noise canceller structure with blocking matrix.

matrix has an effect equivalent to the cutting of this path: The desired signal is blocked. One may then ask why there is a performance degradation for $0^\circ - 20^\circ$ signal-interference separation, even though there is no signal leakage. This is because for small signal-interference separation, the blocking matrix also blocks the *interference*. Therefore, the

Reproduced with permission of the copyright owner. Further reproduction prohibited without permission.

IUNR at the reference noise canceller inputs is undesirably low, and the degradation follows from (2.4). From Figure 4.13, the coupled BF-NC with blocking matrix also performs best for maximum signal-interference separation.

A comparison of Figures 4.10 and 4.12 indicates that the blocking matrix may not be an optimal beamformer for cascading with a noise canceller. In addition to its sensitivity to steering errors, for $0^\circ - 20^\circ$ signal-interference separations, a blocking matrix also lowers the IUNR at the reference noise canceller inputs, thus causing misadjustment in the adaptive process. A beamformer steered to the interference source maximizes the IUNR at the reference noise canceller input, and is thus superior to the blocking matrix in this sense.

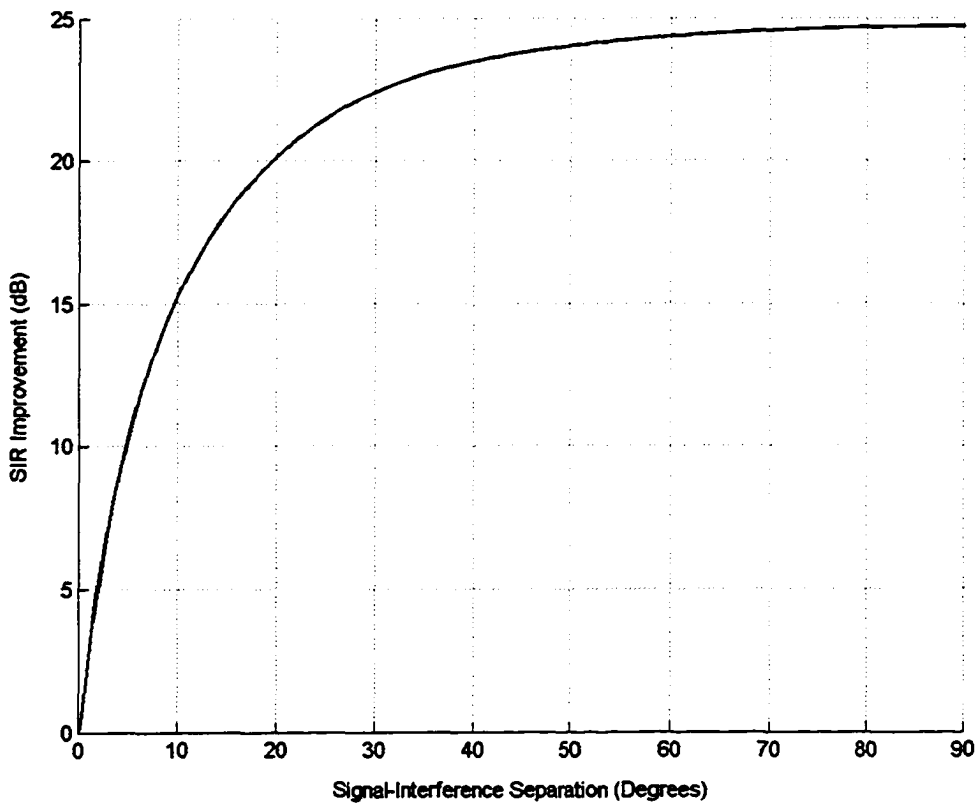

Figure 4.13. Overall signal-to-interference ratio gain of a coupled beamformer-noise canceller structure with blocking matrix.

Reproduced with permission of the copyright owner. Further reproduction prohibited without permission.

4.4.3 Beampattern of a Decoupled Beamformer-Noise Canceller Structure

The effect of including the noise canceller on the beampattern of the decoupled BF-NC structure is shown in Figure 4.14. All applicable parameters are the same as those described in Section 4.4.1. The desired signal beamformer is steered to broadside (perpendicular to array axis), while the interference DSB's look direction is 45°. The frequency of the wavefront is 1.5 kHz.

The beamformer alone achieves only a 5 dB suppression of the interfering signal. The inclusion of the noise canceller forms a deep null in the direction of the interference. Note that the desired signal is attenuated by approximately 3 dB, although the SIR is still very high. This attenuation results from leakage of the desired signal into the reference noise canceller input, leading to a distortion of the output. It is important to distinguish

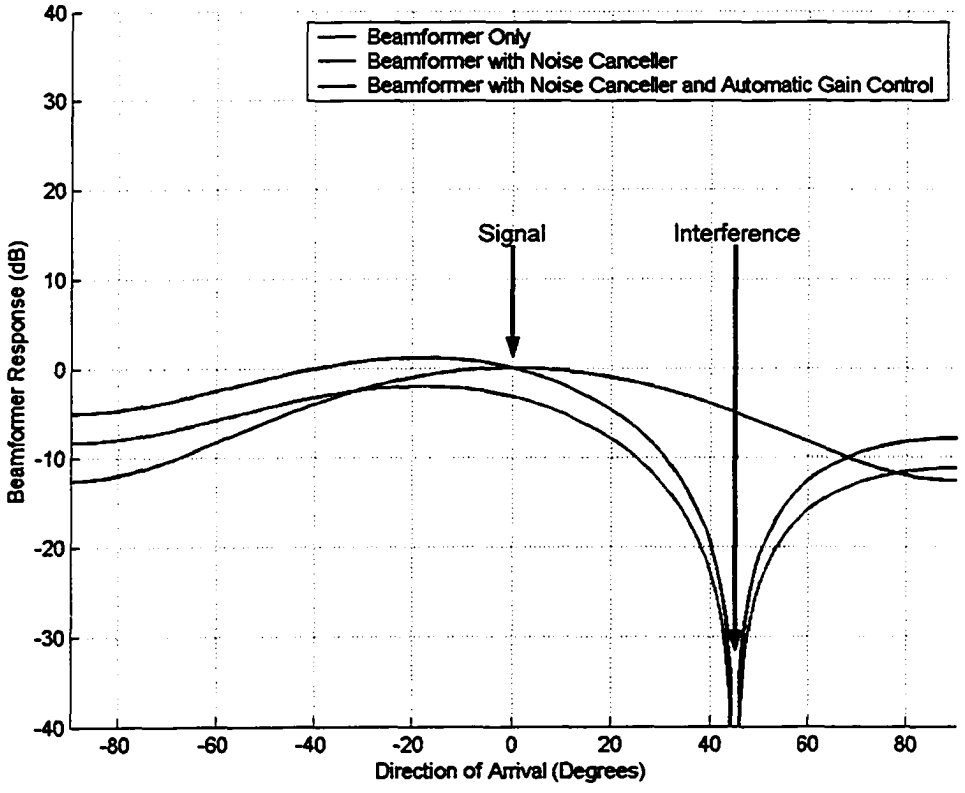

Figure 4.14. Beampatterns of a decoupled beamformer-noise canceller structure.

Reproduced with permission of the copyright owner. Further reproduction prohibited without permission.

desired signal cancellation from desired signal distortion. Desired signal cancellation occurs when the adaptation is carried out with the desired signal source active, and the filter taps are driven to cancel the signal. On the other hand, if adaptation is performed in the absence of the desired signal, no cancellation occurs. However, after adaptation, the desired signal may enter the reference input, pass through the filter and distort the output signal.

Automatic gain control (AGC) may be added to the output of the structure to maintain unity gain response to the desired signal, since the interference is deeply attenuated. The effect of adding an AGC is also shown in Figure 4.14.

4.4.4 Beampattern of a Coupled Beamformer-Noise Canceller Structure

The impact of a noise canceller with a blocking matrix (in the coupled BF-NC structure) on the beampattern is shown in Figure 4.15. All parameters are the same as in the previous section. Once again, the inclusion of the noise canceller leads to a deep null in the direction of the interference. The blocking matrix prevents desired signal leakage into the reference noise canceller inputs, and thus maintains a unity gain response to the desired signal. There is no need to add an AGC. Notice that the response of the decoupled BF-NC with an AGC is virtually identical to the response of the coupled BF-NC with a blocking matrix.

4.4.5 Frequency Dependency of Beampatterns

The beampattern of a BF-NC structure will vary with the frequency of the wavefront. The effect of frequency on the beampattern of the decoupled BF-NC structure is shown in Figure 4.16.

Reproduced with permission of the copyright owner. Further reproduction prohibited without permission.

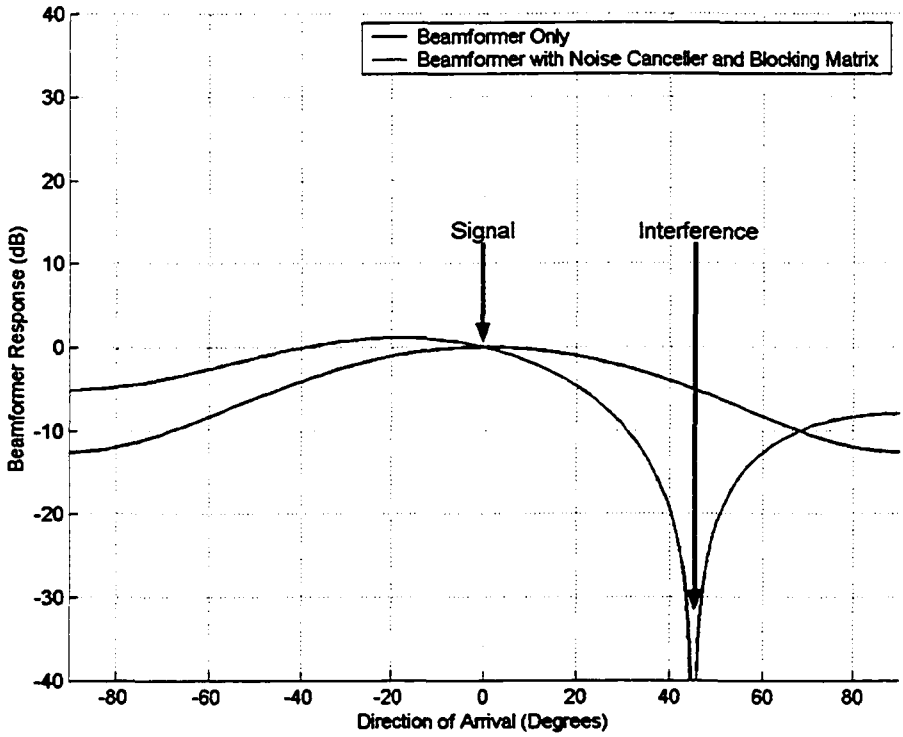

Figure 4.15. Beampatterns of a coupled beamformer-noise canceller structure with blocking matrix.

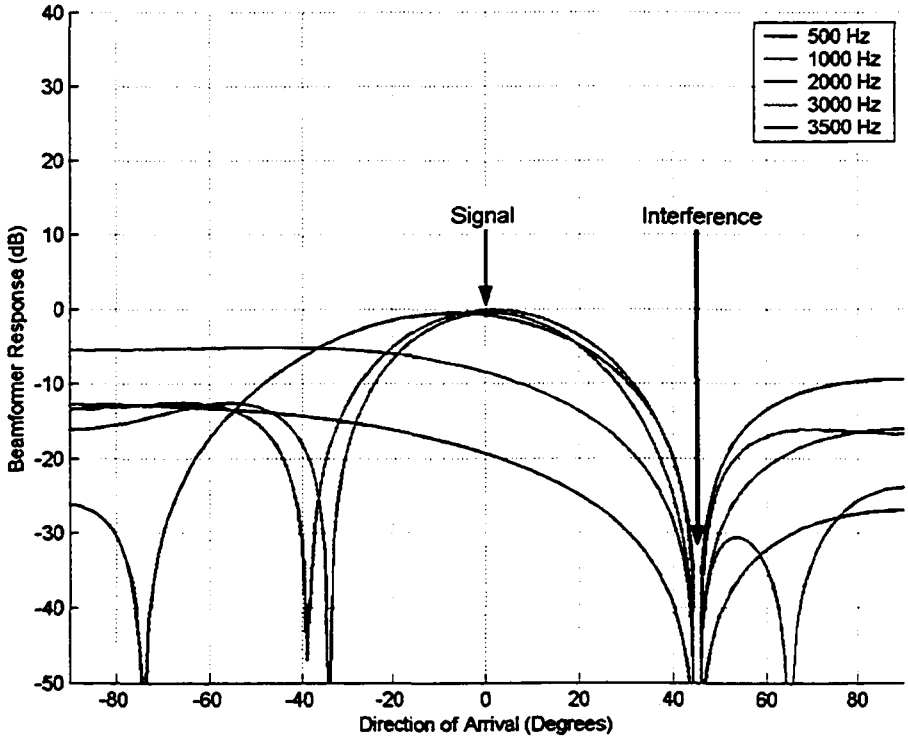

Figure 4.16. Frequency-dependency of beampatterns in a decoupled beamformer-noise canceller structure.

Reproduced with permission of the copyright owner. Further reproduction prohibited without permission.

A deep null in the direction of the interference is formed for all frequencies. However, the response to the desired signal is frequency-dependent: The level of desired signal attenuation is greater for lower frequencies. This is because the level of leakage of the desired signal into the reference noise canceller input varies with the frequency: The main lobe of the reference beamformer will be wider for lower frequencies, and will thus allow a greater amount of desired signal to pass. Furthermore, the transfer function of the converged adaptive filter has a low-pass behavior, and lower frequency leakage is undesirably passed. Any high-frequency leakage is attenuated, and thus a unity gain response is achieved at these frequencies.

An AGC is not appropriate for broadband applications, as the level of amplification needed varies with the frequency. A post-filter that amplifies the lower frequencies may be appropriately designed and added to the structure to achieve unity gain at all frequencies. Such a post-filter will vertically "shift" the beampattern curves such that unity gain is provided at all frequencies. Note that this implies reducing the null in the direction of the interference. The level of amplification required is directly related to the level of signal distortion, which follows from the amount of signal leakage into the reference beam. This post-filter may be placed at the output of the noise canceller, which is shown in Figure 4.17.

The frequency-dependency of beampatterns in the coupled BF-NC structure with a blocking matrix is shown in Figure 4.18.

Reproduced with permission of the copyright owner. Further reproduction prohibited without permission.

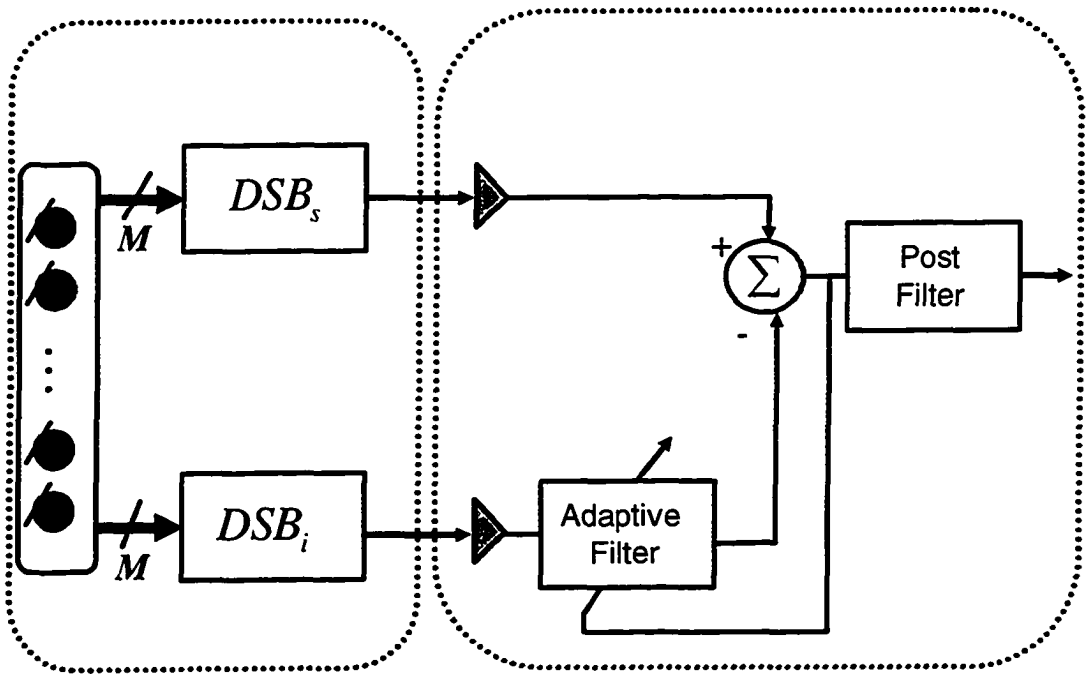

Figure 4.17. Addition of post-filter into decoupled beamformer-noise canceller.

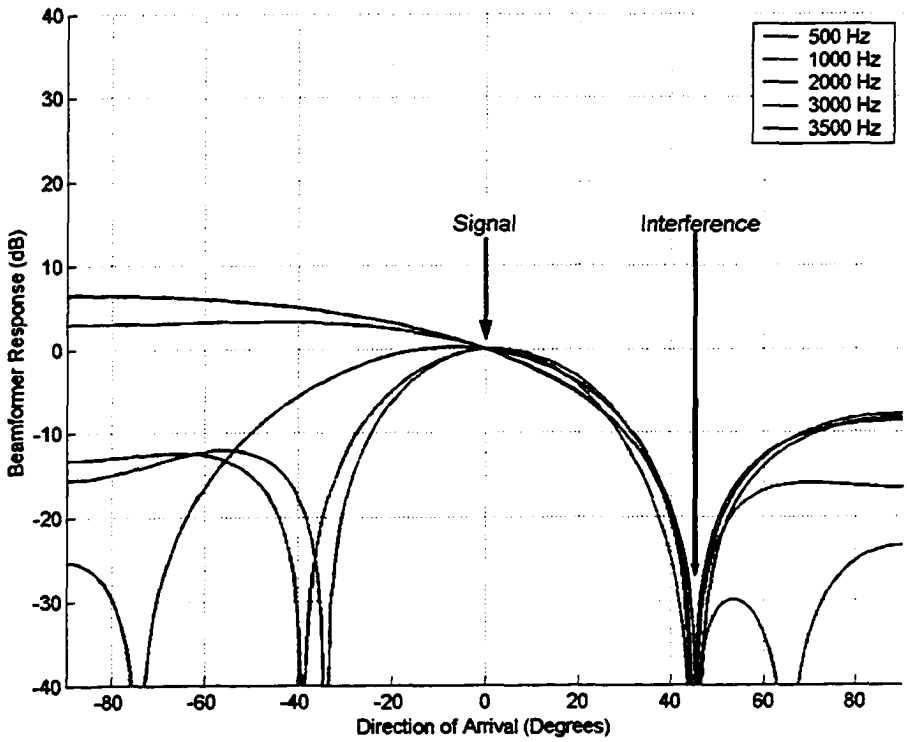

Figure 4.18. Frequency-dependency of beampatterns in a coupled beamformer-noise canceller structure with blocking matrix.

Reproduced with permission of the copyright owner. Further reproduction prohibited without permission.

The addition of the blocking matrix into the noise cancellation process forces the BF-NC's desired signal response to unity-gain at all frequencies. This is because the blocking matrix forms a null in the direction of the desired signal, regardless of the input frequency. Notice, however, that the beam shape itself is frequency-dependent. For example, at lower frequencies, the structure exhibits a high-level of gain across a wide range of directions. In the context of a reverberant environment, this is undesirable, as reflections arriving at these directions will be passed.

4.4.6 White Noise Gain as a Function of Frequency

The effect of cascading the beamformer with the noise canceller on the WNG of the decoupled and coupled structures has been evaluated through (4.22). A 4-element, uniformly-spaced, linear array with inter-element spacing of 0.0425 m is assumed. This spacing allows the entire frequency band of 0 Hz - 4 kHz to be evaluated, which is appropriate when considering the WNG. The sampling frequency is 8 kHz. For the case of the decoupled BF-NC (Figure 4.3), the desired signal DSB is steered to the endfire (parallel to array axis) direction, while the interference DSB is steered to broadside. For the coupled BF-NC with a blocking matrix (Figure 4.6), the desired signal DSB and blocking matrix are steered to the endfire direction. Figure 4.19 depicts the WNG of only the beamformer (equivalent for both decoupled and coupled structures), the decoupled BF-NC scheme, and the coupled BF-NC scheme with blocking matrix.

It is not surprising that the addition of the noise canceller in the decoupled structure reduces the WNG – the DSB at the front-end is the optimal beamformer for maximizing the WNG [9]. The subtraction at the noise canceller back-end increases the amount of noise present in the output. The degradation is most noticeable at the low end

Reproduced with permission of the copyright owner. Further reproduction prohibited without permission.

of the frequency spectrum, as the transfer function of the converged adaptive filter is low-pass. In the coupled structure, the presence of the blocking matrix further degrades the WNG – This is because there are now *M-1* adaptive filters, each of which augments the uncorrelated noise at the output. As mentioned previously, the noise canceller is a purely temporal device that relies on correlation between its two inputs to offer signal enhancement. The ANC is unable to cancel any uncorrelated noise components in its inputs, and thus the degradation of Figure 4.19 ensues.

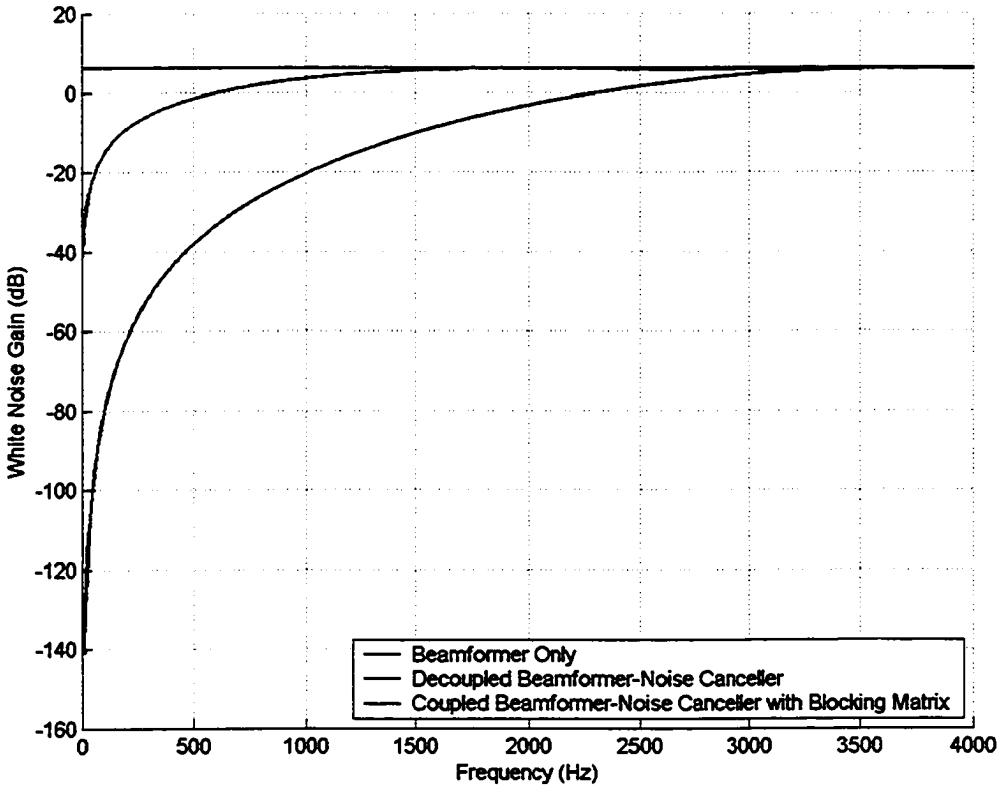

Figure 4.19. White noise gain as a function of frequency.

4.4.7 Directivity as a Function of Frequency

The effect of including the noise canceller on the directivity of the decoupled and coupled BF-NC structures is evaluated through (4.23). All parameters are the same as in the

Reproduced with permission of the copyright owner. Further reproduction prohibited without permission.

previous section. Figure 4.20 displays the DI of only the beamformer, the decoupled BF-NC structure, and the coupled BF-NC structure with blocking matrix.

It is not surprising that the coupled BF-NC with blocking matrix results in superior directivity: The collection of front-end DSB, blocking matrix, and multiple-reference ANC is well-known to be an implementation of the SDB. The SDB is the optimal beamformer in the sense of maximizing the directivity. The decoupled BF-NC structure enhances the directivity over the DSB only in the lower frequency range. This is because a single reference beamformer is limited in its ability to "capture" the noise field. The blocking matrix has multiple outputs, and is thus better suited for this role.

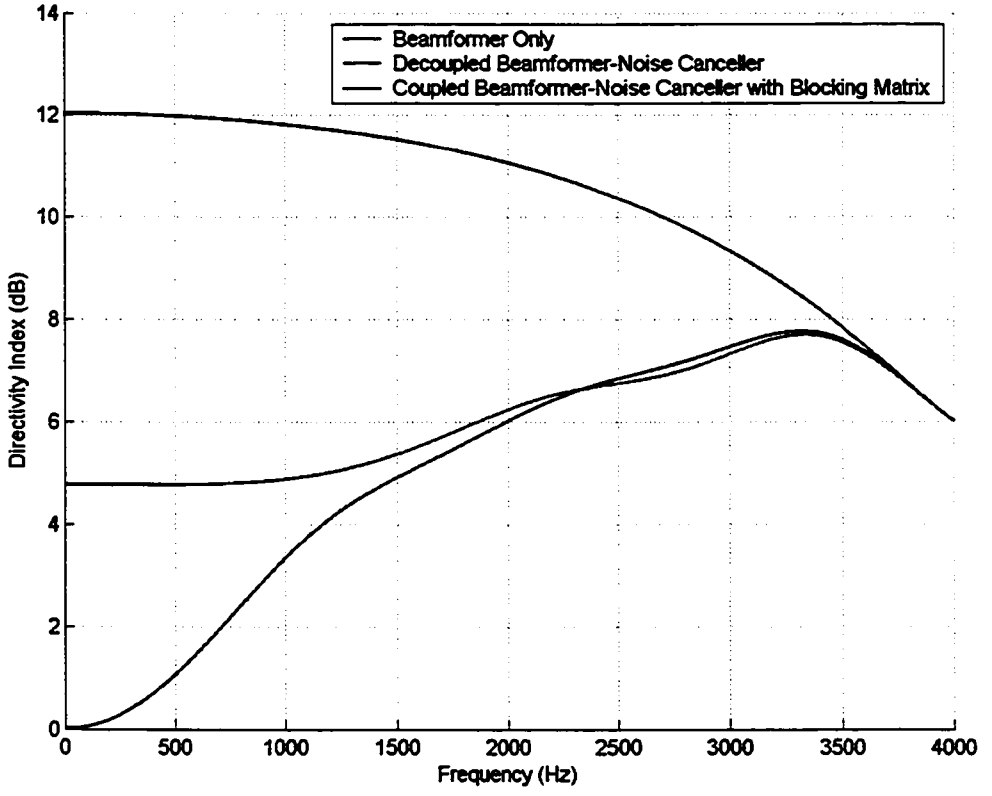

Figure 4.20. Directivity index as a function of frequency.

Reproduced with permission of the copyright owner. Further reproduction prohibited without permission.

Chapter 5

Simulation Evaluation of Beamformer-Noise Canceller Structures

The results of Chapter 4 stem from theoretical beamforming models. While these models do serve to illustrate the relationships between beamforming and noise cancellation, some practical issues are not considered. For example, the transfer functions between beamformer outputs may not always be causal, and thus a delay must be introduced into the desired signal beamformer output to ensure causality. This is shown in Figures 5.1 and 5.2. Furthermore, the theoretical models do not take into account the fact that in a digital implementation, the delays in a DSB need to be rounded into integer multiples of the sampling period. The result is non-ideal beam steering. Moreover, computer simulations provide a simple way of validating theoretical results.

The performance of BF-NC structures is thus evaluated in a computer simulation. The two-DSB, one-ANC structure of Figure 4.3 represents decoupled BF-NC structures. The structure of Figure 4.7, with a DSB as the desired signal beamformer, and the Griffiths-Jim blocking matrix, represents coupled BF-NC structures. Full details of the simulation environment are given in Chapter 3. A key objective of the simulations is to determine the applicability of BF-NC structures to various signal types.

5.1 Investigation of Signal Nature in Beamformer-Noise Canceller Structures

It is important to investigate the applicability of combined BF-NC structures in various signal environments. Three broad cases were considered:

Reproduced with permission of the copyright owner. Further reproduction prohibited without permission.

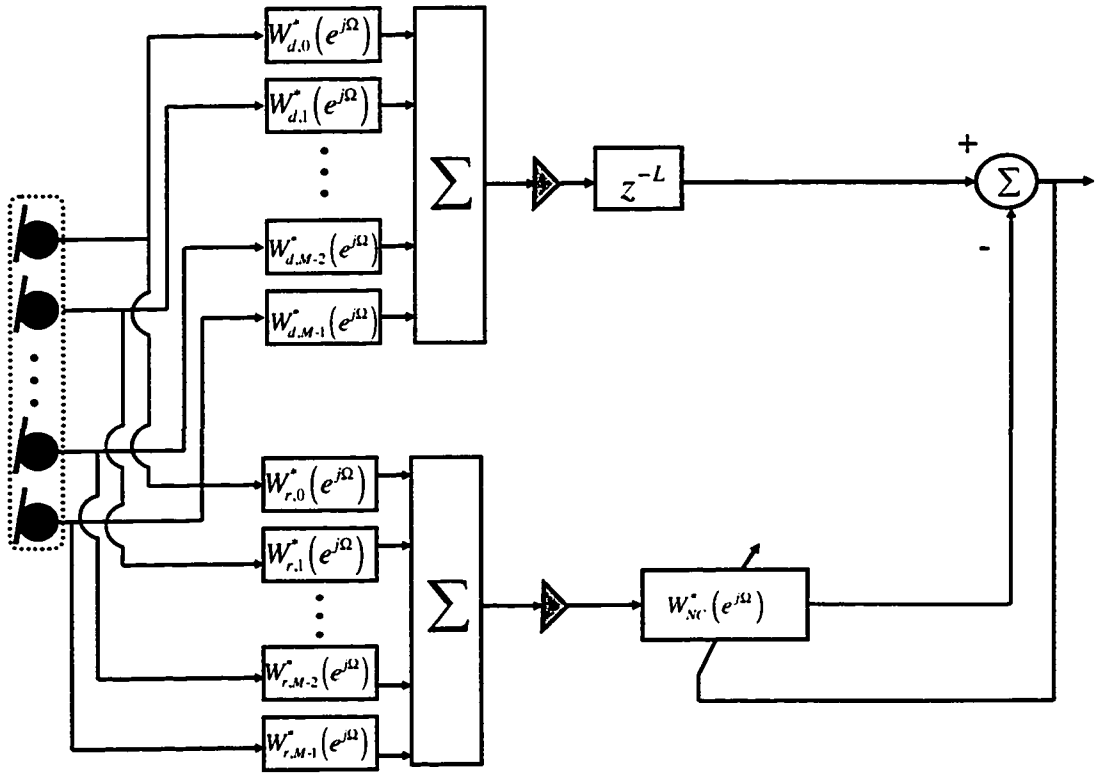

Figure 5.1. Delay for causality in a decoupled beamformer-noise canceller structure.

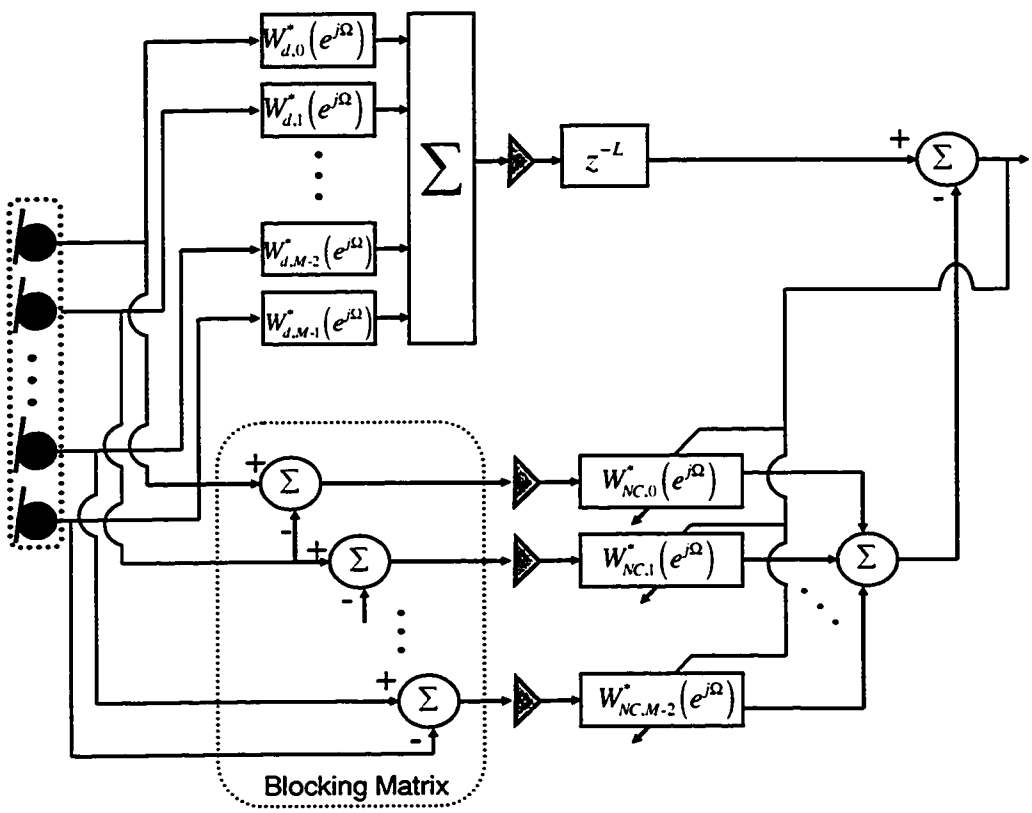

Figure 5.2. Delay for causality in a coupled beamformer-noise canceller structure.

Reproduced with permission of the copyright owner. Further reproduction prohibited without permission.

- A speech source acting as the signal, and a white noise source acting as the interference.
- A white noise source acting as the signal, and a second white noise source acting as the interference.
- A speech source acting as the signal, and a second speech source acting as the interference.

Signal nature is indicative of the frequency content of the signal. Due to the fact that a BF-NC performs *spatial* signal discrimination at the front-end, it is expected that the nature of the signals will not be a limiting factor in the applicability of BF-NC systems. However, there is a subtle issue with the adaptation of the noise cancellers: It is well-known that an adaptive filter converges only at the frequencies which are inputted to it during adaptation. If the signal contains frequency components which are not present during adaptation, the system will not be optimized at those frequencies. Therefore, the case of a white noise signal and speech interference is not considered.

5.2 Simulation Results

Table 5.1 shows the effect of signal nature on the resulting signal enhancement provided by combined BF-NC structures. The numerical entries represent the SIR improvements, from array input to system output, of the front-end beamformer ('BF'), decoupled BF-NC ('Decoupled BF-NC'), and coupled BF-NC with blocking matrix ('Coupled BF-NC'), as a function of the nature of the signal and interference. The values are averaged over 100 trials. The intent is to establish the robustness of combined BF-NC structures with respect to signal nature.

Reproduced with permission of the copyright owner. Further reproduction prohibited without permission.

Table 5.1. Signal enhancement as a function of signal nature.

Signal	Interference	BF	Decoupled BF-NC	Coupled BF-NC
White Noise	White Noise	**4.99 dB**	**24.65 dB**	**20.69 dB**
Male Speech	White Noise	**5.01 dB**	**17.17 dB**	**20.46 dB**
Female Speech	White Noise	**4.99 dB**	**17.49 dB**	**20.64 dB**
Male Speech	Female Speech	**1.62 dB**	**16.03 dB**	**15.33 dB**
Female Speech	Male Speech	**1.34 dB**	**16.50 dB**	**17.51 dB**

Consider first the SIR gains produced by the stand-alone beamformer. These gains reflect the amount of attenuation posed by the desired signal beamformer to the interfering signal. At low frequencies, the inter-sensor spacing of the array is small compared to the wavelength of the signals, and thus, the main lobe of the array is wide. The resulting attenuation of interfering signals is low. The array is designed for the upper frequency range (3.7 kHz), while the energy of the speech signals used in the simulations is concentrated in the 500 Hz-1000 Hz range, as shown in Figure 5.3. Therefore, when the interfering signal is speech, the SIR gain of the front-end beamformer is very small (i.e., ~1.5 dB). When a white noise source acts as the interference, the SIR gains are higher (i.e., ~ 5 dB) due to the presence of high-frequency interfering signal components which are significantly attenuated by the beamformer. A narrowband DSB is limited in its ability to discriminate signals, particularly at frequencies much lower than that of the array design.

Reproduced with permission of the copyright owner. Further reproduction prohibited without permission.

Consider now the decoupled BF-NC structure. The limiting factor in its performance is the amount of leakage of the desired signal into the reference noise canceller input. Moreover, it is expected to perform best with a high-frequency desired

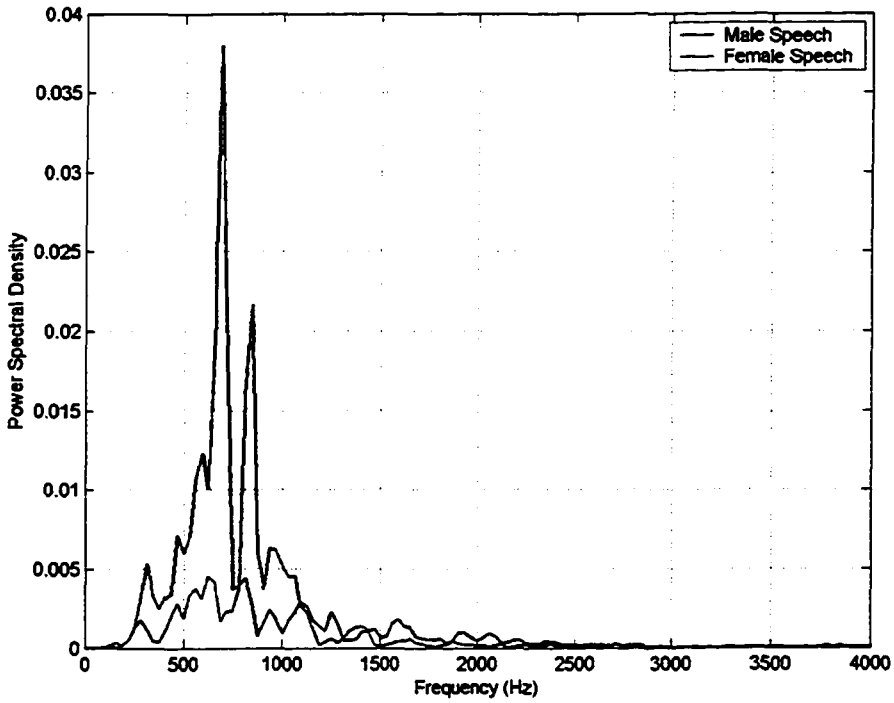

Figure 5.3. Power spectral densities of male and female speech signals used in simulations.

signal, as any high-frequency leakage is attenuated by the adaptive filter, and thus does not distort the output signal. On the other hand, low-frequency leakage is passed by the filter and leads to a distortion of the desired signal. It is therefore not surprising that the decoupled BF-NC performs best when the desired signal is white noise. The performance drops when the desired signal is speech, because the speech signal is predominantly low-pass. Notice that the decoupled BF-NC is not sensitive to the nature of the interfering signal – Once again, this is because the limiting factor is the amount of *desired signal* leakage into the reference noise canceller input.

Reproduced with permission of the copyright owner. Further reproduction prohibited without permission.

Turning now to the interpretation of the SIR gains produced by the coupled BF-NC, it is evident that the nature of the *interfering* signal is key in determining the performance. To be specific, there is a drop-off in output SIR when the interference is speech. Since the blocking matrix prevents leakage of the desired signal into the multiple-reference ANC, the limiting factor in performance becomes the level of uncorrelated noise in the noise canceller inputs. From Figure 4.19, the WNG in a coupled BF-NC with blocking matrix is lowest at low frequencies. Therefore, when the interfering signal is low-pass, the IUNR at the reference noise canceller inputs is lowest. The IUNR dictates the SIR at the noise canceller output, and thus determines the SIR gain of a coupled BF-NC structure. Therefore, when the interfering signal is speech, the IUNR drops, and a reduction in output SIR ensues.

To summarize, the decoupled BF-NC prefers a high-frequency desired signal, while the coupled BF-NC with blocking matrix performs best with a high-frequency interfering signal. When both signal and interference are white noise, the decoupled BF-NC outperforms the coupled BF-NC with blocking matrix due to the lower level of uncorrelated noise in its reference noise canceller input. However, when the desired signal is speech, the inclusion of the blocking matrix in the coupled BF-NC scheme leads to an improvement in SIR. This is because at these frequencies, the attenuation of the desired signal in the decoupled BF-NC outweighs the lower level of uncorrelated noise. Finally, when both signal and interference are speech, the inclusion of the blocking matrix does not significantly affect the output SIR. The decoupled BF-NC suffers from low-frequency leakage, while the coupled BF-NC with blocking matrix suffers from a low IUNR at low frequencies.

Reproduced with permission of the copyright owner. Further reproduction prohibited without permission.

Figure 5.4 depicts the ensemble averaged SIR gains, as a function of frequency, when the desired signal and interference are both white noise (This configuration was chosen for the figure so that the entire frequency band could be examined). At the low frequencies, the amount of desired signal leakage in the decoupled BF-NC is significant, and thus the inclusion of the blocking matrix in the coupled BF-NC is beneficial. On the other hand, at the high-frequency end, the dominant factor becomes the level of uncorrelated noise. Since the DSB is better at suppressing white noise than the Griffiths-Jim blocking matrix, the decoupled BF-NC outperforms the coupled BF-NC with blocking matrix. Notice that the spike in the "beamformer only" curve corresponds to a null in the beampattern at that frequency.

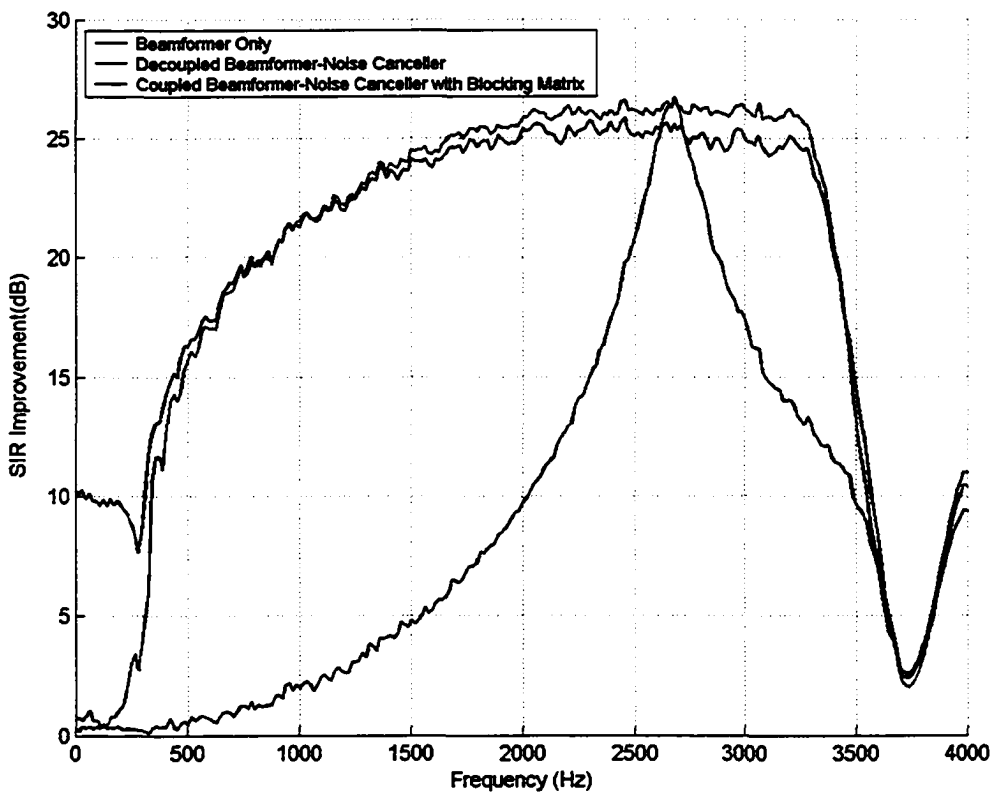

Figure 5.4. Signal-to-interference ratio improvements as a function of frequency.

Reproduced with permission of the copyright owner. Further reproduction prohibited without permission.

To gain further insight into the frequency dependency of the SIR gains, Figure 5.5 shows the interference power levels (as a function of frequency) at the array, output of the front-end beamformer, output of the decoupled BF-NC, and output of the coupled BF-NC with blocking matrix. Likewise, Figure 5.6 displays the frequency-dependent desired signal power levels.

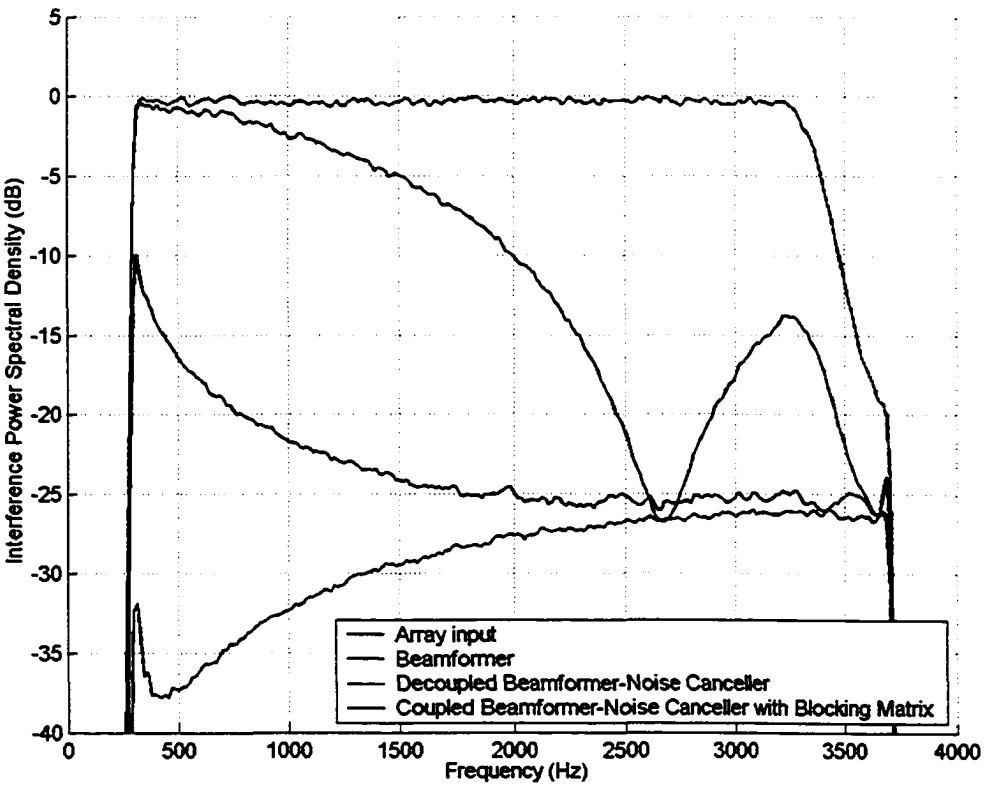

Figure 5.5. Output power spectral densities of interference only, as a function of frequency.

From Figure 5.5, it is clear that the greatest interference cancellation is provided by the decoupled BF-NC. This is because the decoupled BF-NC minimizes the level of uncorrelated noise in the reference noise canceller input, and thus maximizes the coherence between primary and noise canceller inputs, leading to a low minimum-mean-squared-error (MMSE) in the adaptation process. The inclusion of the blocking matrix in the coupled BF-NC raises the level of uncorrelated noise in the reference noise canceller

Reproduced with permission of the copyright owner. Further reproduction prohibited without permission.

inputs, and thus lowers the coherence between primary and reference inputs, leading to a higher MMSE. Therefore, the level of interference cancellation is not as great. The beamformer alone provides only moderate levels of interference reduction

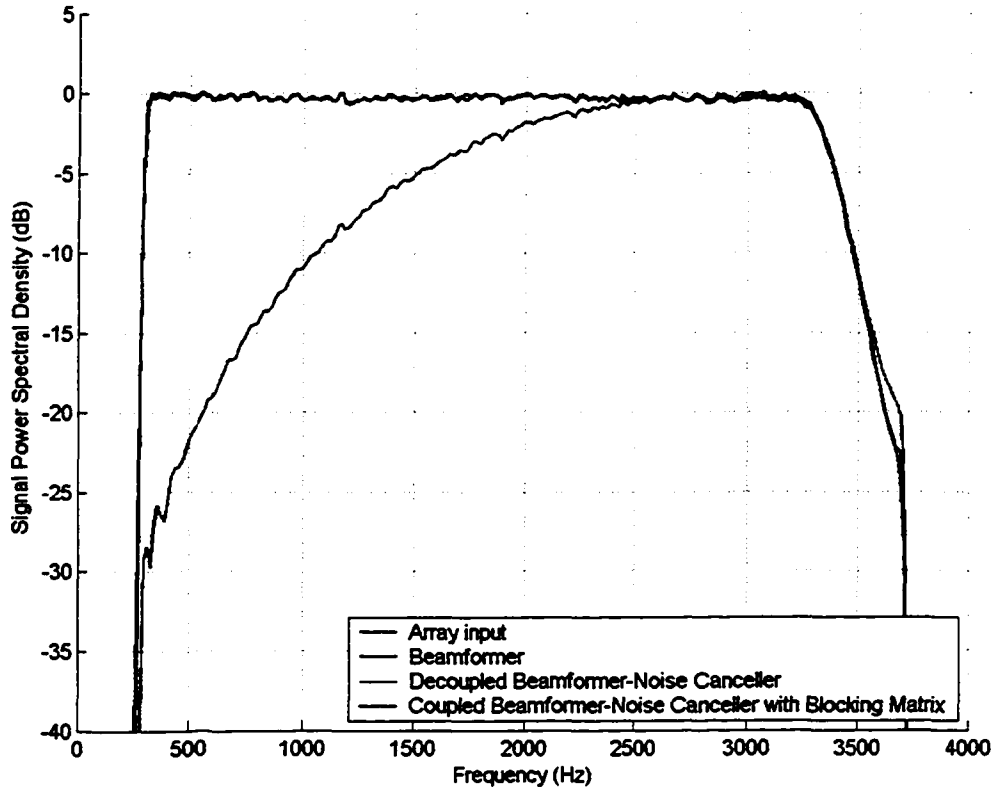

Figure 5.6. Output power spectral densities of desired signal only, as a function of frequency.

Turning now to Figure 5.6, the disadvantage of the decoupled BF-NC is exposed, in the form of desired signal distortion at the low frequency end. This is a direct result of the desired signal being passed through the sidelobes of the interference beamformer. The blocking matrix prevents any such leakage, and thus the coupled BF-NC with blocking matrix preserves the desired signal power levels at the array. The stand-alone beamformer also maintains the signal power. Note that the signal power at the array,

Reproduced with permission of the copyright owner. Further reproduction prohibited without permission.

output of the front-end beamformer, and output of the coupled BF-NC with blocking matrix are virtually identical.

It is interesting to note that while the differences between the decoupled BF-NC and coupled BF-NC with blocking matrix appear minor in the SIR curve of Figure 5.4, the structures differ greatly in the way that these SIRs are achieved: The decoupled BF-NC provides a very high level of interference reduction, which compensates for the loss of desired signal power at the lower frequencies. The coupled BF-NC with blocking matrix does not cause significant desired signal distortion, but attains a lower level of interference cancellation.

The results of Table 5.1 support the hypothesis of BF-NC applicability to various signal environments. A combined BF-NC is essentially an adaptive spatial filter, and thus, as expected, provides signal enhancement across a broad range of signal environments. One may classify the use of a BF-NC for signal enhancement in the case of a speech signal and speech interference as a type of "blind signal separation" [9] in which one signal is to be extracted.

Finally, Figure 5.7 displays the normalized mean-squared-error (MSE) of the noise-only adaptation in BF-NC structures, as a function of number of adaptive algorithm iterations. The curves are averaged over 100 ensembles. The faster convergence of the decoupled BF-NC is evident, and is attributed to the fact that a single adaptive filter is being converged (as opposed to multiple adaptive filters in the case of the coupled BF-NC with blocking matrix), as well as the lower level of uncorrelated noise during adaptation. From the figure, it is also obvious that the MMSE is lower for the decoupled BF-NC. Note that the convergence rate is critical in BF-NC structures, as the adaptation

Reproduced with permission of the copyright owner. Further reproduction prohibited without permission.

is carried out during "silent" (desired signal idle) periods. It is by no means guaranteed that these silent periods are long enough to permit full convergence.

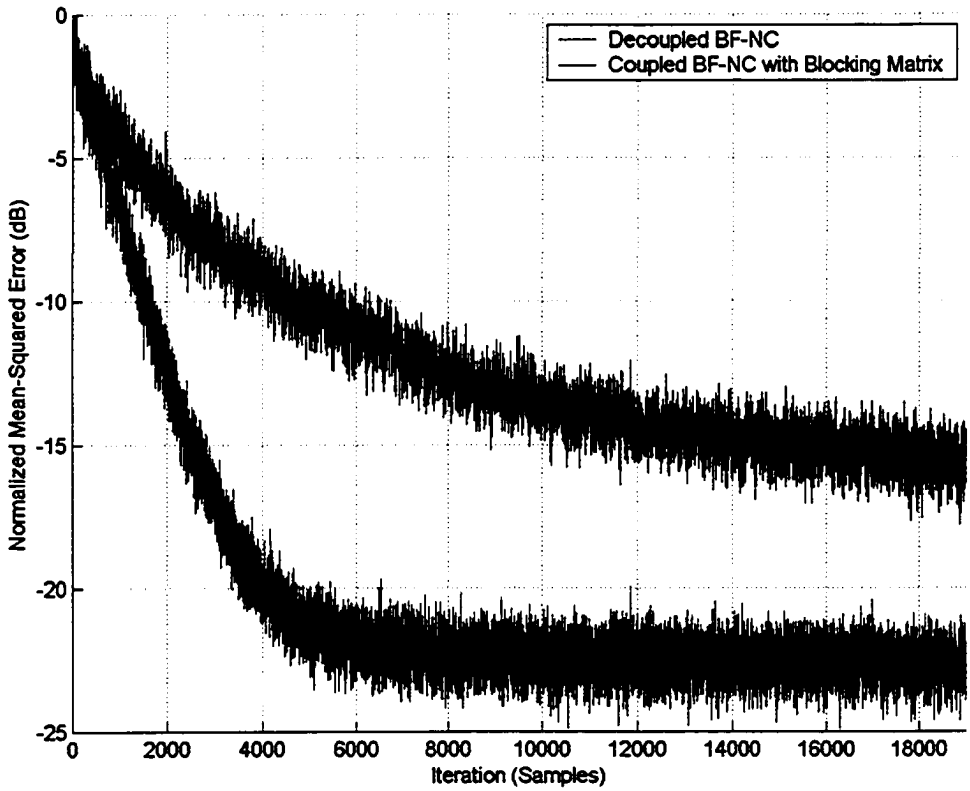

Figure 5.7. Convergence rates of beamformer-noise canceller structures.

Reproduced with permission of the copyright owner. Further reproduction prohibited without permission.

Chapter 6

Experimental Evaluation of Beamformer-Noise Canceller Structures

The results of Chapters 4 and 5 reflect assumptions that do not hold true in real conditions. For example, the far-field plane wave model does not accurately represent wave propagation when the source is in the near-field of the array. The lossless and anechoic signal propagation assumption only holds true in the most artificial of environments. Steering mismatch may occur. Therefore, the performance of BF-NC structures must be evaluated in conditions that correspond to the environments in which BF-NC structures will find applicability. An office room has thus been chosen as the setting. Details of the experimental setup are given in Chapter 3.

6.1 Experimental Procedure

Throughout each experiment, the location of the interference source is held fixed, while the signal source is moved around to various locations. The objective of the evaluation is to determine the improvement in SIR from microphone array to system output for the front-end beamformer, decoupled BF-NC, and coupled BF-NC with blocking matrix.

It is important to note that since the investigation employed real (as opposed to simulated) data, the evaluation cannot be performed with desired signal source and interference playing simultaneously, as it would be impossible to discern the contributions of the signal and interference in the recordings. The signal processing consists of two stages: In the first stage, only the interference is captured with the array, and beamformed accordingly. The adaptive algorithm then computes the optimal transfer

Reproduced with permission of the copyright owner. Further reproduction prohibited without permission.

functions between the primary and reference ANC inputs. The captured interference is then fed back into the converged structure, and the output power is measured. In the second stage, only the desired signal is recorded with the array and subsequent components. The recorded signal is then applied to the converged structure being evaluated, and once again, the output signal power is recorded. The output SIR is then easily determined by combining the results of the two stages. Note that since the system is linear, the latter procedure is valid.

6.2 Experimental Results

Figure 6.1 displays the result of one experiment. The results of all experiments are shown in the Appendix.

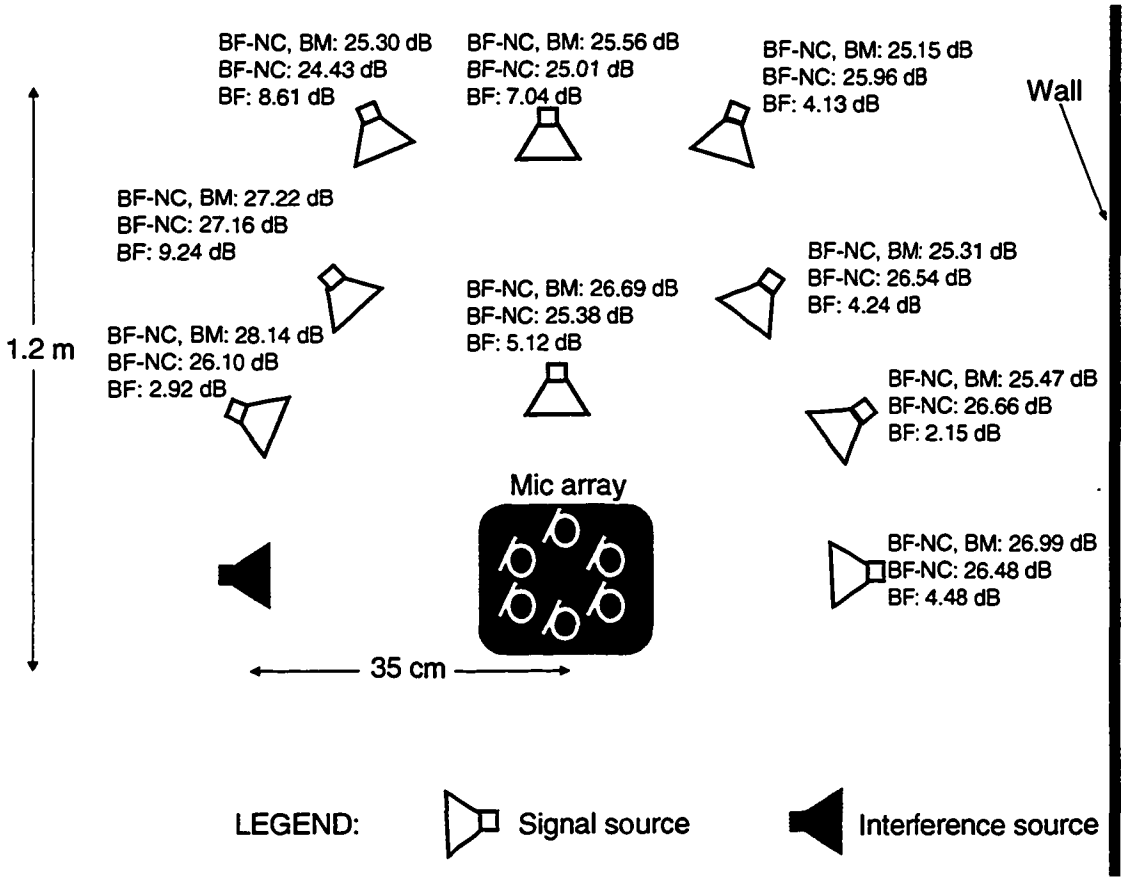

Figure 6.1. Experimentally obtained signal-to-interference ratio improvements for the beamformer, decoupled beamformer-noise canceller, and coupled beamformer-noise canceller with blocking matrix, as a function of signal-source location.

Reproduced with permission of the copyright owner. Further reproduction prohibited without permission.

The numbers indicate the SIR improvement for each signal source location: 'BF' indicates the SIR gain achieved by the front-end beamformer alone, 'BF-NC' indicates the SIR gain achieved by the (decoupled) two-DSB, one-ANC structure of Figure 4.3, and 'BF-NC, BM' indicates the SIR gain achieved by the coupled BF-NC with blocking matrix, shown in Figure 4.7, with a DSB at the front-end, and the Griffiths-Jim blocking matrix.

The sensitivity of the desired signal beamformer to the acoustics of the path from interference source to the array is evident from the figure. For clarity, the results are repeated and key numbers highlighted in Figure 6.2.

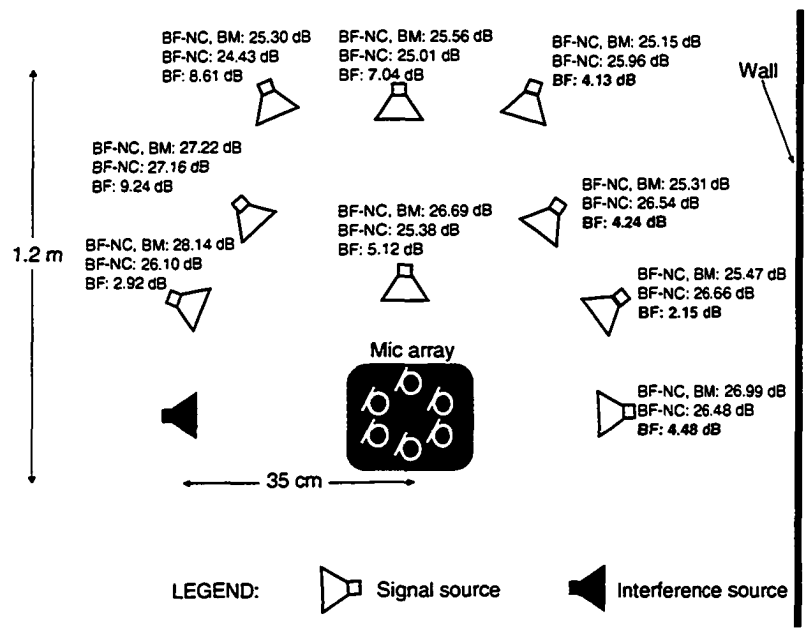

Figure 6.2. Sensitivity of desired signal beamformer to reverberation.

In particular, when the signal source is located near the wall, the desired signal beam strongly picks up interfering signal reflections. This is evidenced from the low beamformer SIR gains experienced when the desired signal source rests near the wall.

Reproduced with permission of the copyright owner. Further reproduction prohibited without permission.

The question of how the lower level of directivity offered by the front-end beamformer affects the performance of the ANC is crucial. Figure 6.3 highlights the BF-NC gains at locations in which the beamformer offers very little SIR gain.

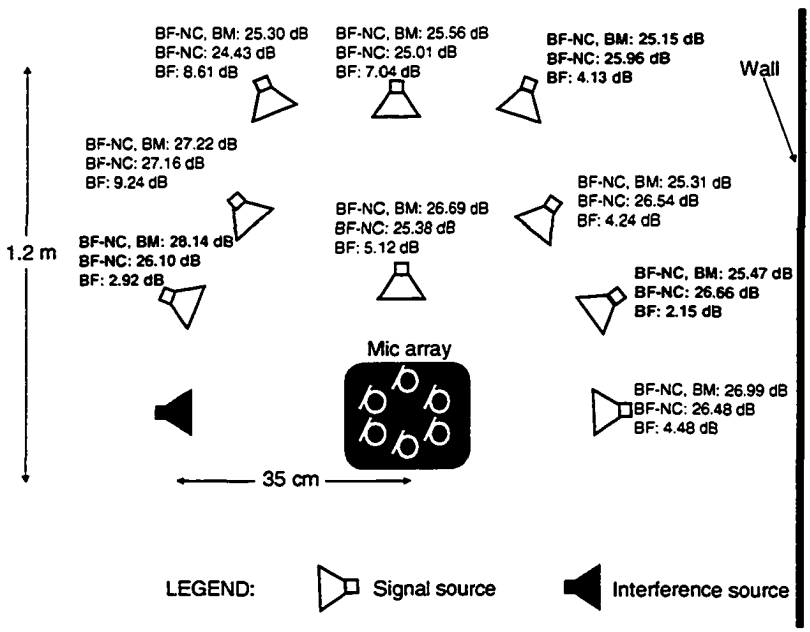

Figure 6.3. Effect of lowered beamformer directivity on performance of noise canceller.

It is apparent that a low SIR gain at the front-end beamformer does *not* translate to reduced ANC SIR gain. The ANC is able to "compensate" for the lowered directivity of the beamformer. Note that the noise cancellers are adapted in the presence of reverberation, and thus, the filter taps will be driven to cancel any interference reflections in the desired signal beamformer output. Because the adaptation is carried out in the absence of the desired signal, cancellation of the desired signal due to signal reflections does not result. Even though reverberation does lead to the leakage of the desired signal in the reference noise canceller input, the filter is no longer being adapted, and thus only a distortion of the signal occurs.

Figure 6.4 highlights the lone location at which the coupled BF-NC with blocking matrix significantly outperforms the decoupled BF-NC (by ~2 dB). It is not surprising

Reproduced with permission of the copyright owner. Further reproduction prohibited without permission.

that this location corresponds to the lowest signal-interference separation in the figure. Without the blocking matrix, there is a significant amount of desired signal distortion as a result of leakage of the signal into the interference beam. The blocking matrix forms a null in the direction of the desired signal source, thus lowering the level of distortion.

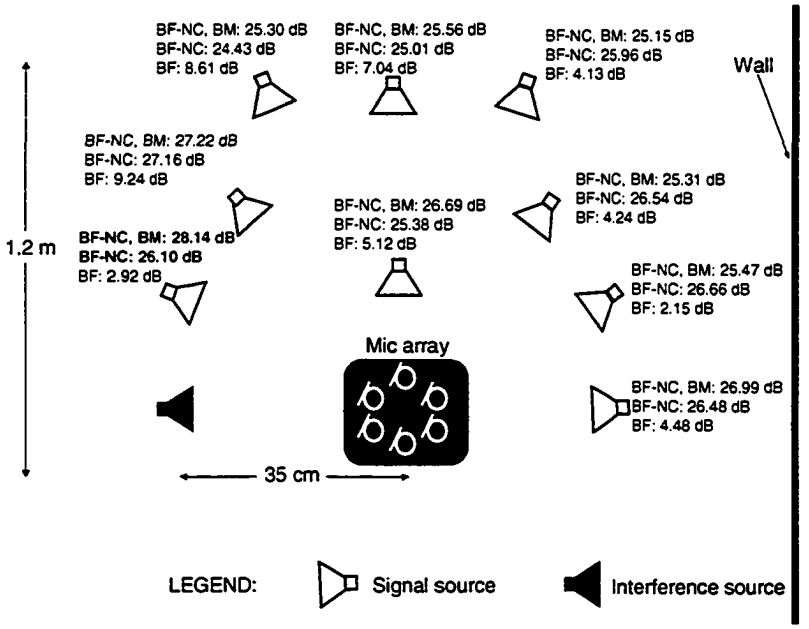

Figure 6.4. Location at which blocking matrix offers greatest signal-to-interference ratio increase.

The reader may wonder why the decoupled BF-NC performs better in some configurations (highlighted in Figure 6.5) than the coupled BF-NC with blocking matrix, which has a significantly higher complexity.

The blocking matrix is designed to prevent desired signal leakage into the reference noise canceller inputs. Because of its multiple outputs, the blocking matrix requires multiple ANCs, each of which amplify any low frequency uncorrelated noise and thus reduce the noise reduction as compared to that of the decoupled BF-NC. Therefore, in cases where desired signal leakage is not the limiting factor in performance, the inclusion of the blocking matrix may actually lower performance, as the level of uncorrelated noise in the system output is boosted.

Reproduced with permission of the copyright owner. Further reproduction prohibited without permission.

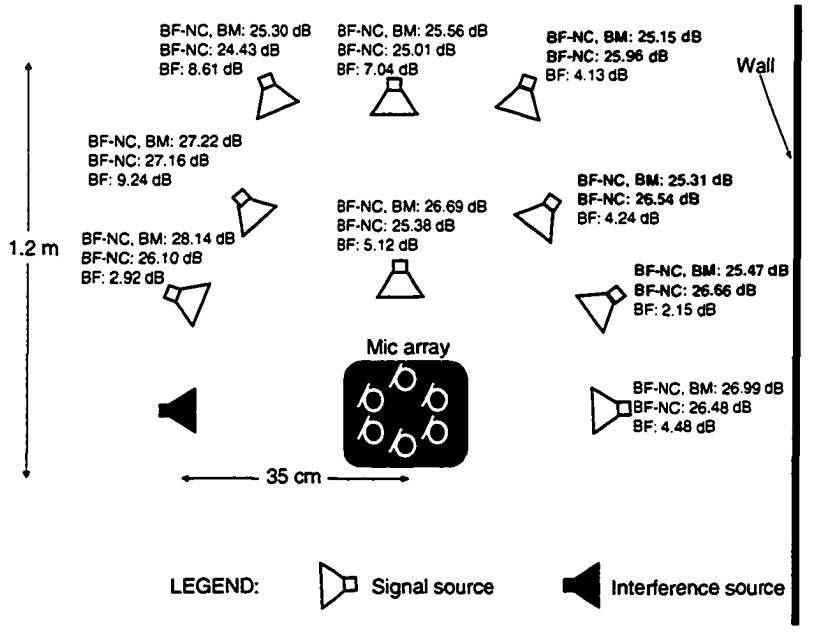

Figure 6.5. Locations at which blocking matrix is detrimental to performance.

Lastly, from Figure 6.1, it is easily observed that the decoupled and coupled BF-NC SIR gains are robust to the signal-interference spatial configuration. This follows from the robustness of the BF-NC to reverberation, which occurs because the adaptation is performed in the absence of the desired signal, thus avoiding the desired signal cancellation phenomenon.

A key design issue in BF-NC structures is that of the length of the adaptive filter(s) comprising the ANC. The selection of L, the delay in the desired signal beamformer output to ensure causality, is also relevant. It has been shown that the value of L should correspond to half the length of the adaptive filter [6]. Figure 6.6 shows the effect of varying the adaptive filter length on the overall SIR gain of the front-end beamformer, decoupled BF-NC, and coupled BF-NC with blocking matrix. The plot stems from a sample experiment run. At each point in the curve, the value of L is half of the adaptive filter length at that point.

Reproduced with permission of the copyright owner. Further reproduction prohibited without permission.

It is obvious that the length of the adaptive filter(s) does not affect the performance of the front-end beamformer. Consider now the decoupled BF-NC: It is evident that the impulse response from interference DSB output to desired signal DSB output is in the order of 50 taps, as the SIR gain stabilizes after reaching this value. On

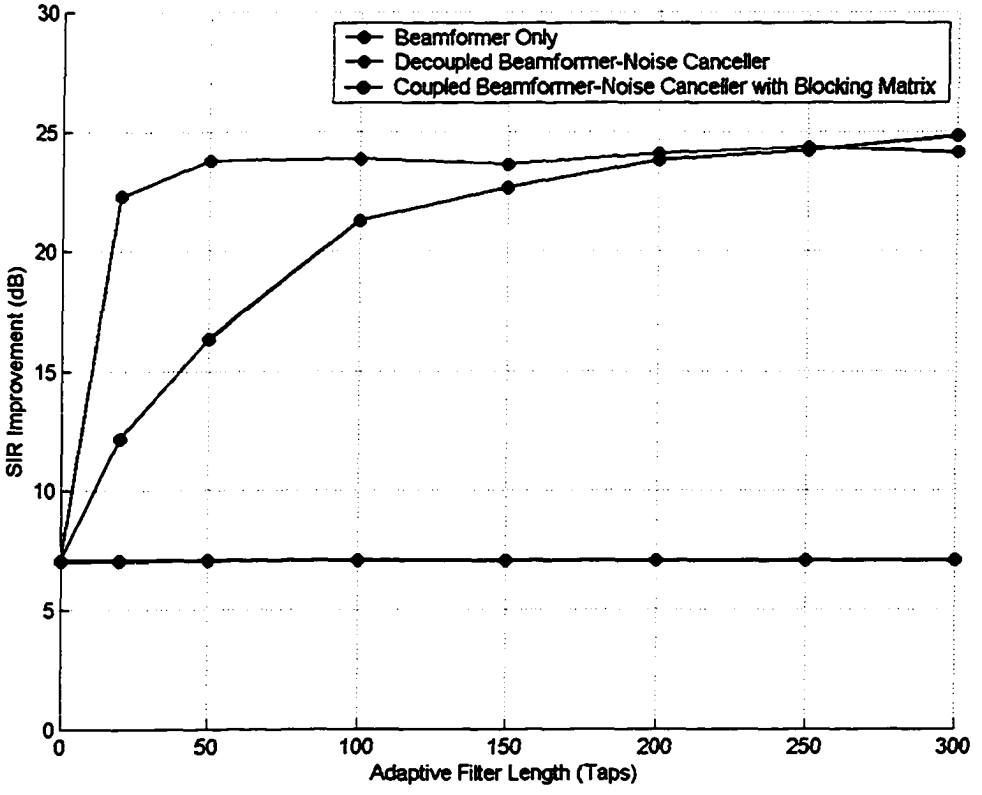

Figure 6.6. Signal-to-interference ratio improvements as a function of adaptive filter length in beamformer-noise canceller structures.

the other hand, the impulse responses between blocking matrix outputs and desired signal DSB output are significantly longer, as the SIR gain has yet to stabilize at 300 taps.

In the two-DSB, one-ANC structure of Figure 4.3, the adaptive filter models the transfer function between two points in space: The source of interference, and the source of the desired signal. On the other hand, the blocking matrix output does not correspond to a specific DOA. Rather, it represents the signal emanating from all directions, with the

Reproduced with permission of the copyright owner. Further reproduction prohibited without permission.

exception of the direction of the desired signal. Intuitively, longer filters are required to model the signal paths from all directions to the direction of the desired signal source.

6.3 Sensitivity of Blocking Matrix to Steering Errors

The experimental findings seem to indicate that lower-complexity alternatives to blocking matrix-based adaptive beamformers may exist. The uncorrelated noise level is not the only problem of the blocking matrix. The sensitivity of the blocking matrix to steering errors is also undesirable. In this section, this sensitivity is explained in terms of the ANC theory presented in Chapter 2.

Consider the following scenario: The desired signal is nominally at broadside, while the interference impinges on the array at a DOA of 60°. Keep in mind that the output SIR of a noise canceller is inversely related to the SIR at the reference noise canceller input through (2.5). Figure 6.7 shows the beampatterns of a blocking matrix and a DSB steered to the interference source. The SIRs attained at the reference noise canceller inputs are shown. In the nominal situation, the blocking matrix achieves a reference SIR of approximately -35 dB, while the reference SIR achieved by the DSB is approximately -23 dB. Therefore, with no steering errors, the blocking matrix indeed provides a desirably low reference SIR.

Now imagine that the signal source moves to a DOA of −20°. The resulting SIRs are shown in Figure 6.8. The signal now falls on a portion of the blocking matrix beampattern that provides very little attenuation, and thus the blocking matrix reference SIR is now only -7 dB. The beampattern of the DSB exhibits a fair amount of attenuation at −20°, and thus, the resulting reference SIR is -12 dB.

Reproduced with permission of the copyright owner. Further reproduction prohibited without permission.

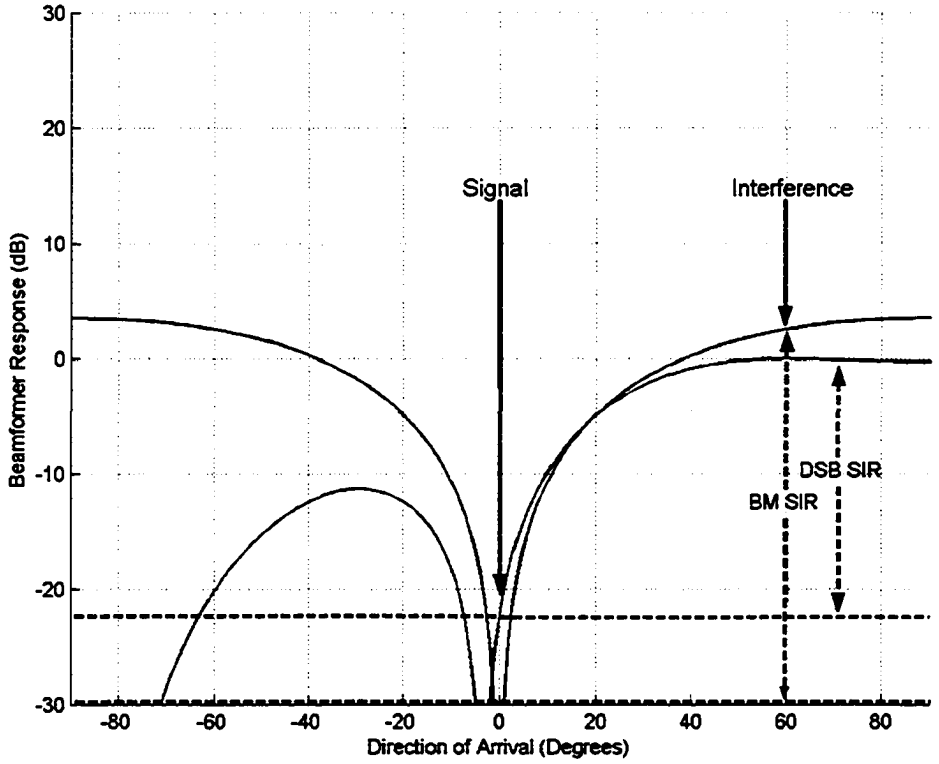

Figure 6.7. Reference signal-to-interference ratios under ideal conditions.

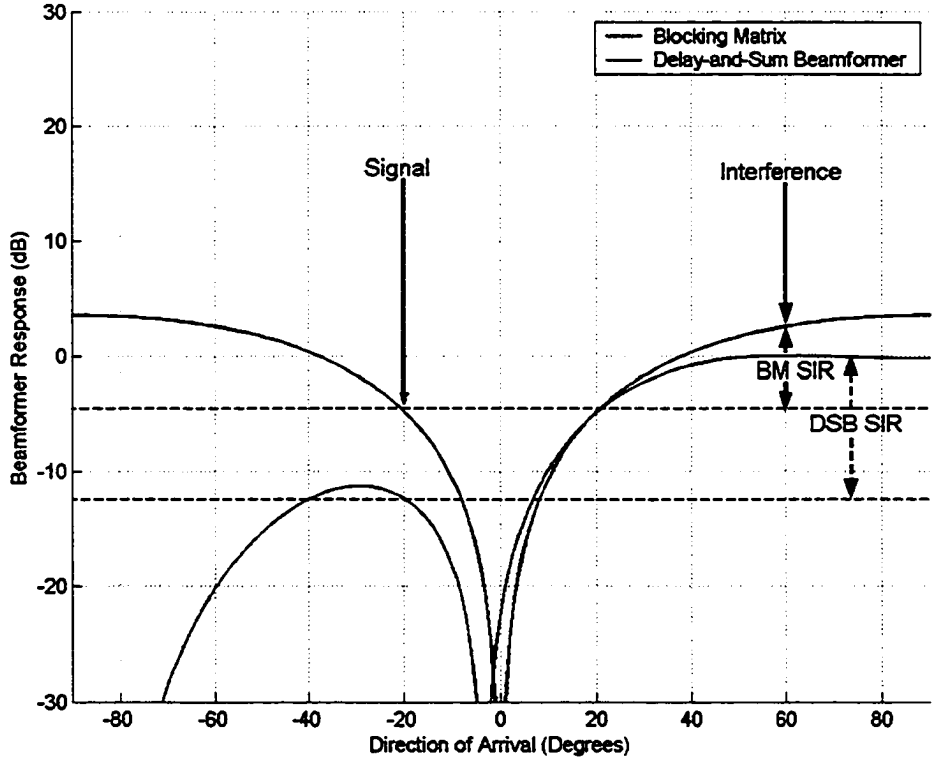

Figure 6.8. Reference signal-to-interference ratios with steering error.

Reproduced with permission of the copyright owner. Further reproduction prohibited without permission.

Therefore, from (2.5), the output SIR of the decoupled BF-NC is 12 dB, while the output SIR of the coupled BF-NC with blocking matrix is 7 dB. Notice that the blocking matrix beampattern exhibits gains of unity or greater at a wide range of angles. Thus, all reflections arriving in this range will leak through the blocking matrix. On the other hand, the DSB provides unity gain only in the direction of the interference, and is thus more robust to reverberation than the blocking matrix.

Reproduced with permission of the copyright owner. Further reproduction prohibited without permission.

Chapter 7

Conclusions and Future Work

7.1 Thesis Contributions

The contributions of this thesis have been:

1. The decoupled BF-NC model was identified [10-12]. It was shown that a decoupled BF-NC is effectively an adaptive beamformer, and may be implemented in fully-adaptive form.
2. The relationships between front-end beamformers and cascaded noise cancellers were characterized by comparing the beampattern, directivity, WNG, and SIR achieved before and after the noise cancellation stage. It was shown that the SIR gain contributed by the desired signal beamformer is inversely related to the SIR gain contributed by the noise canceller [11-12].
3. The applicability of BF-NC structures to various signal environments was established: This included the case of a speech desired signal with speech interference.
4. An experimental model for evaluating BF-NC structures in real conditions was presented. Experimental results showed that the inclusion of a VAD module allows for simpler, robust alternatives to coupled, blocking matrix-based approaches [11-12].

7.2 Concluding Remarks and Future Work

It is somewhat surprising that while structures that combine beamforming with noise cancellation, such as the GSC, have been prominent in signal estimation research efforts,

Reproduced with permission of the copyright owner. Further reproduction prohibited without permission.

the identification of these structures as two-stage systems (i.e., first beamforming, then noise cancellation) has not been done. Rather, these structures have been viewed solely as implementations of MVDR beamformers that allow for the unconstrained optimization of adaptive algorithms. The natural compatibility of beamformers with noise cancellers has not been explored. This work has attempted to characterize the interoperation involved when cascading beamformers with noise cancellers.

The problems of GSC-structured adaptive beamformers are well-known [9]. Many researchers have attempted to solve these issues using a modified version of the GSC [36-42]. All of these approaches are reactive and involve additional GSC features and functionality, thereby increasing the complexity of an already computationally expensive structure. Moreover, the root of the problem, namely the sensitivity of the blocking matrix to reverberation and location errors, has not been targeted. The fact is that reflections of the desired signal will inevitably leak through the blocking matrix whether it is adaptive or not. Even GSC variants that allow for a certain margin of steering error do not eliminate the leakage of reflections arriving outside of the allowable range. The decoupled BF-NC paradigm proposed in this thesis provides a simple, flexible, and novel method of performing adaptive beamforming. Decoupled BF-NC structures will be operated alongside auxiliary modules: A VAD-like module that freezes adaptation when the desired signal becomes active, and a beam-steering module, which will operate as a look-up table. A switching module will determine the beamformer whose output will be fed into the primary input of the ANC, and feed the remaining beams into the auxiliary channels. The result is a highly-directive structure that avoids

Reproduced with permission of the copyright owner. Further reproduction prohibited without permission.

the sensitivities of the blocking matrix. It is for these reasons that it is predicted that such decoupled designs will be at the forefront of future adaptive beamformer designs.

This thesis has mostly assumed a single source of interference. Decoupled BF-NC designs may be further evaluated for the case of several interference sources. Implementations of decoupled BF-NC without a VAD module may also be investigated. As mentioned previously, it would be most desirable to design a simple fixed beamformer that forms both a beam in the direction of the signal, and a null in the direction of the interference. Such a beamformer may then be connected to the reference noise canceller input.

It is paradoxical that while beamformers and noise cancellers combine so naturally, a beamformer contributes the most SIR gain in conditions that lead to the lowest noise canceller SIR gain contribution. Beamformers prefer maximal spatial separation between signal sources in order to discriminate between the sources, while noise cancellers desire maximal correlation between the primary and reference inputs. This correlation decreases as the separation between signal and interference increases. Since the contribution of the front-end beamformer is inversely related to the contribution of the cascaded noise cancellers, the overall system is versatile to spatial configuration. For small separations, the noise canceller removes a large amount of interference from the primary input. For large separations, the beamformer is able to filter out a lot of the interference prior to the noise cancellation stage, which is not as effective due to the reduced correlation between inputs.

Adding a spatially filtering front-end to the noise cancellation process eliminates the need for the installation of external auxiliary sensors. The addition of an intelligent

Reproduced with permission of the copyright owner. Further reproduction prohibited without permission.

beamforming front-end also provides a method for preventing leakage of the desired signal into the reference noise canceller inputs. The relatively low directivity offered by a stand-alone fixed beamformer is augmented by the integration with a noise canceller. This makes the combination of a beamformer with a noise canceller both natural and mutually beneficial.

Reproduced with permission of the copyright owner. Further reproduction prohibited without permission.

References

[1] Wiener, N., *Extrapolation, Interpolation and Smoothing of Stationary Time Series*, with Engineering Applications. New York: Wiley, 1949.

[2] Bode, H., and Shannon, C., "A simplified derivation of linear least squares smoothing and prediction theory," *Proc. IRE*, vol. 38, pp. 417-425, Apr. 1950.

[3] Kalman, R., "On the general theory of control," *Proc. 1st IFAC Congress*, London: Butterworth, 1960.

[4] Kalman, R., and Bucy, H., "New results in linear filtering and prediction theory," *Trans. ASME, ser. D., J. Basic Eng.*, vol. 83, pp. 95-107, Dec. 1961.

[5] Kailath, T. "A view of three decades of linear filtering theory," *IEEE Trans. Information Theory*, vol. IT-20, pp. 145-181, March 1974.

[6] Widrow, B.., et al., "Adaptive noise canceling: principles and applications," Proc. IEEE, vol. 63, 1975, pp. 1692-1716.

[7] Van Veen, B.D., and Buckley, K.M., "Beamforming: A versatile approach to spatial filtering," *IEEE ASSP Mag.*, vol. 5., no. 2, Apr. 1988, pp. 4-24.

[8] Dudgeon, D., and Johnson, D., *Array Signal Processing*. New Jersey: Prentice-Hall, 1993.

[9] Brandstein M. and Ward, D., *Microphone Arrays*, Berlin: Springer-Verlag, 2001.

[10] Dmochowski, J., and Goubran, R.A., "Noise cancellation using fixed beamforming," *Proc. IEEE International Workshop of Haptic, Audio, and Visual Environments and Their Applications*, pp. 141-145, Oct. 2004.

[11] Dmochowski, J., and Goubran, R.A., "Combined Beamforming and Noise Cancellation", *Proc. IEEE Instrumentation and Measurement Technology Conference*, May 2005, submitted and accepted.

[12] Dmochowski, J., and Goubran, R.A., "Decoupled Beamforming and Noise Cancellation: An Alternative to Classical Adaptive Beamforming", *IEEE Transactions Instrumentation and Measurement*, August 2006, submitted and under review.

[13] Haykin, S., *Adaptive Filter Theory*, Prentice-Hall, 3rd Edition, 1996.

[14] Comprenolle, D. Van, "Switching Adaptive Filters for Enhancing Noisy and Reverberant Speech from Microphone Array Recordings," Proc. IEEE Int. Conf. Acoust., Speech, Signal Processing (ICASSP), Phoenix, Arizona, USA, April 1990, vol.2, pp. 833-836.

[15] Frost, O.L., "An algorithm for linearly constrained adaptive array processing", *Proc. IEEE*, vol. 60, pp. 926-935, Aug. 1972.

[16] Cox, H. et al., "Robust adaptive beamforming", *IEEE Trans. Acoust. Speech Signal Processing*, vol. 35, pp. 1365-1375, Oct. 1987.

[17] Monzingo, R.A., and Miller, T.W., *Introduction to Adaptive Arrays*, John Wiley and Sons, New York, 1980.

[18] Griffiths, L.J., and Jim, C.W., "An alternative approach to linearly constrained adaptive beamforming," *Trans. IEEE Ant. Prop.*, AP-30, 1982, pp. 27-34.

[19] Buckley, K.M., "Broad-band beamforming and the generalized sidelobe canceller", *IEEE Trans. Acoust. Speech Signal Processing*, vol. 34, pp. 1322-1323, Oct. 1986.

[20] Er., M.H. and Cantoni, A., "Transformation of linearly constrained broadband processors to unconstrained partition form", *IEE Proc. Pt. H.*, vol. 133, pp. 209-212, June 1986.

[21] Nordholm, S., et al., "The Broad-band Wiener Solution for Griffiths-Jim Beamformers," *IEEE Transactions on Signal Processing*, Vol. 40, No. 2, February 1992, pp. 474-478.

[22] Claesson, I., and Nordholm, L., "A spatial filtering approach to robust adaptive beamforming," *IEEE Trans. Antennas Propagation*, pp. 1093-1096, September 1992.

[23] Affes, S., and Grenier, Y., "A signal subspace tracking algorithm for microphone array processing of speech," *IEEE Trans. Speech Audio Processing*, vol. 5, no.5, pp. 425-437, September 1997.

[24] Er, M.H., and Ng, B.C., "A new approach to robust beamforming in the presence of steering vector errors," *IEEE Transactions on Signal Processing*, vol. 42, no. 7, pp. 1826-1829, July 1994.

[25] Fudge, G.L., and Linebarger, D.A., "A calibrated generalized sidelobe canceller for wideband beamforming," *IEEE Trans. Signal Processing*, pp. 2871-2875, October 1994.

[26] Hoshuyama, O., et al., "A real-time robust adaptive microphone array controlled by an SNR estimate," *Proc. IEEE ICASSP 1998*, pp. 3605-3678, May 1998.

[27] Zheng, Y.R., Goubran, R.A., and El-Tanany, M., "Experimental evaluation of a nested microphone array with adaptive noise cancellers", *IEEE Transactions on Instrumentation and Measurement*, Vol. 53, Issue 3, pp. 777-786, June 2004.

Reproduced with permission of the copyright owner. Further reproduction prohibited without permission.

[28] Doclo, S., and Moonen, M., "SVD-based optimal filtering with applications to noise reduction in speech signals," Proc. IEEE Workshop Applicat. Signal Processing to Audio and Acoust. (WASPAA'99), New Paltz, NY, USA, October 1999, pp. 143-146.

[29] Doclo, S., and Moonen, M., "Robustness of SVD-based Optimal Filtering for Noise Reduction in Multi-Microphone Speech Signals," Proc. 1999 IEEE Int. Workshop Acoust. Echo and Noise Control (IWAENC' 99), Pocono, PA, USA, pp. 143-146

[30] Doclo, S. et al., "Multi-microphone noise reduction using GSVD-based optimal filtering with ANC postprocessing stage," Proc. DSP2000 Workshop, Hunt, TX, USA, October 2000

[31] Doclo, S. et al., "Multi-microphone noise reduction using GSVD-based optimal filtering with ANC postprocessing stage," Proc. DSP2000 Workshop, Hunt, TX, USA, October 2000.

[32] Doclo, S. et al., "Combined Acoustic Echo and Noise Reduction using GSVD-based Optimal Filtering," Proc. IEEE Int. Conf. Acoust., Speech, Signal Processing (ICASSP2000), Istanbul, Turkey, June 2000, vol. 2, pp. 1061-1064.

[33] Knapp, C., and Carter, C., "The Generalized Correlation Method for Estimation of Time Delay," IEEE Trans. on Acoustics, Speech, and Signal Processing, Vol. ASSP-24, No. 4, August 1976.

[34] Ward, D.B., et al., "FIR filter design for frequency-invariant beamformers," *IEEE Signal Processing Lett.*, vol. 3, no. 3, pp. 69-71, Mar. 1996

[35] Bitzer, J., et al., "An alternative implementation of the superdirective beamformer", *Proc. IEEE Workshop Applicat. Signal Processing to Audio Acoust.*, pp. 7-10, New Paltz, NY, USA, Oct. 1999.

[36] Widrow, B., and McCool M., "A comparison of adaptive algorithms based on the methods of steepest descent and random search," *IEEE Trans. Antennas Propagat.*, pp. 615-637, Sep. 1976.

[37] Er, M.H., and Cantoni, A., "An unconstrained partitioned realization for derivative constrained broad-band antenna array processors," *IEEE Trans. Acoust., Speech Signal Processing*, pp. 1376-1379, Dec. 1986.

[38] Jablon, N.K., "Adaptive beamforming with the generalized sidelobe canceller in the presence of array imperfections," *IEEE Trans. Antennas Propagat.*, pp. 996-1012, Aug. 1986.

[39] Greenberg, J.E., and Zurek, P.M., "Evaluation of an adaptive beamforming method for hearing aids," *J. Acoust. Soc. Amer.*, vol.91, no.3, pp.1662-1676, Mar. 1992.

[40] Hoshuyama, O., et al., "A robust adaptive beamformer with a blocking matrix using coefficient constrained adaptive filters," *Trans. IEICE*, vol. E82-A, no.4, pp. 640-647, Apr. 1999.

[41] Hoshuyama, O., et al., "A robust adaptive beamformer for microphone arrays with a blocking matrix using constrained adaptive filters," *IEEE Trans. Signal Processing*, vol. 47, no.10, pp. 2677-2684, Oct. 1999.

[42] Hoshuyama, O., et al., "A robust adaptive microphone array control based on output signals of different beamformers," *Proc. IEICE 12th DSP Symp.*, A3-4, Nov. 1997.

Reproduced with permission of the copyright owner. Further reproduction prohibited without permission.

Appendix

Full Experimental Results

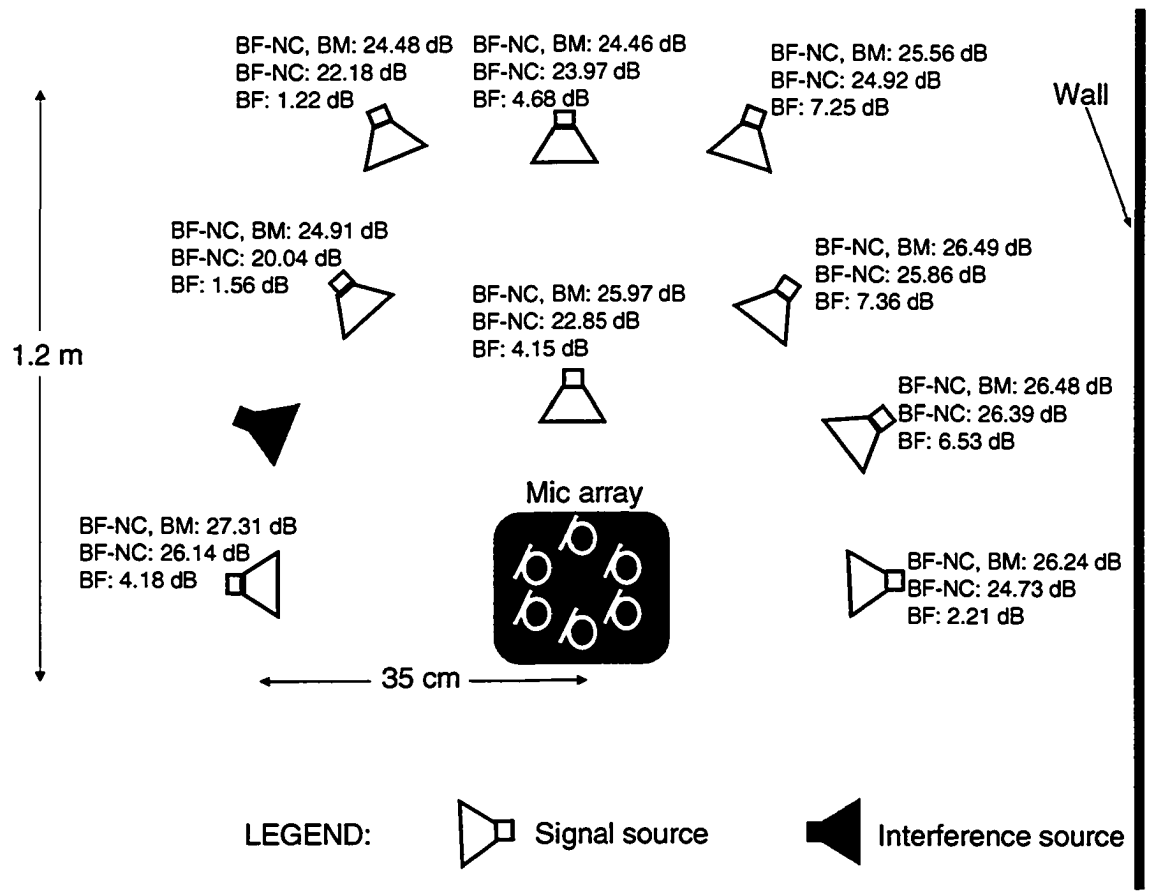

Reproduced with permission of the copyright owner. Further reproduction prohibited without permission.

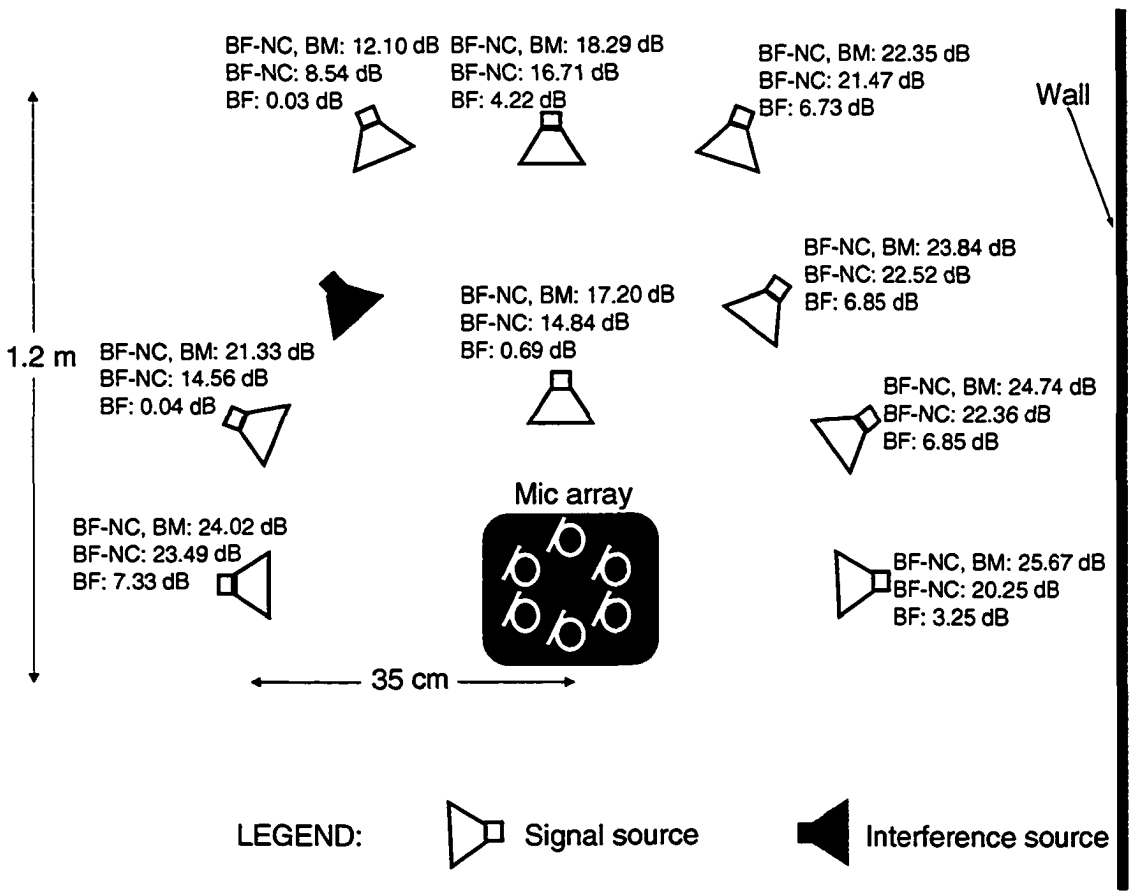

Reproduced with permission of the copyright owner. Further reproduction prohibited without permission.

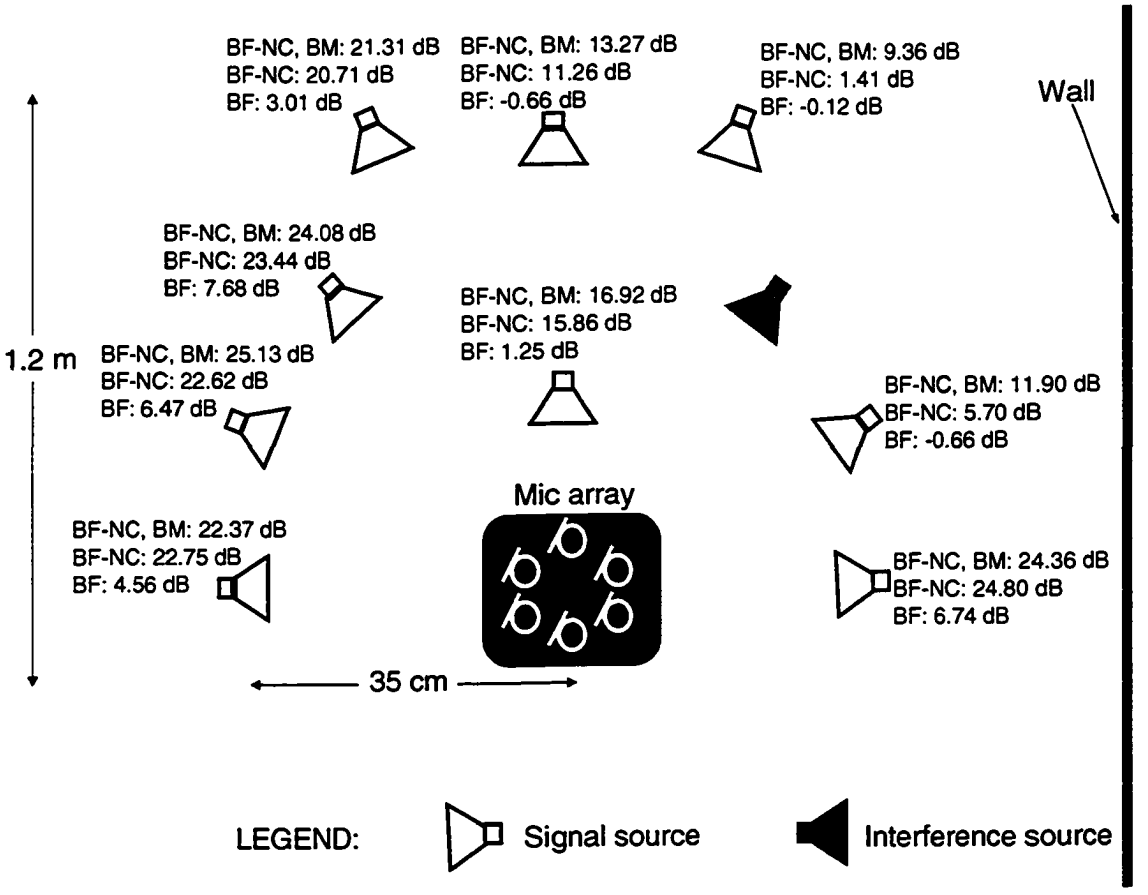

Reproduced with permission of the copyright owner. Further reproduction prohibited without permission.

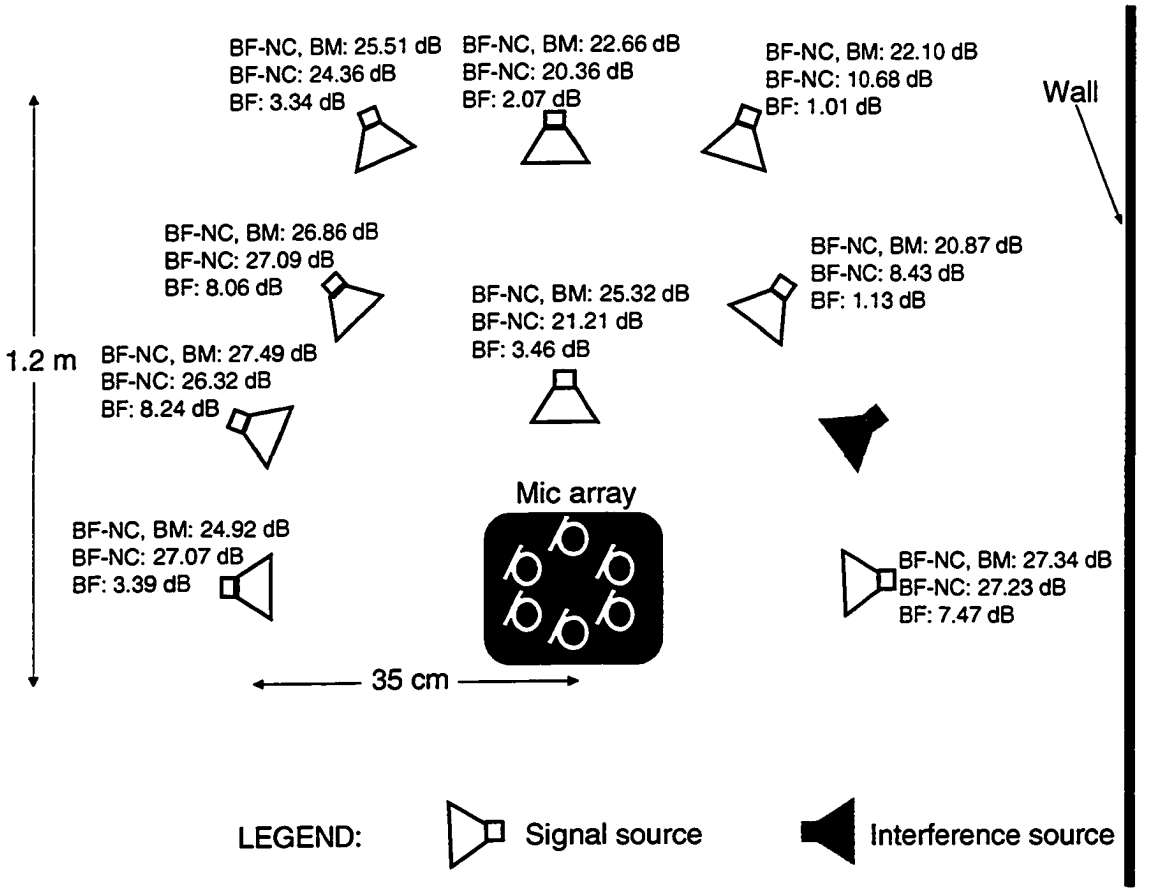

Reproduced with permission of the copyright owner. Further reproduction prohibited without permission.

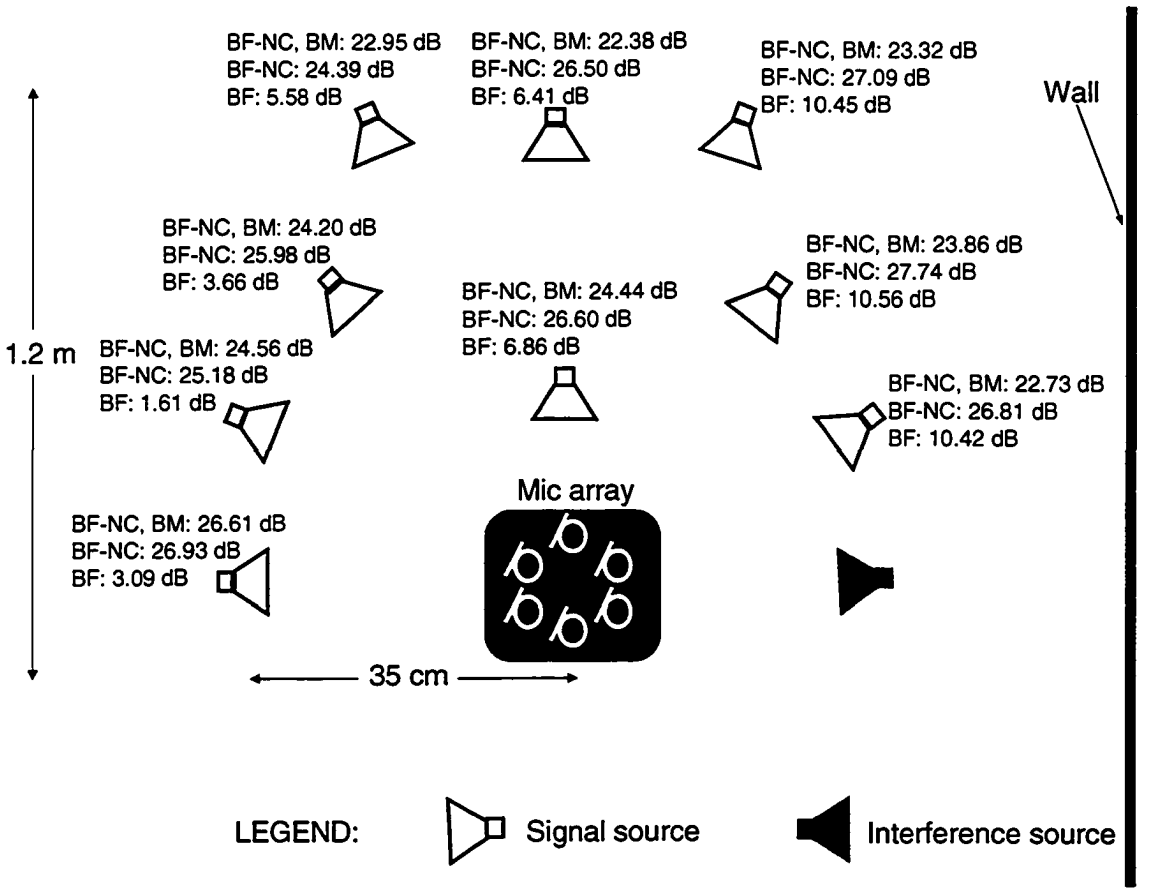

Reproduced with permission of the copyright owner. Further reproduction prohibited without permission.